NTNU – Trondheim
Norwegian University of
Science and Technology

Tension-loaded bolted connections in steel structures

Elin Stensrud Skavhaug
Svanhild Irene Østhus

Civil and Environmental Engineering
Submission date: June 2015
Supervisor: Arild Holm Clausen, KT
Co-supervisor: Arne Aalberg, KT
Erik Grimsmo, KT

Norwegian University of Science and Technology
Department of Structural Engineering

Department of Structural Engineering
Faculty of Engineering Science and Technology
NTNU- Norwegian University of Science and Technology

ACCESSIBILITY

OPEN

MASTER THESIS 2015

SUBJECT AREA:	DATE:	NO. OF PAGES:
Computational Mechanics	19.06.2015	20+146+32

TITLE:

Tension-loaded bolted connections in steel structures

Strekkpåkjente skrueforbindelser i stålkonstruksjoner

BY:

Elin Stensrud Skavhaug
Svanhild Irene Østhus

SUMMARY:
The purpose of this thesis is to study the behaviour of bolted steel connections subjected to tension. Quasi-static conditions have been considered. By performing laboratory tests on single bolts and simple T-stub connections the failure modes of the bolts have been examined. Finite element models are created and validated to represent the behaviour observed in the laboratory.

Different grip length configurations have been tested for a single bolt and nut assembly subjected to pure tension. Both partially and fully threaded bolts have been considered. It was found that partially threaded bolts with three threads between the unthreaded part of the shank and the bearing surface of the nut experienced thread stripping. This is inconsistent with the recommendations given in NS-EN 1090-2, which states that one full thread is sufficient to avoid thread stripping. Finite element models are able to recreate the behaviour of all configurations tested with acceptable accuracy. In addition to the grip length, the material properties and geometry of the threads are identified as the crucial factors for the failure modes of the bolts.

Simple T-stub connections with one bolt in each flange have been tested to examine the behaviour of the bolts when they are subjected to a combination of tension and bending. The center distance between the bolts was varied to examine the behaviour…

RESPONSIBLE TEACHER: Professor Arild Holm Clausen

SUPERVISOR(S): Arild Holm Clausen, Arne Aalberg, Erik Løhre Grimsmo

CARRIED OUT AT: SIMLab, Department of Structural Engineering, NTNU

NORGES TEKNISK-NATURVITENSKAPELIGE UNIVERSITET
INSTITUTT FOR KONSTRUKSJONSTEKNIKK

MASTER THESIS 2015

Elin Stensrud Skavhaug and Svanhild Irene Østhus

Tension-loaded bolted connections in steel structures

(Strekkpåkjente skrueforbindelser i stålkonstruksjoner)

This master thesis is a part of a research project concerned with the behaviour of connections subjected to extreme loads, e.g. dropped objects and sudden column-removal scenarios. Connections are often the critical component in a structure, and if they fail, progressive collapse is imminent. In an early phase of the project, it was observed that the capacity of a connection was limited by thread stripping between the nut and shank in a bolt where tension was the main loading action. This calls for a closer investigation of how different aspects such as the length of the threaded part of the shank and the location of the nut affect the deformation and load capacity of the connection.

The experimental programme of this master thesis involves tests on single bolts as well as test on a T-stub connection with one bolt in each flange. It is of particular interest to explore possible scatter in the single-bolt tests, and this calls for a rather large number of samples. Concerning the T-stub connection, a part of the thesis is to design it in such a way that the desired fracture mode is obtained. The experimental results should be compared with the response from finite element analyses as well as the capacity due to Eurocode 3.

Some keywords for activities related to this master thesis project may include:

- Literature survey: Behaviour of bolted connections (articles, codes, text books).
- Material tests: Uniaxial tension tests. Identification of parameters for numerical model.
- Single-bolt tests: Survey exploring the effect of different parameters. Reporting
- T-stub tests: Design of sample and experimental survey. Reporting.
- Numerical analyses: FEM simulations of tests.
- Design code: Comparison of results with estimates from Eurocode 3.

The candidate may agree with the supervisors to pay particular attention to specific parts of the investigation, or include other aspects than those already mentioned.

The thesis is to be organized as a research report, recognizing the guidelines provided by Department of Structural Engineering.

Supervisors: Erik Grimsmo, Arne Aalberg and Arild Holm Clausen

The report is to be handed in not later than 24 June 2015.

NTNU, 7 January 2015

Arild Holm Clausen

Abstract

The purpose of this thesis is to study the behaviour of bolted steel connections subjected to tension. Quasi-static conditions have been considered. By performing laboratory tests on single bolts and simple T-stub connections the failure modes of the bolts have been examined. Finite element models are created and validated to represent the behaviour observed in the laboratory.

Different grip length configurations have been tested for a single bolt and nut assembly subjected to pure tension. Both partially and fully threaded bolts have been considered. It was found that partially threaded bolts with three threads between the unthreaded part of the shank and the bearing surface of the nut experienced thread stripping. This is inconsistent with the recommendations given in NS-EN 1090-2 [1], which states that one full thread is sufficient to avoid thread stripping. Finite element models are able to recreate the behaviour of all configurations tested with acceptable accuracy. In addition to the grip length, the material properties and geometry of the threads are identified as the crucial factors for the failure modes of the bolts.

Simple T-stub connections with one bolt in each flange have been tested to examine the behaviour of the bolts when they are subjected to a combination of tension and bending. The center distance between the bolts was varied to examine the behaviour when subjected to increased bending effects. Connections with partially threaded bolts all failed due to thread stripping. The fully threaded bolts experienced both thread stripping and bolt failure. The complexity of the stress distribution when large bending effects are present was difficult to recreate with a simplified finite element model. Acceptable accuracy up to maximum force was possible to achieve for the smallest bolt center distance. The response of the finite element model was very mesh sensitive, and difficult to recreate with limited computational capacity when applying an explicit solution algorithm.

II

Sammendrag

Formålet med denne masteroppgaven er å studere atferden til skrudde stålforbindelser utsatt for strekkbelastninger. Kun kvasi-statiske lastbetingelser er tatt i betraktning. Laboratorietester er utført både på enkeltbolter og enkle knutepunkter av T-stykker for å undersøke boltenes bruddmoder. Elementmetoden er brukt for å lage og validere modeller som gjenskaper oppførselen observert i laboratoriet.

Ulike avstander mellom hode og mutter har blitt testet for en enkel skrueforbindelse som utsettes for ren strekk. Både del- og helgjengede bolter har blitt betraktet. Det ble oppdaget at delvis gjengede bolter med tre gjenger mellom ugjenget del av bolt og mutterens bæreflate opplever gjengebrudd. Dette strider med anbefalingene gitt i NS-EN1090-2 [1], der det opplyses at en hel gjenge er tilstrekkelig for å unngå gjengebrudd. Modellene som ble laget ut fra elementmetoden er i stand til å gjenskape oppførselen til alle konfigurasjonene som ble testet med god nøyaktighet. Materialegenskapene og gjengenes geometri anses som avgjørende faktorer for bruddmodene, i tillegg til antallet gjenger mellom hode og mutter.

Enkle forbindelser sammensatt av to T-stykker med en bolt på hver side av steget er testet for å undersøke boltenes oppførsel når de utsettes for en kombinasjon av strekk og bøyning. Senteravstanden mellom boltene ble variert for å undersøke om mengden bøyningseffekter påvirker bruddmoden. Alle knutepunkter med delgjengede bolter opplever gjengebrudd. Helgjengede bolter opplever både gjengebrudd og tverrsnittsbrudd. Den komplekse spenningsfordelingen som oppstår med store bøyningseffekter er vanskelig å gjenskape med bruk av elementmetoden. Akseptabel nøyaktighet opp til maksimal kraft er mulig for den minste senteravstanden. Elementmetodemodellens respons er svært avhengig av elementstørrelser. Det er derfor utfordrende å gjenskape den med begrenset beregningskapasitet når en eksplisitt løsningsalgoritme blir benyttet.

Preface

This master thesis has been performed at the Norwegian University of Sience and Technology for the Department of Structural Engineering. All laboratory work performed for this thesis has been carried out at the research center Structural Impact Laboratory (SIMLab).

We would like to express our gratitude for the help and guidance we have received from our supervisors Professor Arild H. Clausen, Associate Professor Arne Aalberg and PhD candidate Erik L. Grimsmo. Their help have been of vital importance for the progress of our thesis. A special thank to Erik L. Grimsmo for the support and accessibility. The quick response has been outstanding and highly appreciated.

We would also like to thank Postdoc Egil Fagerholt, researchers David Morin and Torodd Berstad, and chief engineer Trond Auestad. Egil Fagerholt has given valuable help and guidance with the installation of DIC, which made it possible to retrieve data from the laboratory tests. David Morin has introduced us to SIMLab Metal Model (SMM) and assisted us in solving problems concerning the use of this model, and Torodd Berstad helped run comprehensive analyses on a supercomputer. Finally, we would like to thank chief engineer Trond Auestad, for his patience and help to perform 62 laboratory tests.

Trondheim, Friday 19th June, 2015

Elin Stensrud Skavhaug

Svanhild Irene Østhus

Contents

List of Figures

List of Tables

1 Introduction

The work presented in this thesis is part of a research project at SIMLab, which concerns the behaviour of bolted connections subjected to extreme loads. This chapter presents the outline of the thesis in terms of the considered problem, previous research, the experimental program conducted and the scope of the thesis.

1.1 Bolted connections

Bolted connections are widely used due to their simple requirements regarding installation and ductile behaviour. Connections where flanges are subjected to tension are very common in steel structures, i.e. beam-to-column connections, bolted end-plates, flange cleats in bending and base plates in bending under tension. These connections should be able to withstand large deformations of the flange and/or end plate in addition to elongation of the bolts. The flange and the bolts form the tension zone of the connection, and may be modelled using an equivalent T-stub. The T-stub connection is useful for examining the behaviour of common structural components.

Connections are often the critical components in a structure. Their behaviour is often limited by the bolts. It is therefore of utter importance to understand how the bolts will behave when subjected to extreme loads. Previous observations have shown that thread stripping may limit the capacity of the bolted connection. This is a brittle failure mode that may lead to sudden collapse.

1.2 Previous work

Relevant literature is presented in Chapters 3 and 9. Previous studies conducted on steel fasteners at elevated rates of strain have shown that the number of

threads in the grip length may influence the failure mode. Alexander [18] has found that the number of threads influence the bolt breaking strength, but the thread stripping strength is not affected. This implies that the failure mode of a bolt may change from bolt breaking to thread stripping when the number of threads in the grip length is reduced. Based on experimental studies, a method for estimating the failure mode of threaded fasteners has been developed. However, this method does not account for the number of threads in the grip length.

None of the previous studies conducted on T-stubs considered thread stripping as a possible failure mode since it was not observed in any of the experimental results reported. The main focus of earlier research has been general failure modes, deformations of flanges and the stiffness of the system rather than the behaviour of the bolts. Swanson [7] discovered that the bolt location and flange thickness may influence the pressure distributions in the T-stub. The research considered in the literature review is based on pre-tensioned bolts, but pre-tensioning has not been applied in the laboratory work conducted for this thesis because it will reduce the tension capacity of the bolts.

1.3 Experimental program

The experimental program is carried out at SIMLab, NTNU. A total of 32 single bolts and 18 T-stub connections have been tested. All tests are performed under quasi-static loading conditions to check if geometry and material properties will affect the behaviour.

The large number of tests of the single bolt will reveal possible scatter concerning the failure modes for different grip lengths. Four different configurations of the T-stub connection have been considered in order to investigate different geometrical properties. All configurations are designed to fail due to a combination of yielding of the flange and bolt failure. Twelve material tests have been performed in order to determine the material properties of the bolts and T-stubs.

1.4 Scope of work

Connections are as mentioned often the critical components in a structure, and failure of a single connection may lead to collapse of the entire structure. It is therefore very important to understand their behaviour. This thesis study the behaviour of single bolt and nut assemblies and a simple T-stub connection. The

main focus is to investigate the failure modes of the bolts when tension is the main loading action. For the single bolts the number of threads in the grip length is of concern. Both partially and fully threaded bolts will be considered to reveal possible differences.

The results from the experimental work are compared to the loading capacity according to NS-EN 1993-1-8 and to the conducted numerical analyses. Finite element models (FE models) have been implemented in order to recreate the behaviour observed in the laboratory tests. Parametric studies are performed in an attempt to reveal what influences the failure mode of the bolts.

The thesis is divided into two parts. Part I considers the single bolts, while Part II considers the T-stub connections. Each part consists of a literature review, presentation of the laboratory work, identification of the material parameters, implementation of finite element models, and the parametric study conducted on these. The results are discussed and a conclusion is presented together with suggestions for further work.

2 Theory

This chapter contains a summary of the most important underlying theory used throughout the thesis.

Sections 2.1-12.4 give a brief description of yield line design and how the design resistance and stiffness of a T-stub connection are calculated.
Then the basic principles of digital image correlation are presented in Section 2.4.

The elastic-plastic material model presented in Section 2.5 will be used to establish a stress-strain relationship for the materials used in the laboratory work in both parts of the thesis. In addition to these material properties the fracture criterion Cockcroft-Latham presented in Section 2.6 will be used.

SIMLab Metal Model is presented in Section 2.7. This implementation of a material model is used to employ the fracture criterion in the finite element models.

Section 2.8 gives a brief introduction to the explicit numerical solution algorithm that will be used in the finite element analyses of this thesis.

2.1 Yield line design

The yield line theory was developed by K. V. Johansen [19] for use in calculations of the ultimate load capacity of reinforced concrete slabs subjected to transverse loading. The theory is a generalization of the plastic hinge method used for beams in frame structures.

It is based on the assumption that all plastic deformation is localized to a number of yield lines that form a kinematic mechanism as displayed in Figure

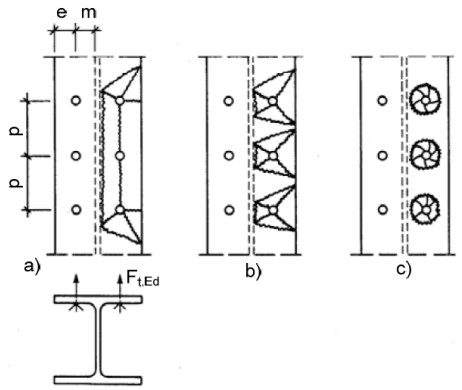

Figure 2.1: Possible kinematic mechanisms in unstiffened column flange. Adapted version of Figure 11.5 in [8]

2.1. The remaining part of the plate stays elastic and undeformed.

The critical load is obtained by finding the mechanism which requires the least amount of work to develop. This may be found using the principle of virtual work, which contemplates that the internal plastic work in the system W_p must be equal to the work done by the externally applied load W_E,

$$W_P = W_E \tag{2.1}$$

The work done by rotation along the yield line is the same as the work done by rotation along the projected length of the yield line onto the support axis, which gives the expression for the internal plastic work,

$$W_P = \Sigma m_P \cdot \phi_i \cdot l_i \tag{2.2}$$

The moment resistance per unit length, m_P, of a plate with thickness t and yield stress f_y is given as $m_P = \frac{1}{4} f_y t^2$. The length of the projected yield line onto the support axis with angle ϕ_i is l_i.

The external work is given as the force multiplied with the displacement,

$$W_E = \int q(x,y) \cdot w(x,y) dA \tag{2.3}$$

where $q(x, y)$ is the applied load per unit area and $w(x, y)$ is the transverse displacement.

The yield line theory is based on the upper bound theorem and is therefore a non-conservative approach unless the correct mechanism is chosen. However, to determine the correct kinematic mechanism in construction features is important to ensure correct capacity. This tend to be a cumbersome process since there is an infinite number of different mechanisms that must be checked.

2.2 Equivalent T-stub

According to the design standard NS-EN 1993-1-8 [17] it is possible to use an equivalent T-stub in tension to model the design resistance of the following basic bolted connections:

- Column flange in bending
- End-plate in bending
- Flange cleat in bending
- Base plate in bending under tension

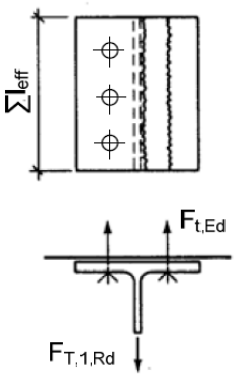

Figure 2.2: Yield lines in equivalent T-stub. Adapted version of Figure 11.5 in [8]

This model is based on known mechanisms of yield lines at the flange, parallel and close to the web and the bolt holes, as displayed in Figure 2.2.

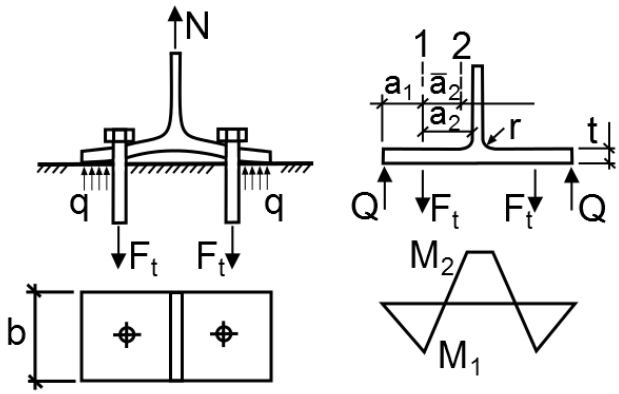

Figure 2.3: Forces in a tension loaded T-stub connection

Due to prying forces it is possible that the forces in the bolts are larger than what would be expected considering the external force on the system. Figure 2.3 show how the bending deformations in the flange causes a distributed pressure q between the flange and the base. In the calculation model this pressure is replaced by a concentrated force Q placed by the flange ends. This results in a moment distribution similar to the one shown in Figure 2.3.

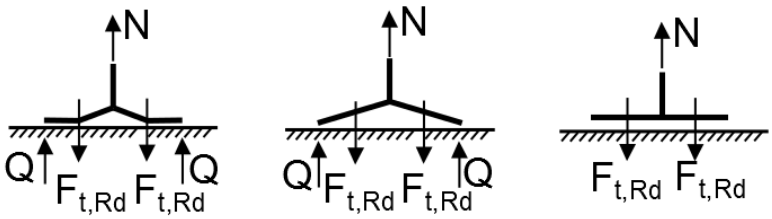

(a) Mode 1 (b) Mode 2 (c) Mode 3

Figure 2.4: Failure modes of tension loaded T-stub

Figure 2.4 displays the three possible failure modes of a tension loaded T-stub, which are:

- Mode 1 - Complete yielding of flange
- Mode 2 - Bolt failure with yielding of flange

- Mode 3 - Bolt failure

The design resistance $F_{T,Rd}$ for the flange of each failure mode is given in Table 6.2 in NS-EN 1993-1-8 [17]. Parts of the table are shown in Table 2.1. The resistance of a T-stub is determined by which of the three modes provides the lowest value. In Table 2.1, $M_{\mathrm{pl,Rd}} = 0.25 \sum l_{\mathrm{eff}} t_{\mathrm{f}}^2 f_{\mathrm{y}} / \gamma_{\mathrm{M0}}$, where $\sum l_{\mathrm{eff}}$ is the smallest effective length found from the possible failure mechanisms.

Table 2.1: Design Resistance $F_{\mathrm{T,Rd}}$ of a T-stub flange [17]

	Prying forces may develop, i.e. $L_{\mathrm{b}} \leq L_{\mathrm{b}}{}^*$		No prying forces
Mode 1	Method 1	Method 2 (alternative method)	$F_{\mathrm{T,1\text{-}2,Rd}} = \frac{2M_{\mathrm{pl,1,Rd}}}{m}$
without backing plates	$F_{\mathrm{T,1,Rd}} = \frac{4M_{\mathrm{pl,1,Rd}}}{m}$	$F_{\mathrm{T,1,Rd}} = \frac{(8n-2e_w)M_{\mathrm{pl,1,Rd}}}{2mn-e_w(m+n)}$	
with backing plates	$F_{\mathrm{T,1,Rd}} = \frac{4M_{\mathrm{pl,1,Rd}}+2M_{\mathrm{bp,Rd}}}{m}$	$F_{\mathrm{T,1,Rd}} = \frac{(8n-2e_w)M_{\mathrm{pl,1,Rd}}+4nM_{\mathrm{bp,Rd}}}{2mn-e_w(m+n)}$	
Mode 2	$F_{\mathrm{T,2,Rd}} = \frac{2M_{\mathrm{pl,2,Rd}}+n\sum F_{\mathrm{t,Rd}}}{m+n}$		
Mode 3	$F_{\mathrm{T,3,Rd}} = \sum F_{\mathrm{t,Rd}}$		

The effective length l_{eff} depends on the positioning of the bolts and whether the column flange is stiffened, unstiffened, or if it is an end-plate. For an unstiffened flange the effective length is calculated from the formulas given in Table 6.4 [17] displayed in Table 2.2. If there are several rows of bolts on the T-stub these have to be checked individually as well as a part of a group of bolt-rows. It is referred to NS-EN 1993-1-8 [17] for similar tables for cases with stiffened flange and end-plate.

2.3 Stiffness of the T-stub connection

The total stiffness of the T-stub connection can be compared with a spring in a serial connection, where each basic component contributes to the total stiffness. The relation between the stiffness, k_{tot}, displacement, u, and force, F, is given as

$$F = k_{tot} \cdot u \tag{2.4}$$

Table 2.2: Effective lengths for an unstiffened column flange [17]

Bolt-row Location	Bolt-row considered individually		Bolt-row considered as part of a group of bolt-rows	
	Circular patterns $l_{\text{eff,cp}}$	Non-circular patterns $l_{\text{eff,nc}}$	Circular patterns $l_{\text{eff,cp}}$	Non-circular patterns $l_{\text{eff,nc}}$
Inner bolt-row	$2\pi m$	$4m + 1.25e$	$2p$	p
End bolt-row	The smaller of: $2\pi m$ $\pi m + 2e_1$	The smaller of: $4m + 1.25e$ $2m + 0.625e + e_1$	The smaller of: $\pi m + p$ $2e_1 + p$	The smaller of: $2m + 0.625e + 0.5p$ $e_1 + 0.5p$
Mode 1	$l_{\text{eff},1} = l_{\text{eff,nc}}$ but $l_{\text{eff},1} \leq l_{\text{eff,cp}}$		$\sum l_{\text{eff},1} = \sum l_{\text{eff,nc}}$ but $\sum l_{\text{eff},1} \leq \sum l_{\text{eff,cp}}$	
Mode 2	$l_{\text{eff},2} = l_{\text{eff,nc}}$		$\sum l_{\text{eff},2} = \sum l_{\text{eff,nc}}$	

where

$$k_{tot} = \frac{1}{2}\frac{1}{\sum \frac{1}{k_i}} \tag{2.5}$$

k_i represents the stiffness from component i. For T-stub connection subjected to tension, only the flange and the bolts will contribute, as illustrated in Figure 2.5. As the calculations are based on one T-stub, the total stiffness of the system, which contains two T-stubs, will be reduced with a factor of $1/2$.

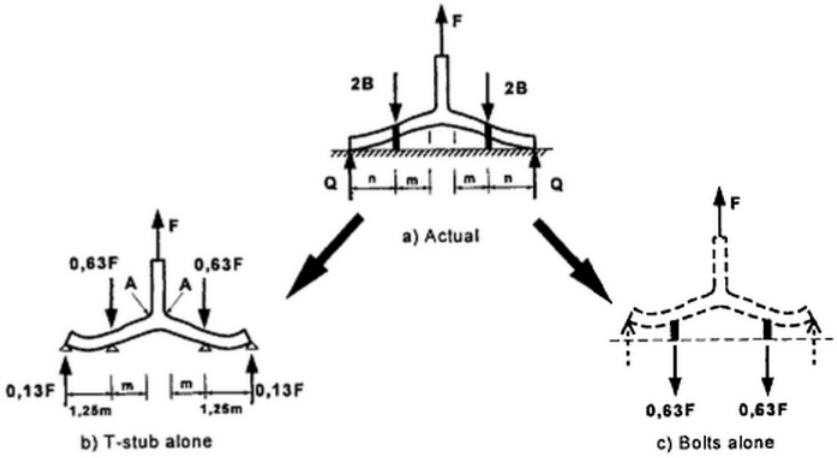

Figure 2.5: Elastic deformation of T-stub [9]

In NS-EN 1993-1-8 [17], the following stiffness coefficients, k_j, are described as
Plate in bending:

$$k_5 = \frac{0.9 \cdot l_{\text{eff}} \cdot {t_p}^3}{m^3} \tag{2.6}$$

Bolt in tension:

$$k_{10} = \frac{1.6 \cdot A_s}{L_b} \tag{2.7}$$

where A_s is the tensile stress area and L_b is the bolt elongation length, which is equal to the grip length of the bolt in addition to half the length of the bolt head and the nut.

The stiffness coefficients are given in the unit millimetre. To achieve the correct unit of the stiffness contribution retrieved from NS-EN 1993-1-8, the following relation is defined as

$$k_i = E \cdot k_j \tag{2.8}$$

where Young's Modulus, E, is taken into account.

2.3.1 Determination of the stiffness coefficients

A deviation of the stiffness coefficients described in NS-EN 1993-1-8 [17], will be presented.

Flange in bending

The stiffness coefficient for the flange is based on calculations of the equivalent T-stub connection, where one flange in taken into consideration. The distance n, defined in Figure 2.5, is set to $1.25m$, which is the maximum length of n used in NS-EN 1993-1-8.

The unit load method is utilized to determine the stiffness of the flange, where the displacement is given as

$$u = \int_L M1 \frac{M2}{EI} dx = 0.079 \frac{Fm^3}{EI} \tag{2.9}$$

where $M1$ and $M2$ is the corresponding moment diagram for the external and virtual load, displayed in Figure 2.6.

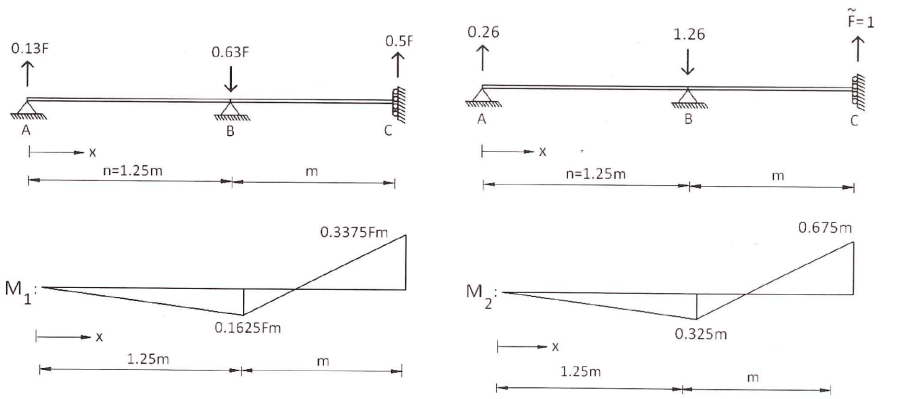

(a) Moment diagram due to external forces

(b) Moment diagram due to virtual load

Figure 2.6: Static models [10]

The calculations of strength is based on the plastic capacity, while the stiffness of the flange is based on the elastic capacity. By combining these formulas, the bending stiffness is described by an initial effective length, $l_{\text{eff.ini}}$, where

$$I = \frac{l_{\text{eff.ini}} \cdot t^3}{12} \tag{2.10}$$

which leads to

$$F = 0.079\frac{EIu}{m^3} = 1.055\frac{l_{\text{eff.ini}} \cdot t^3 \cdot E \cdot u}{m^3} \tag{2.11}$$

With $W_{pl} = 1.5W_{el}$, the relation between elastic and plastic load capacity is defined as

$$F_{\text{Rd.pl}} = \frac{3}{2} \cdot F_{\text{Rd.el}} \tag{2.12}$$

where the elastic load capacity is described as [9]

$$F_{\text{Rd.el}} = \frac{M_{\max}}{0.322m} \tag{2.13}$$

and the plastic load capacity corresponds to failure mode 1 NS-EN 1993-1-8 [17]

$$F_{\text{T.1.Rd}} = \frac{4M_{\text{pl.Rd}}}{m} = \frac{l_{\text{eff}}t^2 f_y}{m\gamma_{\text{M0}}} \tag{2.14}$$

By solving Equation 2.12, the following relation between the initial and plastic effective lengths is determined as

$$l_{\text{eff.ini}} = 0.859 \cdot l_{\text{eff}} \tag{2.15}$$

Inserting Equation 2.15 in Equation 2.11, gives the following formula

$$F = \frac{0.906 l_{\text{eff}} t^3 E u}{m^3} \tag{2.16}$$

The stiffness coefficient of the flange is then utilized by combining the Equations 2.16 and 2.8, which results in the following relation

$$k_{\text{flange}} = \frac{0.906 l_{\text{eff}} t^3}{m^3} \approx k_5 \tag{2.17}$$

Bolt in tension

The contribution from the bolt is based on calculations of the stress- strain relation for a rod in tension, and can be expressed by the formula

$$u = \frac{F_b L_b}{E A_b} \Rightarrow F_b = \frac{E A_b u}{L_b} \tag{2.18}$$

where F_b is the force contributed at the bolt and A_b is the cross section of the bolt. From Figure 2.6a, the load distribution in the bolt is set to $0.63F$. With known force, the stiffness coefficient for the bolt can be calculated by

$$k_b = \frac{1.587 A_b}{L_b} \approx k_{10} \tag{2.19}$$

2.4 Digital Image Correlation (DIC)

Digital Image Correlation (DIC) is an optical technique for measuring strain and displacement at the surface of the specimen. It is widely employed as a laboratory measurement tool due to the simple setup and specimen preparation [20]. The measurements are based on comparison of digital images taken of the specimen during the test. Due to the randomly distributed speckle pattern applied on the specimen, the elongation is easy to register. To implement the DIC method, a calculation area needs to be specified on the reference image. A grid of evenly spaced virtual elements are applied, where the elements recognize and deform

with the highlighted speckles.

DIC uses a mathematical transformation algorithm to retrieve data from the test. The digital images are stored as matrices, where each grey-scale point,the pixel, represent a matrix. The movement of the pixels are evaluated in the computer algorithm. To translate the three dimensional coordinates (X,Y,Z) at the specimen, to the corresponding two dimensional image coordinates (u,v), a camera coordinate system (X_0,Y_0,Z_0) is defined. This model, referred to as the "pinhole projection model" in accordance to Fagerholt [11], is illustrated in Figure 2.7.

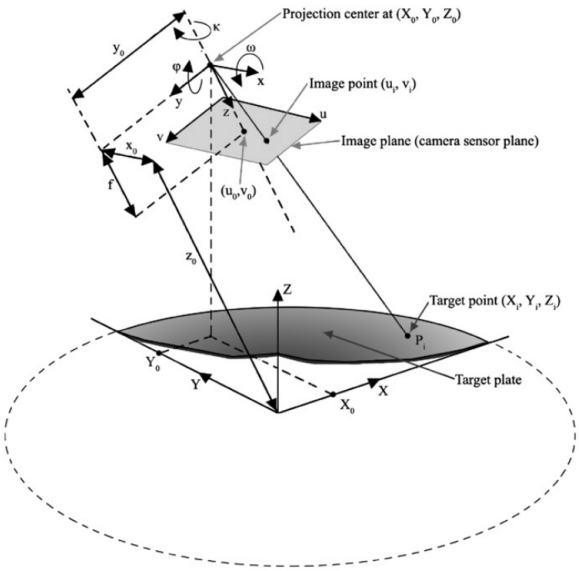

Figure 2.7: Pinhole projecting model, transforming specimen coordinates to image coordinates [11]

The measurements are quite sensitive, and high quality of the images is essential to get satisfactory accuracy. This can be achieved with good light settings, stable camera setup and high resolution of the images.

To retrieve the data of deformation between two points, a vector is inserted at the reference photo, where no force is applied.

DIC uses the unit pixel. This unit can easily be converted into millimetre by appending the known conversion ratio into the DIC software.

From the formula below, the vector elongation is calculated

$$e_x = \frac{L_x}{L_0} - 1 \tag{2.20}$$

where e_x is the elongation of vector at time t_x, L_x is the length of vector at time t_x and L_0 is the length of vector at initial time t_0.

Since DIC operates with registered elongation, measured from the image series, the method is best suited for samples where large deformations occurs. Measurements from the elastic domain will not provide satisfactory accuracy, as opposed to the deformation registered in the plastic domain. The use of DIC to determine Young's Modulus will therefore not be appropriate.

2.5 Material Mechanics

One of the main challenges in finite element analyses is to determine a proper material model, which yields the correct material behaviour when external loads are applied. To understand and be able to predict the response of the material, a full examination of the material is necessary. Figure 2.8 shows a typical stress-strain relation for a tensile test. The stress-strain relation gives important information about the material, and is commonly used to characterize the material properties. This chapter presents all the different aspects of the material features.

2.5.1 Elasticity

The first domain, i.e before yielding, displayed in Figure 2.8 is characterized as the elastic domain. The deformations are assumed to be infinitesimal, which makes it reasonable to assume linear elastic behaviour. Steels are commonly assumed isotropic, which implies that no direction is preferred in the elastic material. This results in only two independent elastic coefficients, Young's Modulus, E, and Poisson's Ratio, ν . NS-EN 1993-1-1 [21] define the material properties for steel as shown in Table 2.3.

Hooke's Law describes the linear elastic stress-strain relation. In isotropic materials, the general formula of Hooke's Law is simplified to

$$\sigma = E\varepsilon^e \tag{2.21}$$

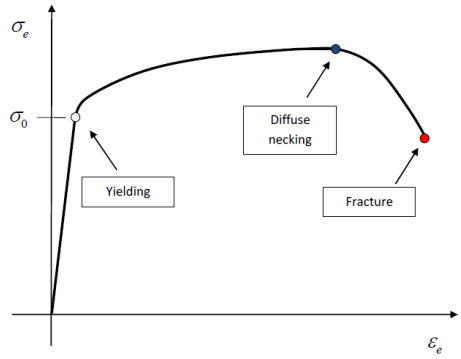

Figure 2.8: Typical stress-strain relation in tensile tests [12]

Table 2.3: Material parameters

E [GPa]	210
ν [-]	0.3
ρ [kg/m^3]	7850

Where σ refers to the stress and ε^e to the elastic strain. In the elastic domain, the deformation is reversible and path independent. By unloading within this area, the test recovers to the original configuration. The elastic behaviour persist until the stress or strain reaches the yield limit. Typical strain limit, ε^e, is in order of 0.001-0.005 [12]. The plastic domain is beyond this limit.

2.5.2 Plasticity

From recoverable deformation in the elastic domain, the deformation now starts to deform plastically, i.e. permanently. The true strain, ε_t, consists of both elastic stain, ε^e, and plastic strain, ε^p, as shown in Figure 2.9.

$$\varepsilon_t = \varepsilon^p + \varepsilon^e \tag{2.22}$$

The theory of plasticity mainly consists of three parts, yield criterion, flow rule and work hardening rule. A brief overview of these will be presented.

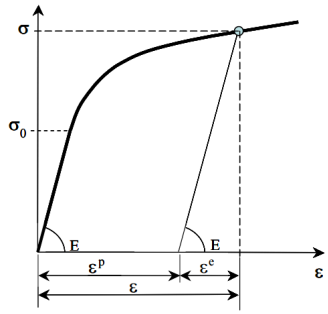

Figure 2.9: Distribution of elastic and plastic strain [13]

Yield Criteria

The yield criterion marks the end of the elastic domain, and the beginning of the plastic domain. The yield stress is the limit where the deformations starts to appear permanently.

$$f(\sigma) = \sigma_{eq} - \sigma_Y = 0 \tag{2.23}$$

where σ_{eq} is the equivalent stress and σ_Y is the yield stress.

For isotropic metals, Von Mises stress is frequently used as the equivalent stress.

$$\sigma_{eq} = \sqrt{\frac{1}{2}((\sigma_1 - \sigma_2)^2 + (\sigma_2 - \sigma_3)^2 + (\sigma_3 - \sigma_1)^2)} \tag{2.24}$$

For uniaxial tests, the formula is simplified as

$$\sigma_{eq} = \sqrt{\frac{1}{2}\sigma_1^2} = \sigma_1 \tag{2.25}$$

where σ_1 refers to the stress in the longitudinal direction of the specimen.

The yield condition, described in Equation 2.23, implies that the yielding occurs when $f(\sigma) = 0$, which means that $f(\sigma) < 0$ in the elastic domain.

Flow rule

As Hooke's Law is necessary to define the relation between the stress and the strain in the elastic domain, the flow rule has the same function in the plastic

domain [13]. In the associated flow rule, the incremental plastic strain tensor, $\dot{\varepsilon}^p_{ij}$, is proportional with the gradient to the yield function, $\frac{\delta f}{\delta f \sigma_{ij}}$, as described below

$$\dot{\varepsilon}^p_{ij} = \dot{\lambda}\frac{\delta f}{\delta f \sigma_{ij}} \tag{2.26}$$

Combined with the Von Mises criterion, the plastic strain rate tensor, $\dot{p}$, is defined as

$$\dot{\varepsilon}^p_{ij} = \frac{3\dot{\lambda}}{2\sigma_{eq}}\sigma_{ij} \tag{2.27}$$

where $\dot{\lambda}$ is a non-negative scalar, $\dot{\lambda} \geq 0$. This is to ensure non-negative dissipation, which means that plastic work must be non-negative for plastic processes. Assuming $\dot{p} = \dot{\lambda}$, the equivalent plastic strain rate, $\dot{p}$, is described as

$$\dot{p} = \sqrt{\frac{2}{3}\dot{\varepsilon}^p_{ij}\dot{\varepsilon}^p_{ij}} \tag{2.28}$$

and equivalent plastic strain,p, is defined as

$$p = \int_0^t \dot{p}\,\mathrm{d}t \equiv \int_0^t \dot{\lambda}\,\mathrm{d}t \tag{2.29}$$

Work Hardening Rule

As the material starts to deform plastically, it starts to harden. Isotropic hardening is utilized to account for the work-hardening in the material.

The isotropic hardening rule is defined as

$$f(\sigma, R) = (\sigma) - (\sigma_0 + R) = 0 \tag{2.30}$$

Voce Rule is employed to describe the work hardening variable R

$$R(p) = \sum Q_R(1 - exp(-\frac{Q_R}{\theta_R}p)) \tag{2.31}$$

where Q_R and θ_R are hardening parameters determined from the tension tests. Illustrated in Figure 2.10, the hardening rate tends to zero as the plastic strain increases.

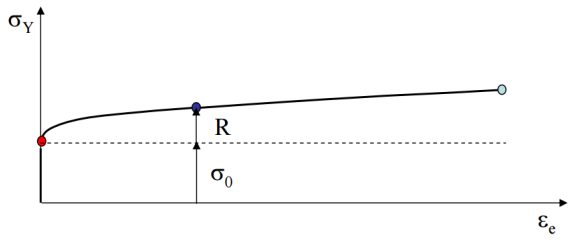

Figure 2.10: Voce Rule hardening curve [14]

2.5.3 Uniaxial tensile test

To characterize the material parameters, the uniaxial tension test is frequently employed. This section presents an outline of the process that gives the best representation of the behaviour of the test specimen. The engineering stress and strain are retrieved from the test, and converted to true stress and strain which may be used to retrieve material properties up to necking. By employing Bridgman's correction method it is possible to calibrate the material properties after necking as well.

Engineering strain and stress

The engineering strain, ε_e, and the engineering stress, σ_e, are only valid for small strains, since they are based on the initial cross-section area.

$$\varepsilon_e(t) = \frac{u(t)}{L_0} \tag{2.32}$$

$$\sigma_e(t) = \frac{F(t)}{A_0} \tag{2.33}$$

were $u(t)$ and $F(t)$ refers to the displacement and force at time t, and L_0 and A_0 describe the initial dimensions, length and cross-section area.

True stress and strain

Large deformations will occur during the tensile testing. The reduction of cross-section area must be taken into account to get a sufficient stress-strain relation. Owing to this, true stress, σ_t, and true strain, ε_t, is the preferable relation to use,

since they are based on the current cross-section area, A, and the current length, L.

$$d\varepsilon_t = \frac{dL}{L} \Rightarrow \varepsilon_t = \int_{L_0}^{L} \frac{1}{L}\,\mathrm{d}L = ln\frac{L}{L_0} \tag{2.34}$$

$$\sigma_t = \frac{F}{A} \tag{2.35}$$

Plastic deformations are volume preserving, which gives the relation $A_0 \cdot L_0 = A \cdot L$. The true strain can further be described as by the initial diameter, d_0, and the current diameter, d, as shown in Equation 2.36.

$$\varepsilon_t = ln\frac{L}{L_0} = ln\frac{A_0}{A} = -2ln\frac{d}{d_0} \tag{2.36}$$

The relation between true stress and engineering stress and strain is given as

$$\sigma_t = \frac{F}{A_0} \cdot \frac{L}{L_0} = \sigma_e exp(\varepsilon_t) = \sigma_e(1 + \varepsilon_e) \tag{2.37}$$

Necking

At necking, i.e maximum stress in Figure 2.8, the uniform stress-strain relation is no longer valid. The state of stress changes from uniaxial stress to triaxial stress for a rod, and to biaxial stress for a thin strip test.

Necking occurs when

$$\frac{d\sigma_t}{d\varepsilon} = \sigma_t \tag{2.38}$$

To predict the stress-strain relation beyond necking, several methods have been developed. For rods,which are most affected by the triaxial stresses, Bridgman's correction is one of the most commonly used methods [22].

Bridgman's Correction Method

Bridgman's correction method is established from the assumptions listed below [23]

1) The contour of the neck remains circular throughout the arc of a circle
2) The cross section of the neck remains circular throughout the test.
3) The von Mises criterion for yielding applies.
4) The strain are constant over the cross section of the neck.

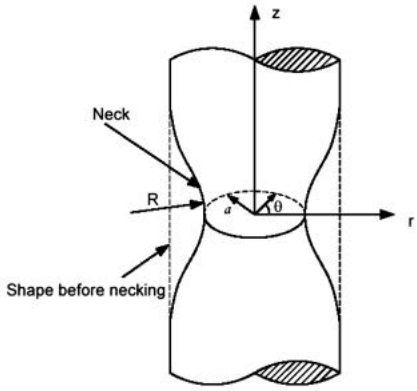

Figure 2.11: Presentation of the Bridgman's assumptions [15]

These assumptions result in the Bridgman's correction formula,

$$\sigma_{eq} = \frac{\sigma_t}{(1 + \frac{2R}{a}) \ln(1 + \frac{a}{2R})} \tag{2.39}$$

where R is the radius of the curvature and a is the smallest radius of the specimen, as illustrated in Figure 2.11.

Based on an empirical expression for the neck geometry, presented by Le'Roy et al. [24], the ratio $\frac{a}{R}$ is simplified to

$$\frac{a}{R} = \kappa(p - p_{necking}), \tag{2.40}$$

where $p_{necking}$ describes the plastic strain at necking and $\kappa \approx 1.1$ for steel.

2.6 Fracture criterion

A fracture criterion is requisite to provoke fracture in finite element analyses. In this thesis the criterion proposed by Cockcroft-Latham is implemented. The Cockcroft-Latham integral, W, is based on the total amount of plastic work, depending on both stress and strain, viz.

$$W = \int_0^p max(\sigma_1, 0)dp \tag{2.41}$$

where σ_1 is the maximum principle stress. The values of σ_1 and p are retrieved from an element at the centerline, where fracture is initiated. Fracture is defined as W reaches its critical value, W_{cr}.

2.7 SIMLab Metal Model

SIMLab Metal Model (SMM), a tool developed by NTNU/SINTEF, implements the material model into the finite element analyses. SMM operates through a material input card consisting of nine flags that control the different features. Each flag represent different material parameters, such as Young' modulus, yield stress and work hardening. For Abaqus/Explicit two different material cards are available, one for axisymmetric and one for non-symmetric models. The SMM can be used on all types of metals, and is applicable to shell and brick elements.

SMM has the advantage of including fracture criterion into the numerical analyses. In SMM, the Cockcroft-Latham fracture criterion is utilized directly, where the elements are deleted when the fracture criteria, $W = W_{cr}$ is reached.

2.8 Explicit numerical solution algorithm

Abaqus/Explicit is a preferable solution algorithm for use in contact problems. By utilizing the central difference algorithm, equilibrium iterations are not necessary, which makes each time increment computationally inexpensive. The main obstacle with an explicit solution method is the conditional stability. To maintain stability, the time step used in equilibrium iterations, Δt, has to be lower than the critical time step Δt_{cr},

$$\Delta t \leq \Delta t_{\mathrm{cr}} \tag{2.42}$$

If this is not the case, the solution will not converge.

The critical time step is defined by the smallest characteristic element dimension, L^e, and the dilitation wave speed c_{d} [25],

$$\Delta t_{\mathrm{cr}} = \frac{L^e}{c_d} \tag{2.43}$$

The dilatation wave speed can be expressed by Young's modulus and the material density,

$$c_d = \sqrt{\frac{E}{\rho}} \tag{2.44}$$

It is important that the finite element analyses are computational efficient. The critical time step is usually so small that running FE analyses with the time period used in quasi-static laboratory tests will require an infinite number of iterations. To increase the efficiency of the explicit solution algorithm, either mass scaling or time scaling may be utilized. From Equations 2.43 and 2.44 it is clear that increasing the mass density will increase the critical time step. This approach is preferred for FE models where some elements are small compared to others. If all elements are approximately the same element size, time scaling is often used. By reducing the time period the system becomes more computational efficient without changing the critical time step.

Utilization of time scaling must be done with caution as it may introduce unwanted effects caused by the inertia forces if the time period is scaled too much. The amount of inertia forces in the system is observed in the kinetic energy plot provided by Abaqus/Explicit. To be sure that these forces do not influence the response of the system, the kinetic energy of the system should not exceed a value of 10 % of the internal energy. A typical plot of the internal and kinetic energies is displayed in Figure 2.12.

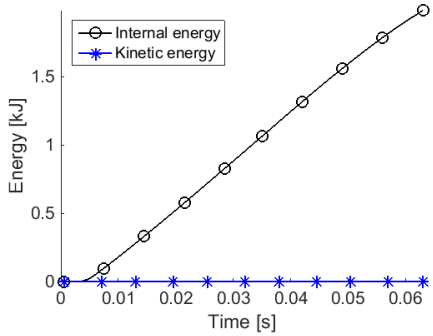

Figure 2.12: Plot of internal and kinetic energy of the deformed system

Part I

Bolts

3 Literature review

The bolt and nut assembly, referring to the externally and internally threaded members, is widely used in engineering structures, owing to the easy installation and replacement. Since often being the critical part of a structure, the stress, deformation and damage distribution of the bolt and nut assembly has been of great interest among scientists. Den Hartod [26] observed that the stress concentrations in the threaded assembly are not uniformly distributed along the length of the threaded part. Owing to the strain setup in the bolt-nut engagement, the maximum intensity of the load distribution occurs at the bearing of the nut. Sopwith [27] has developed a detailed analytical theory for the distribution of load in the threads, which has received acceptance worldwide.

The main focus of the bolt research involves the capacity and failure mode of the threaded connection. This chapter presents some of the previous work performed on threaded assemblies.

3.1 Chen et al.: "A study of the helical effect on the thread connection by three dimensional finite element analysis" [2]

Chen et al. studied the helical effect on the threaded connection by three-dimensional finite element analysis. The effect of both geometry and friction on the load distribution of each thread were analysed. They investigated both axisymmetric and full three-dimensional models of one-inch 8UNC, 12UNC and 16UNC threaded connections. It was observed that the helical effect in the axisymmetric and three-dimensional models has insignificant distinction in the load distribution for the 8UNC and 12 UNC models. As for the one-inch 16 UNF, a deviation of 12% higher load distribution at the first thread measured at the axisymmetric model compared to the full three-dimensional model was found.

By comparing with the analytical analyses by Yamamoto's method, both the axisymmetric and the three-dimensional model have a higher value of load distribution at the first thread. It was also observed that the friction coefficient does not affect the load distribution significantly, although an increase of friction improved the load distribution some.

3.2 Hobbs et al.: "Investigation into the Effect of the Nut Thread Run-Out on the Stress Distribution in a Bolt Using Finite Element Method" [3]

Hobbs et al. investigated the stress distribution in bolts with different nut thread run-out combinations. Both two-dimensional and three-dimensional finite element analyses have been carried out for M12 bolts, and further compared with photoelastic results. As the two-dimensional axisymmetric model ignores the thread helix angle and the thread run-outs in the nut, both chamfered run-out and flat run-out are studied, where different positions around the helix have been tested. The results from the analyses were in good agreement with the results retrieved from the photoelastic results. The peak normalized stress values are within 0.25%, although a large deviation of stress was registered along the threaded connection, further away form the clamped face of the nut. With the use of chamfered run-out, with a rotation of 90 degrees of the thread helix, the peak stress is approximately 10% higher compared with the photoelastic results. The three-dimensional analyses agree with the photoelastic results, when both run-out replicated and friction are included.

3.3 Fransplass et al.: "Numerical study of the tensile behavior of threaded steel fasteners at elevated rates of strain" [4]

Fransplass et al. investigated the behaviour of threaded steel fasteners, M5 with property class 4.6, at elevated rates of strain using numerical analyses. A two-dimensional axisymmetric finite element model of the threaded assemblies was used in the numerical simulations. The material parameters were identified with use of inverse modelling of different material tests at different rates of strain. By studying the same thread run-out combinations investigated by Hobbs [3] combined with different strain rates, the correct failure modes were obtained. With

respect to the maximum load, the deviation between the tests and simulations were less than 4% for bolt fracture and under 9% for thread stripping. Compared to simulations with low strain rates, it was observed that high strain rates gave a better prediction of the maximum force levels. It was also noticed that the number of threads in the grip length affected the failure mode. With no threads in the grip length, the connection failed in thread stripping, while nine threads in the grip length resulted in bolt breaking.

3.4 Alexander: "Design of Threaded Assemblies" [18]

Alexander studied the threaded assembly, and developed methods to describe the strength design of mechanical fasteners employing the ISO R68 thread profile. The work was accepted by the Technical Committee 2 of ISO.

The three possible failure modes for the threaded assembly with corresponding failure loads developed by Alexander are described as

- Bolt Breaking
$$F_{bb} = \sigma_s \cdot A_s i \tag{3.1}$$
- External thread stripping (bolt)
$$F_{bs} = \sigma_s \cdot AS_{si} \cdot C1 \cdot C2 \cdot 0.6 \tag{3.2}$$
- Internal thread stripping (nut)
$$F_{ns} = \sigma_n \cdot AS_{ni} \cdot C1 \cdot C3 \cdot 0.6 \tag{3.3}$$

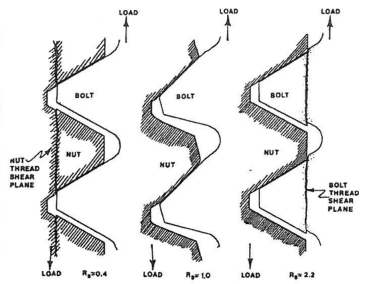

Figure 3.1: Failure modes

Alexander argues that bolt breaking occurs when the threaded engagement is long and the material of both the bolt and the nut coincide with each other. When the threaded engagement is short, thread stripping will appear. Dependent on the weakest material, the thread stripping will occur in either the internal or the external threads.

There are several factors influencing the strength of the threads, among these, geometrical and material factors.
The tensile stress area of the bolt, A_{si}, is directly proportional to the bolt ultimate tensile strength,F_{bb}. The shear area of internal and external threads together with the length of the threaded engagement have huge impact the load capacity and failure mode. The countersink in the nut reduces the contact area of the threaded assembly, which make the length of the threaded engagement, LE_i considerably lower than the nut height. Experimental investigation has given the presence of countersink an effectiveness of 40% of the nut height. This implies that only 40% of the strength is contributed at a nut with a countersink compared to a nut without one.

Material parameters such as ultimate strength of external and internal threads, σ_s and σ_n have a strong influence on the shear strength of the threads. The strength ratio, R_s controls the degree of thread bending between the nut and bolt thread. During loading, plastic deformation will occur in the threads. The bending of the threads decreases the effective shear area, and reduce the angle of the contact surface. This will further develop wedging action of the threads and causes dilation of the nut, where the minor diameter of the nut has increased. As the ratio between the nut wall thickness and nominal diameter, s/D, decreases, the dilation becomes more evident. The influence of the dilation is accounted for in the strength reduction factor $C1$, while the reduction factors $C2$ and $C3$ take the thread bending into consideration. Figure 3.2 show how the strength reduction factors are dependent on R_s and s/D. Figure 3.2b is divided into zones of nut and bolt stripping, relative to the strength ratio.

Coefficient of friction between the bolt and the nut has a high influence of the factors $C2$ and $C3$. By reducing the friction coefficient, the nut will dilate more easily, which result in lower stripping resistance.

The number of threads in the grip affects the bolt strength. The bolt breaking strength may increase $10-20\%$ by reducing the threads within the grip, while the stripping strength is nearly unchanged. This leads to change of failure, from bolt breaking to stripping, when the number of threads in the grip length is reduced.

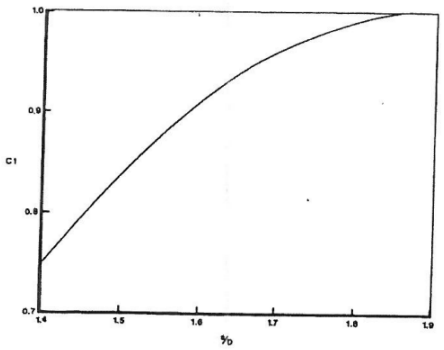

(a) Strength reduction factor, C1, for nut dilation

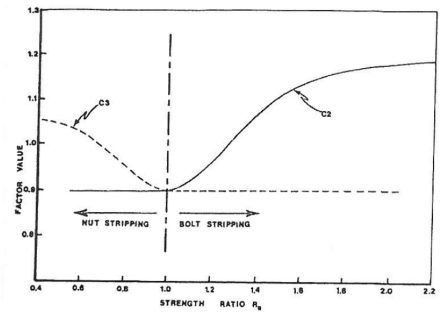

(b) Strength reduction factors, C2 and C3, for threaded bending

Figure 3.2: Strength reduction factors for threaded bending

4 Laboratory work

The laboratory work has been an extensive part of the project. In this chapter the laboratory work is documented in form of review of the methods used in the laboratory and presentations of results. Interesting observations are also addressed at the end of the chapter.

A total of 32 quasi-static uniaxial tension tests have been carried out in the laboratory, see Table 4.1. The purpose of these tests has been to check whether changes in the grip length of a bolt may affect the physical response of the bolt and trigger different failure modes. All tests were performed on M16 bolts with property class 8.8. Both fully and partially threaded bolts have been considered.

Table 4.1: Survey of tests

Bolt type	Grip length [mm]	Number of tests
Partially threaded	118	5
	122	5
	124	2
	130	5
	141	5
Fully threaded	118	5
	141	5

4.1 Geometry

The grip length of a bolt is defined as the distance between the bolt head and nut. It is measured from the underside of the bolt head to the bearing surface of the nut. An overview of the different grip length configurations tested is given in

Table 4.1. Five tests have been executed for every configuration except the grip length 124 mm where only two tests were carried out. This corresponds to 22 tests for partially threaded bolts and 10 test for fully threaded bolts. Figure 4.1 shows sketches of the different grip lengths used for the partially threaded bolts, and Figure 4.2 displays the configurations tested on bolts that are fully threaded.

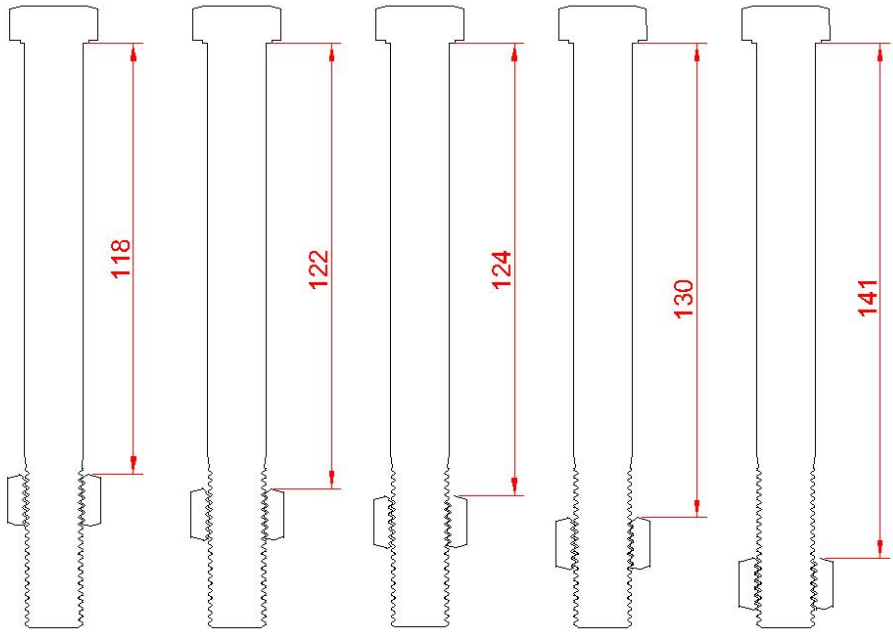

Figure 4.1: Grip length configurations for partially threaded bolts

Since the focus of this laboratory work is directed on the type of failure mode, there has not been done any detailed inspections of the fractures observed in the laboratory other than classifying which failure mode has occurred. The three possible failure modes that the bolts may exhibit are fracture of the cross section, stripping of the external threads on the bolt or stripping of the internal threads on the nut. However, in this particular case it is chosen to view the two cases of thread stripping as one failure mode referred to as thread stripping.

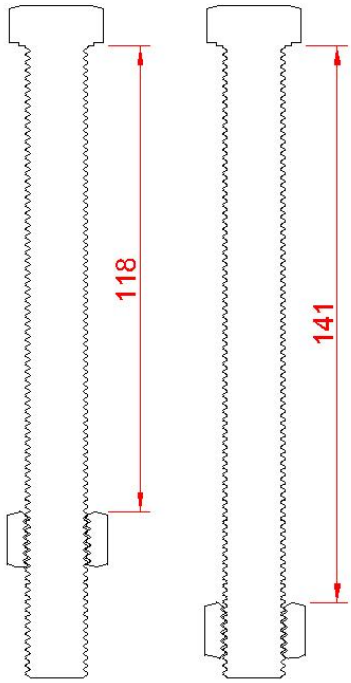

Figure 4.2: Grip length configurations for fully threaded bolts

4.2 Test setup

All laboratory tests are carried out in a screw-driven uniaxial test machine delivered by Instron. The bolt is fastened with purpose-made fixtures and thick circular plates as shown in Figure 4.3a.

To ensure even load distribution from the circular plates onto the bolt, brushers are placed inside the circular plates. These brushers reduce the diameter of the hole through the circular plates, which then makes the longitude axis of the bolt and nut coincide with the longitude axis of the plate to ensure symmetric loading conditions.

The tests were performed under deformation control by a continous movement of the upper bolt head in Figure 4.3. To ensure quasi-static loading conditions low velocities were applied. The deformation rates were in general 0.0133mm/s

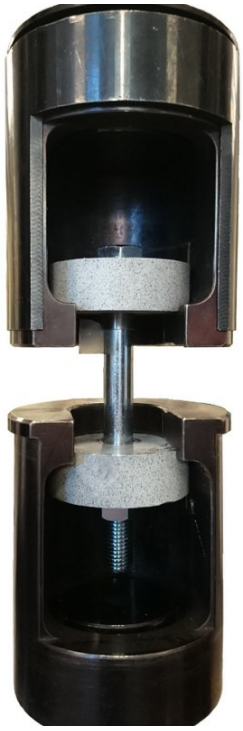

(a) Detailed view

(b) Overview

Figure 4.3: Test setup

and 0.0150mm/s for the partially threaded bolts and 0.0333mm/s for the fully threaded bolts. The increase in velocity for the partially threaded bolts was introduced as a result of very long test durations for the first seven tests. The increase in velocity is assumed not to influence the physical response of the remaining tests.

The physical response of the bolt and nut is logged by machine software at a frequency 1 Hz. In addition DIC is used to measure the deformation of the bolt and nut for two tests from every configuration. This is done by using a camera that takes pictures of the bolt and nut at the frequency 1 Hz. Figure 4.3b shows the DIC setup.

4.3 DIC

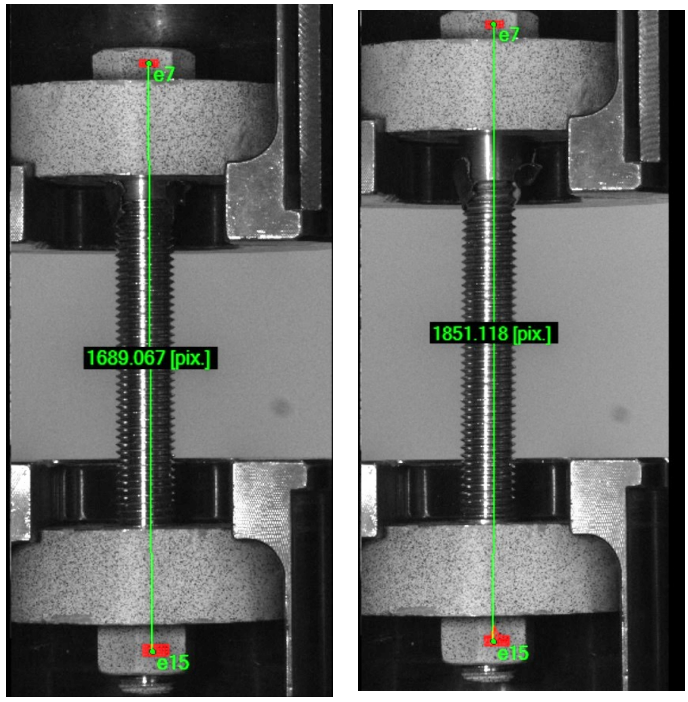

(a) Initial vector length (b) Vector length at time, t

Figure 4.4: Vector elongation in DIC

For the component tests, two dimensional DIC analyses are used to determine the elongation of the bolts during the tests. This will rule out possible elastic deformations included in the displacement log from the machine. Figure 4.4 shows the basis of the elongation retrieved from DIC. A vector is used to measure the distance between the head and nut in each frame. Due to disturbance of the element mesh upon rough surfaces, the utilized element mesh was applied on the middle of the nut and bolt head. Owing to compression registered at the bolt head and nut, the retrieved elongation was further corrected to obtain an accurate deformation of the bolt between the described grip length. Details about the measured correction is presented in Appendix A.

4.4 Results

The failure mode and maximum tension force, $F_{t,Ed}$, observed for each test specimen are presented in Table 4.2. The tests are denoted PT for partially threaded and FT for fully threaded bolts. The three digit number indicates the grip length in millimetres, and the last two digits denote the test number. The failure modes are denoted TS for thread stripping and F for bolt failure. The force-displacement curves from the machine log are presented in Figures 4.5 - 4.11, and the replicate tests show excellent agreement.

As a measure of the components ductility, the external work is calculated up to the point of maximum loading by use of numerical integration, see Table 4.2. This is because the response of the tension loaded bolt would in reality be load driven rather than displacement driven which is the case in this laboratory work. A load driven response indicates that the fracture of the bolt will occur at the maximum applied loading.

From Table 4.2 and the plots of the force-displacement curves in Figures 4.5 - 4.11, the following is observed:

- There are no variations in the failure mode for tests of the same grip length.
- Thread stripping occurs only for partially threaded bolts with grip lengths of 122 mm or shorter. All other tests experienced bolt failure.
- The maximum force for each grip length varies less than 1.67% from the median value of the set.
- The average maximum force for partially threaded bolts with grip length 118 mm is 151.65 kN, while it is 140.59 kN for fully threaded bolts with the same grip length. This trend is also the case for the bolts with grip length of 141 mm.
- Although the maximum force in the fully threaded bolts is lower than for the partially threaded ones with the same grip length, the partially threaded bolts with grip length 141 mm can only absorb 35.90% of the energy that the fully threaded bolts. For the grip length 118 mm this ratio is 25.90%.
- The external work for each grip length varies less than 13.17% from the median value of the corresponding set. For 27 tests this variation is less than 5% of the median value.

Table 4.2: Results from laboratory tests

Test	Failure mode	$F_{t,Ed}$ [kN]	External work [Nm]
PT-118-01	TS	150.76	303.45
PT-118-02	TS	153.75	317.67
PT-118-03	TS	151.22	297.99
PT-118-04	TS	151.66	290.63
PT-118-05	TS	150.88	280.20
PT-122-18	TS	152.50	336.69
PT-122-19	TS	152.33	344.94
PT-122-20	TS	152.64	352.80
PT-122-21	TS	152.13	372.45
PT-122-22	TS	151.05	343.92
PT-124-16	F	153.16	370.52
PT-124-17	F	151.28	353.38
PT-130-11	F	148.67	420.83
PT-130-12	F	148.30	366.72
PT-130-13	F	150.22	371.87
PT-130-14	F	148.12	368.84
PT-130-15	F	149.41	376.13
PT-141-06	F	147.52	450.92
PT-141-07	F	146.39	454.00
PT-141-08	F	147.24	460.84
PT-141-09	F	147.38	437.31
PT-141-10	F	145.26	467.40
FT-118-23	F	140.50	1147.5
FT-118-24	F	140.74	1183.9
FT-118-25	F	140.53	1183.1
FT-118-26	F	141.23	1119.7
FT-118-27	F	139.95	1117.8
FT-141-28	F	140.43	1212.4
FT-141-29	F	140.09	1240.4
FT-141-30	F	140.79	1364.1
FT-141-31	F	140.38	1206.3
FT-141-32	F	141.18	1302.1

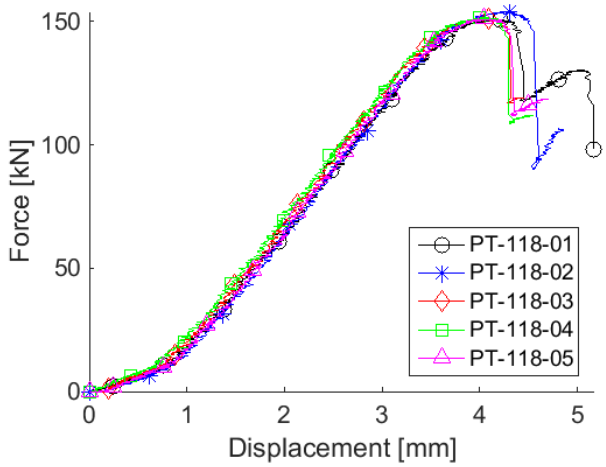

Figure 4.5: Partially threaded bolts, grip length 118 mm

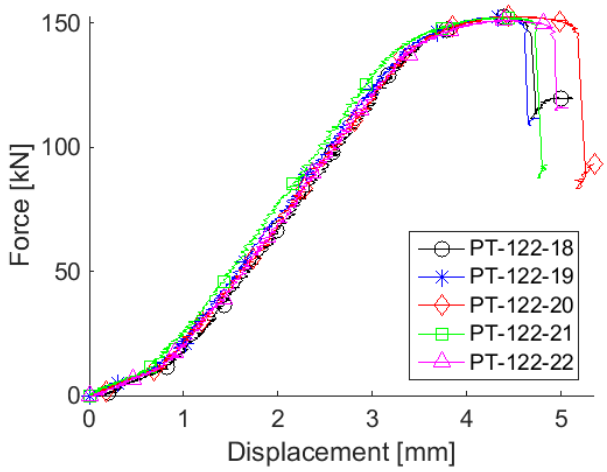

Figure 4.6: Partially threaded bolts, grip length 122 mm

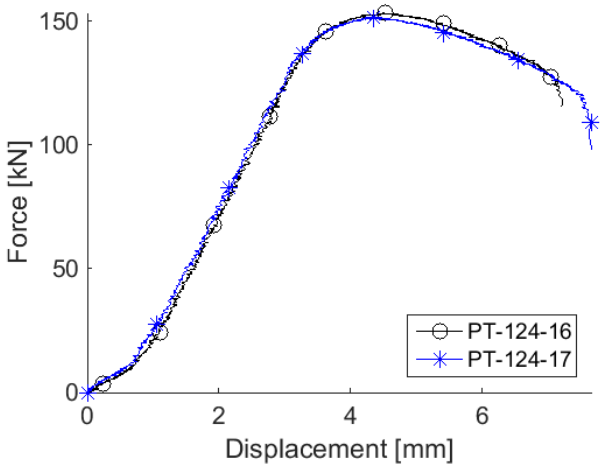

Figure 4.7: Partially threaded bolts, grip length 124 mm

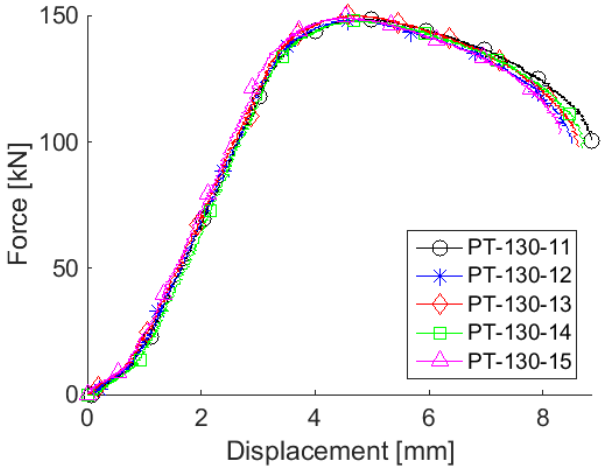

Figure 4.8: Partially threaded bolts, grip length 130 mm

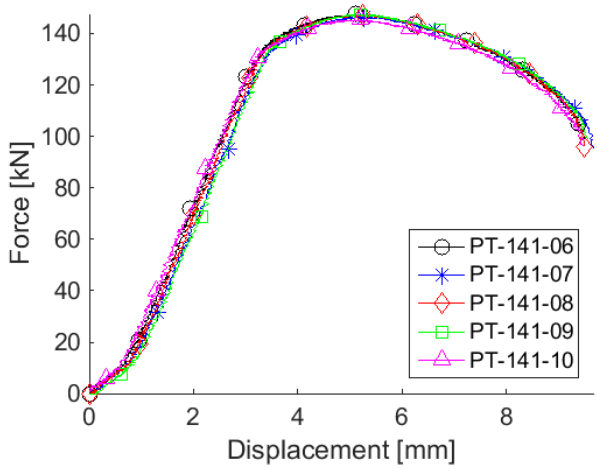

Figure 4.9: Partially threaded bolts, grip length 141 mm

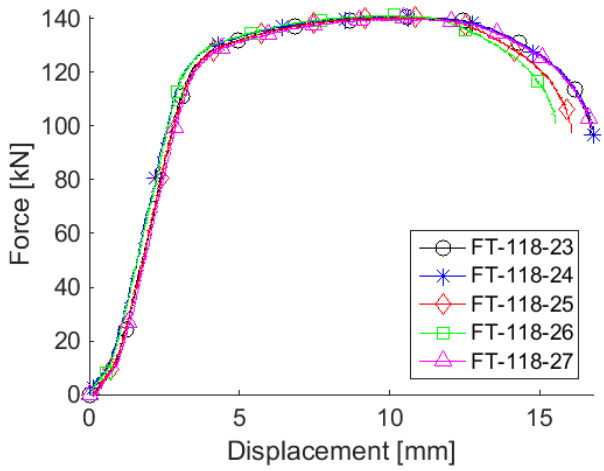

Figure 4.10: Fully threaded bolts, grip length 118 mm

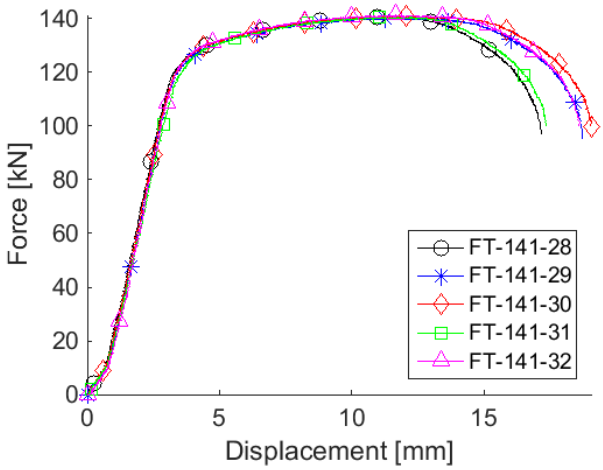

Figure 4.11: Fully threaded bolts, grip length 141 mm

4.5 Vickers Hardness test

Vickers hardness test is a commonly used method to determine the hardness in materials, particular in metals. The hardness number is determined by a known load over the surface area of the recess. In these tests, a load of 10 kgf was applied over a time period of 10 seconds. The tests have been preformed on a partially and fully threaded bolt, M16x160, and a nut M16. The tests were first cut in two, before they were sent to testing. As the hardness tests revealed a fairly constant hardness through the cross-section, the materials were assumed homogeneous in terms of material properties. Figures 4.12 and 4.13 show the test results, where Vickers numbers are presented below the indentation points.

Small variations within the material listed in Table 4.3, imply that the material properties will exhibit the same material within the cross-section. However, the hardness variation between the tested nut and the bolts is significant. Pursuant to Alexander [18] this might be an indicator for the behaviour observed at several of the bolt tests, which failed due to thread stripping. Owing to the small amount of performed tests, it is hard to say if this is a generally distinction of the nut hardness compared to the bolt.

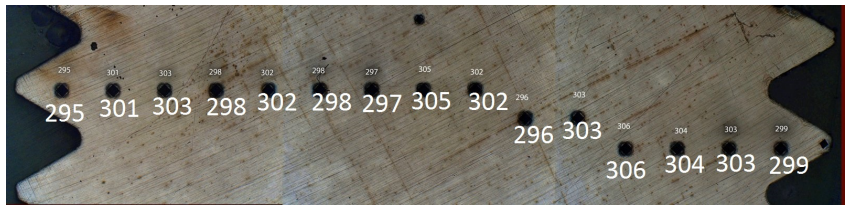

(a) Partially threaded bolt

(b) Fully threaded bolt

Figure 4.12: Vickers Hardness test on M16x160 bolts

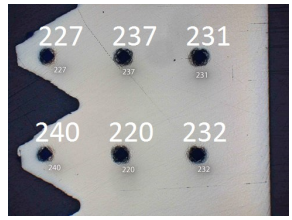

Figure 4.13: Vickers hardness test on nut M16

Table 4.3: Vickers Hardness test result

Test	PT bolt	FT bolt	Nut
Average hardness $[\frac{\text{kgf}}{\text{mm}^2}]$	301	293	231
Maximum derivation [%]	2.9	7.5	8.3
Nut hardness/Bolt hardness[%]	76.7	78.9	-

4.6 Discussions

An estimate of the tension resistance of a bolt, $F_{t,Rd}$, is given as [17]

$$F_{t,Rd} = \frac{k_2 f_{ub} A_s}{\gamma_{M2}} \tag{4.1}$$

where f_{ub} is the ultimate tensile strength, A_s is the tensile stress area of the bolt, γ_{M2} is a general partial factor and k_2 is an empirical factor. With $\gamma_{M2} = 1.25$ and $k_2 = 0.9$ the tension resistance of a M16 bolt with material properties 8.8 is calculated in Equation 4.2.

$$F_{t,Rd} = \frac{0.9 \cdot 800\text{N/mm}^2 \cdot 157\text{mm}^2}{1.25} = 90.43\text{kN} \tag{4.2}$$

The maximum tensile forces, $F_{\text{t,Ed}}$ registered during the laboratory work are presented in Table 4.2. All tests exceed the value calculated in Equation 4.2, indicating that NS-EN 1993-1-8 provides a conservative estimate of the tension resistance. This is mainly due to the fact that the yield stress of the material is found to be much higher than the nominal values provided. The material properties are presented in Chapter 5. In addition the general partial factor and empirical factors introduced in the design code reduce the nominal tension resistance further.

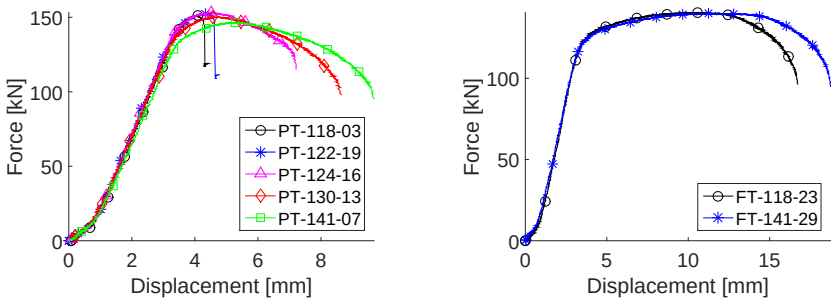

(a) Partially threaded (b) Fully threaded

Figure 4.14: Force-displacement curves for different grip lengths

Figure 4.14 displays the force-displacement curves for different grip lengths for partially and fully threaded bolts. It is clear that the increase in grip length of the partially threaded bolts changes the failure mode of the bolt. Shorter

grip lengths impose thread stripping. According to NS-EN 1090-2 [1], one full thread between the unthreaded part of the shank and the nut surface is enough to prevent thread stripping. Based on the experimental test in this thesis this requirement is not sufficient, since a grip length of 122 mm corresponds to at least three full threads between the unthreaded part of the shank and the nut.

The grip length of 124 mm differs only by one thread from the grip length of 122 mm, and both tests performed with this configurations failed due to bolt failure. This corresponds with the observations made by Alexander stating that the bolt breaking resistance is affected when the number of threads within the grip length is reduced, but the thread stripping resistance remains unchanged, which may cause the failure mode to change.

The calculated external work presented in Table 4.2 is graphically displayed in Figure 4.17 for each grip length configuration. The external work is far less for the partially threaded bolts than the fully threaded bolts with same grip lengths. In general larger grip lengths absorb more energy. This implies that the grip length affects the ductility of the bolt, which is observed in Figure 4.15, where the threads in the bolt with grip length 124mm is considerably deformed compared to the bolt with grip length 118mm. Figure 4.14 displays how the deformation of the bolt increases when the grip length is increased. This is the case for both partially and fully threaded bolts. When the grip length is increased, the length of the area subjected to strain increases. This implies that larger grip lengths are subjected to larger deformations when the strain remains unchanged.

Figure 4.15: Comparison between bolt tests with grip length 124mm and 118mm

Figure 4.16b displays how the number of threads included in the grip length influences the ductility additionally. The partially threaded bolts with grip length 141 mm can only absorb 35.90% of the energy absorbed by the fully threaded

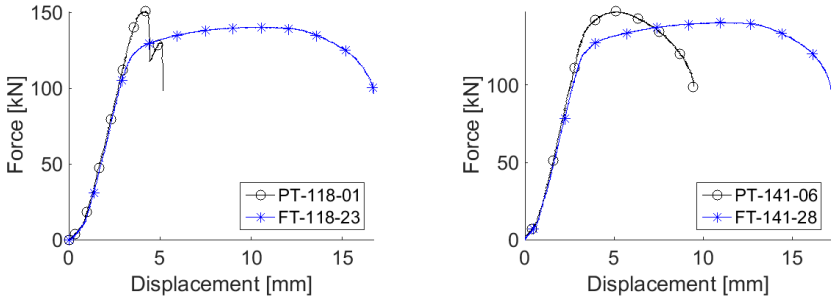

(a) Grip length 118 mm (b) Grip length 141 mm

Figure 4.16: Partially threaded and fully threaded bolts with same grip length

bolts with same grip length. Due to the difference in cross-sectional area of the partially threaded bolt, the unthreaded part of the shank will not yield. The part of the bolt subjected to plastic deformations is therefore reduced to the threaded part of the grip length only. This corresponds to 13 threads for the partially threaded bolt with grip length 141 mm, while the grip length equals 70 threads for the fully threaded bolt. The same principle as for the increased grip length applies, where an increase in length of threaded area implies larger deformations of the bolt.

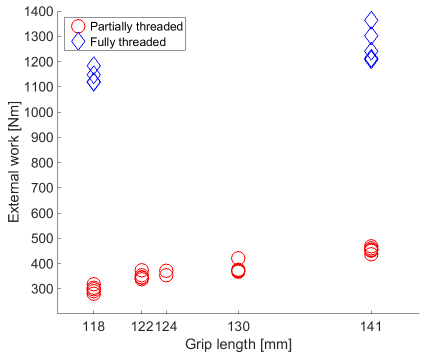

Figure 4.17: External work for each grip length

As described in Section 3.4, a variation of bolt and nut material properties will affect the failure mode. The results from Vickers Hardness test indicate that

the nut material is significantly weaker than the material of the fully and partially threaded bolts. However, more tests should be conducted to verify if this is a consistent feature.

The uncertainties regarding occurrence of thread stripping will be investigated by implementing a finite element model and conducting a parametric study. Based on observations stating that variation in maximum force and external work is fairly small for each grip length configuration it is decided to use the displacement calculated by using two dimensional DIC analysis as described in Section 4.3 to verify the physical response of the finite element model. The force-displacement curves from DIC analysis are displayed in Figures 4.18 and 4.19. Note that DIC was not used during tests PT-124-16 and PT-124-17, and therefore these are not investigated further. Also note that the grip length configuration of 118 mm for partially threaded bolts only has one curve for comparison because of problems with the DIC software. This should not be a problem since the curves in Figure 4.5 show good agreement.

The difference in slopes in the elastic region in Figures 4.18d and 4.19b verify that DIC analysis does not provide the accuracy needed to determine Young's modulus as discussed in Section 2.4.

The external work is recalculated for all tests that has undergone DIC analysis. This will exclude any contributions from the test machine. The results are presented in Table 4.4. The trends regarding ductility which have previously discussed also apply for these DIC results.

Table 4.4: External work calculated from DIC

Test id	External work [Nm]
PT-118-05	100.89
PT-122-21	162.96
PT-122-22	155.73
PT-130-14	187.70
PT-130-15	220.21
PT-141-09	228.55
PT-141-10	253.56
FT-118-26	868,00
FT-118-27	987,43
PT-141-31	1213,2
PT-141-32	1133,5

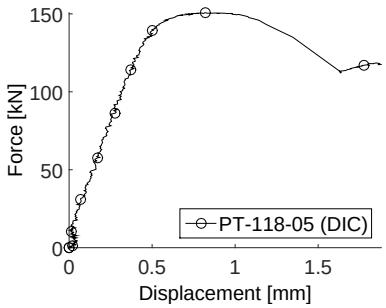

(a) Grip length 118 mm

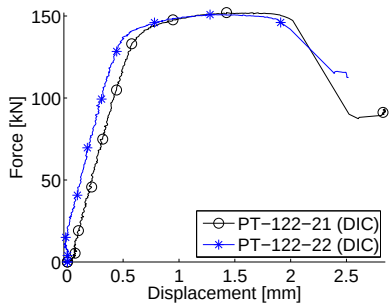

(b) Grip length 122 mm

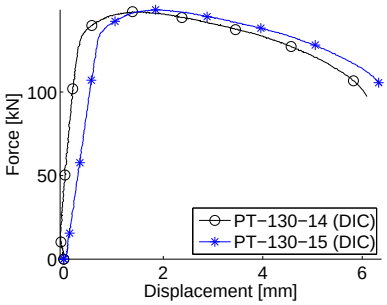

(c) Grip length 130 mm

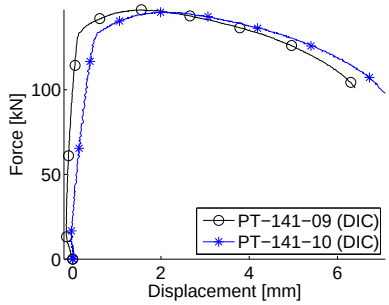

(d) Grip length 141 mm

Figure 4.18: Force-displacement curves from DIC-analyses for partially threaded bolts

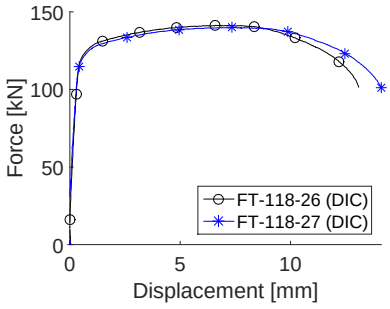

(a) Grip length 118 mm

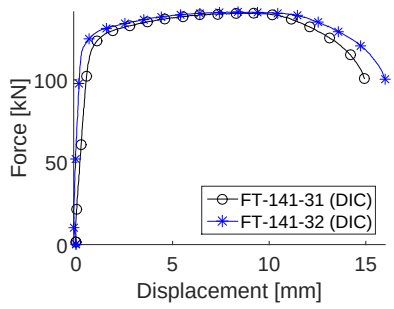

(b) Grip length 141 mm

Figure 4.19: Force-displacement curves from DIC-analyses for fully threaded bolts

5 Identification of material parameters

The foundation of the prescribed material behaviour is based on the force-displacement curve retrieved from the test machine and DIC in the laboratory. As material tests from the same batch have been carried out by students in course *TKT4511 Computational Mechanics Specialization Project*, fall'14, no further material tests are preformed. Three partially threaded and two fully threaded bolt material tests are taken into consideration when developing a suitable model. Figure 5.1 displays the results from the material tests, where small deviations of less than 3% are observed. Hence one material test from each test series is chosen as the initial material test.

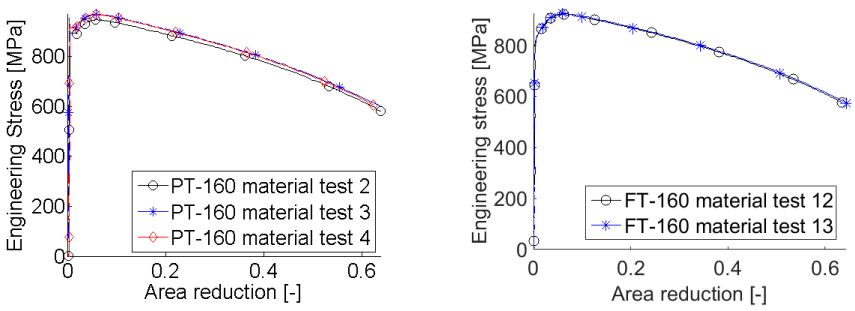

(a) Partially threaded

(b) Fully threaded

Figure 5.1: Stress-strain curves for material tests of M16x160 bolts

5.1 DIC

DIC is utilized to retrieve the strain from the material tests. The deformation is assumed axisymmetric, implying that one camera will give satisfactory description of the diameter elongation. With a frequency of 1 Hz, the amount of images throughout the test is considered to give a suitable foundation for tracking the movement. The strain vector is applied at the reference image at the same location where the neck later will initiate. With the identified diameter along the test series, the true cross-section is easily determined. A reference measure of the material tests makes it possible to convert the unit from pixel to millimetre. Figure 6.4 shows the vector elongation carried out using DIC.

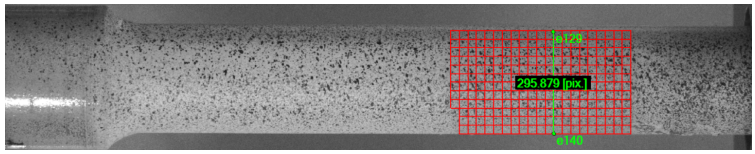

(a) Undeformed test specimen

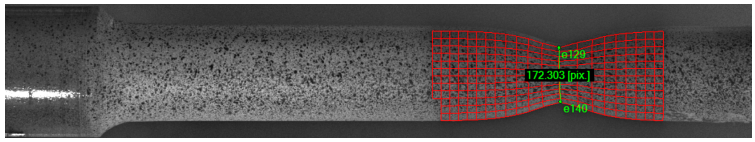

(b) Necking of test specimen

Figure 5.2: Elongation vector

5.2 Calibration of the material parameters

As described in Section 2.5, the data from the uniaxial tensile test are only valid until the specimen reaches its maximum load and diffuse necking occurs. In order to find an applicable description of the material behaviour beyond necking, isotropic hardening by Voce Rule has been utilized. Figure 5.3 shows the contribution of triaxial stress removed by Bridgman's correction method.

5.2.1 Material test simulations

To ensure that the defined material parameters describe the correct material behaviour in the numerical analyses, a finite element model of the tension test is

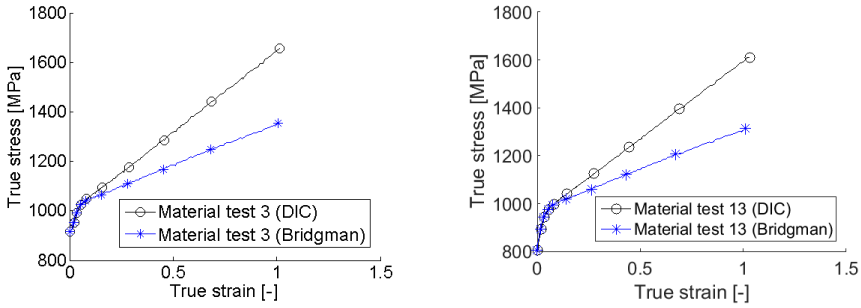

(a) Partially threaded bolt (b) Fully threaded bolt

Figure 5.3: Corrections of triaxial stresses

created. An iterative process is then performed, where the Voce material parameters are changed in attempt to achieve a behaviour similar to the one observed for the physical tests.

The FE models are based on the same assumptions as the initial models for the bolts presented in chapter 6, where an axisymmetric model is carried out, using explicit solver. Simlab Metal Model (SMM) has been used to describe the material properties. The failure criterion is not included at this stage.

Figure 5.4: FEM model for M16x160 material test

With final Voce parameters prescribed, the failure criterion could be defined. Cockcroft-Latham failure criterion have been utilized, where maximum principle stress and equivalent plastic strain are retrieved from the critical element at the neck region. Figure 5.5 shows the development of fracture, starting from the inner element. Cockcroft-Latham failure criterion was carried out for several element

sizes due to high mesh sensitivity.

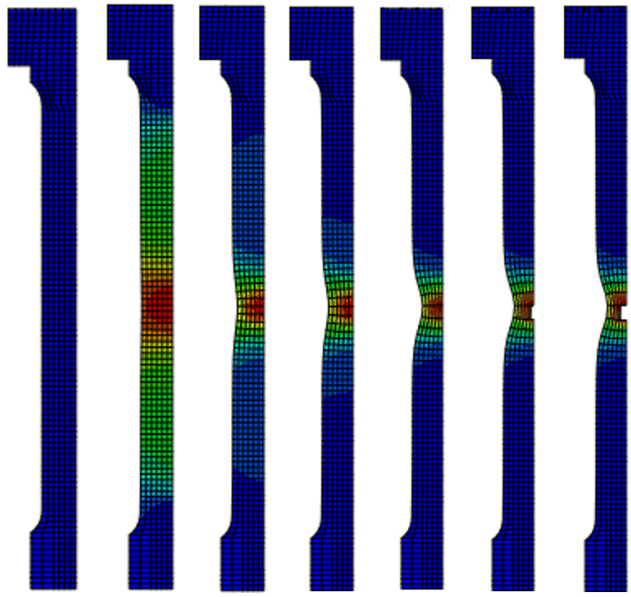

Figure 5.5: Propagation of fracture

5.2.2 Final material test simulation

Suitable material properties were determined after calibrations. Figure 5.6 shows the force-displacement curves for the final models, where the curves are plotted up to failure. The corresponding material properties are listed in Table 5.1.

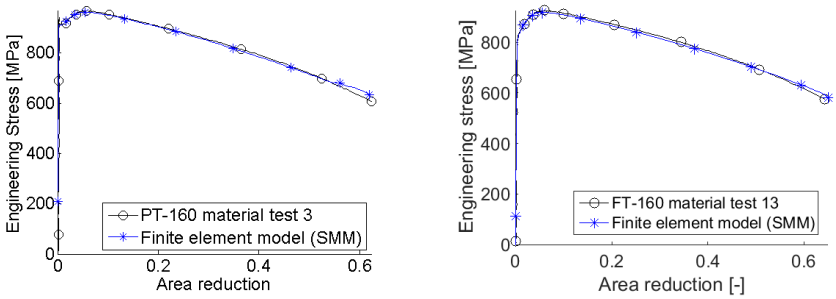

(a) Partially threaded (b) Fully threaded

Figure 5.6: Stress-strain curves for finite element models of material tests

Table 5.1: Material parameters for the M16x160 material tests

	Partially threaded	Fully threaded
σ_0 [MPa]	917.0	804.9
θ_1 [MPa]	7622	7125
$Q_{\mathrm{R},1}$ [MPa]	169.4	168.7
θ_2 [MPa]	$-1.000 \cdot 10^4$	280.6
$Q_{\mathrm{R},2}$ [MPa]	-68.47	4496
θ_3 [MPa]	303.7	-
$Q_{\mathrm{R},3}$ [MPa]	300.0	-
W_{cr} [MPa]	1475	1559

6 Finite element models

Finite element analyses have been performed to recreate the behaviour observed in the laboratory tests. With the use of Abaqus/Explicit, an explicit integration scheme is utilized. This is preferable owing to the main problem in the analyses, contact, which occurs in the threaded connection.

Due to time efficiency, the complex helix shape on the bolt has been considerable simplified in the finite element models. Instead of modelling a three-dimensional helix shaped bolt, an axisymmetric two-dimensional bolt model is utilized. From previous studies [2], this simplification has shown to give sufficient result compared to the three dimensional model.

Initial models have been created for both the partially and fully threaded bolt models. As the incorrect failure mode occurred in two of the partially threaded initial models, further investigations were performed to find the sensitivity related to the failure mode. Parameters concerning mesh, nut strength material and geometry have been considered.

6.1 Initial model

Six different initial models have been created to represent each configurations tested, i.e fully threaded (FT) bolts, with grip lengths 118mm and 141mm and partially threaded (PT) bolts with grip lengths 118mm, 122mm, 130mm and 141mm. All initial models are created based on the properties presented in the following sections. The materials used are presented in Chapter 5.

6.1.1 Geometry

The geometry of the bolt, M16x160 and nut M16 with property class 8.8, is based on ISO standards [28] [29] [30] combined with primary measurements of the bolts

and nuts at the laboratory. The geometry of the threads were modelled in accordance to ISO 68-1 [28] and ISO 965-1 [29]. Details regarding the dimensions are presented in Appendix B. Figure 6.1 displays the geometry of the fully threaded and partially threaded bolts utilized in the FE models.

(a) Partially threaded

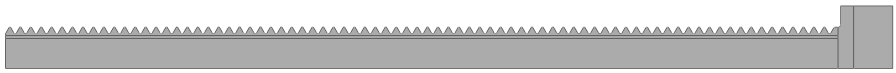

(b) Fully threaded

Figure 6.1: Initial geometry for bolt M16 x160

The outer diameter of the bolt and internal diameter of the nut are equal in each model to get a sufficient basis of comparison owing to the different grip lengths. Owing to the neglection of the helical shape, some adjustments had to be done to make it possible to achieve the desired grip length with correct number of threads in the axisymmetric model.

6.1.2 Mesh and element characteristics

The bolts and nuts are modelled with continuum axisymmetric 4-node reduced integration elements, CAX4R. As the models consist of complex geometry where

large loads are applied, the elements are expected to distort significantly. First order elements are therefore preferable over second order elements due to less sensitivity to distortion [16]. The reduced integration will reduce the computational time required. A concern using this element type is the appearance of hourglassing effects, which may cause unreliable results. Hourglassing implies that the element has no strain in bending as illustrated in Figure 6.2. This deformation is characterized as a zero-energy mode. Enhanced hourglass control can be used to limit problems caused by hourglassing. Artificial strain energy induces the energy stored in hourglassing resistance and transverse shear in the elements [31]. It is therefore important to check that the artificial strain energy is low compared to the internal energy of the system.

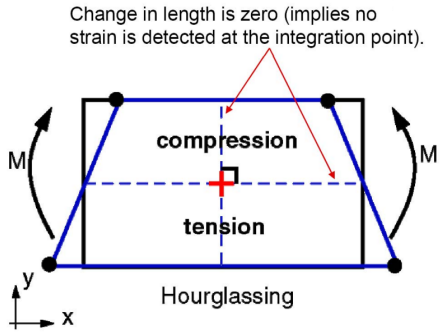

Figure 6.2: Bending behaviour for single first-order reduced integration element [16]

The initial models consist of varying element sizes. To intercept the divergence of the behaviour at the contact area, the element size at the threaded connection is given a finer mesh compared to the shank and the outer part of the nut.

Table 6.1 gives an overview of the element sizes in the initial models for FT and PT bolt models. As the partially threaded bolt models will be prioritized in further investigations, a coarser mesh has been applied to limit the computation time. The same element size is utilized in the threads in both the bolt and the nut, this is referred to as local mesh size in Table 6.1. Analogous, the global mesh indicates the mesh in the shank of the bolt and the outer part of the nut. The elements are approximately quadratic, with same element size in both directions. Figure 6.3 shows the distinction between the local and global element size in the bolt and nut.

Table 6.1: Element sizes utilized in the initial models

Part	Element size [mm]
Local mesh on PT bolts	0.2
Global mesh on PT bolts	1.0
Local mesh on FT bolts	0.2
Global mesh on FT bolts	0.5

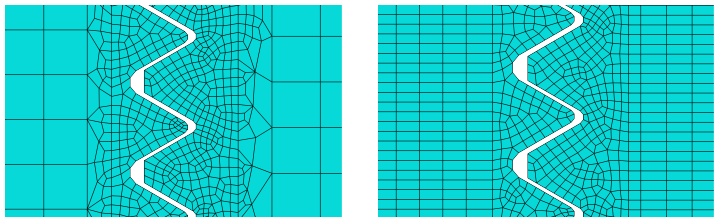

(a) PT bolt models (b) FT bolt models

Figure 6.3: Initial mesh selection

6.1.3 Boundary conditions

Figure 6.4 displays the boundary conditions, where the fixed boundary condition and force are implicated as triangles and arrows. As described in Chapter 4, the physical tests were loaded at the bolt head, and withheld at the nut. To recreate the scenario in the finite element models, boundary conditions are applied. At the top surface of the nut, a boundary condition is inserted to prevent the nut from moving in vertical direction, where a velocity is applied at the bottom of the bolt head.

6.1.4 Interactions

The surface-to-surface approach has been implemented in the interaction between the nut and the bolt. The surface-to-surface contact involves two specified predetermined surfaces, described as master and slave surface. As distinct from the master surface, the slave surface allows penetration. Hence, the choice of slave and master surface depends on the mesh size, where the master surface contains finer mesh. As similar sized elements have been chosen in the threads for both the bolt and the nut, the choice of master surface is assumed not to affect the

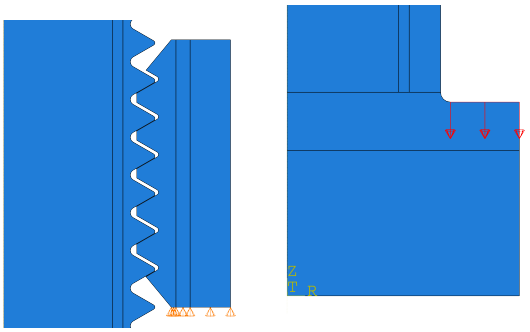

(a) Fixed nut

(b) Applied load at bolt head

Figure 6.4: Applied boundary conditions

behaviour in the finite element models.

Surface-to-surface contact between the nut and the bolt is implemented with two interaction properties, tangential and normal behaviour. The tangential behaviour is employed using the penalty algorithm with finite sliding. Penalty method is the default method for the finite sliding with surface-to-surface approach in Abaqus/Explicit. Finite sliding is favourable since it allows arbitrarily large motion between the interacting surfaces [32]. According to the NS-EN 1090-2 [1], the friction coefficient for rolled surfaces is 0.2. This is assumed to represent the tested bolts. "Hard" contact was chosen for the normal behaviour, which prevents large penetration of the surfaces.

6.1.5 Computational efficiency

To obtain an computationally efficient quasi-static solution in Abaqus/Explicit, the load rate has been increased. This requires less time increments, which leads to a lower computational cost. A velocity of 500mm/s for the partially threaded bolts and 250mm/s for the fully threaded bolts are found not to cause inertia forces.

The default in Abaqus/Explicit apply loads immediately, and remains constant throughout the step. Instant loading may induce a propagation of stress wave, which may produce undesired results [33]. To minimize these adverse effects, smooth step amplitude curve is employed. This implies a ramping up of the

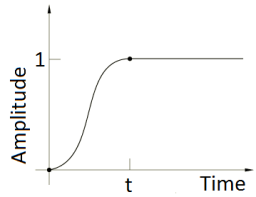

Figure 6.5: Amplitude of smooth step

load, from zero to full load, during time t, as described in Figure 6.5. A smooth step with $t = 0.05 \cdot T$ is utilized in the analyses, where T is the total time period of the analyses.

6.1.6 Result of the Initial Models

All the initial models are implemented with the same properties discussed. Figure 6.6 shows the force-displacement curves, where the initial FE models are compared with the corresponding experimental results.

The maximum tensile forces, $F_{\mathrm{t,Ed}}$, and the external work of the initial FE models are compared with average values from DIC in Table 6.2.

Table 6.2: Results for the initial FE models

Model	$F_{\mathrm{t,Ed}}$ [kN]	Deviation DIC average [kN]	Deviation DIC average [%]	External work [Nm]	Deviation DIC average [Nm]	Deviation DIC average [%]
PT-118	167.97	17.2	11.4	181.29	80.41	79.70
PT-122	162.67	11.2	7.37	183.89	24.54	15.40
PT-130	156.49	7.94	5.35	233.59	29.64	14.53
PT-141	153.34	7.09	4.85	272.68	13.12	13.12
FT-118	145.88	4.88	3.35	1007.9	80.21	7.960
FT-141	145.45	4.59	3.16	1171.2	2.130	0.182

From Figure 6.6 and Table 6.2 the following observations are made:

- A generally good accordance is observed in stiffness between the FE models and the laboratory tests.

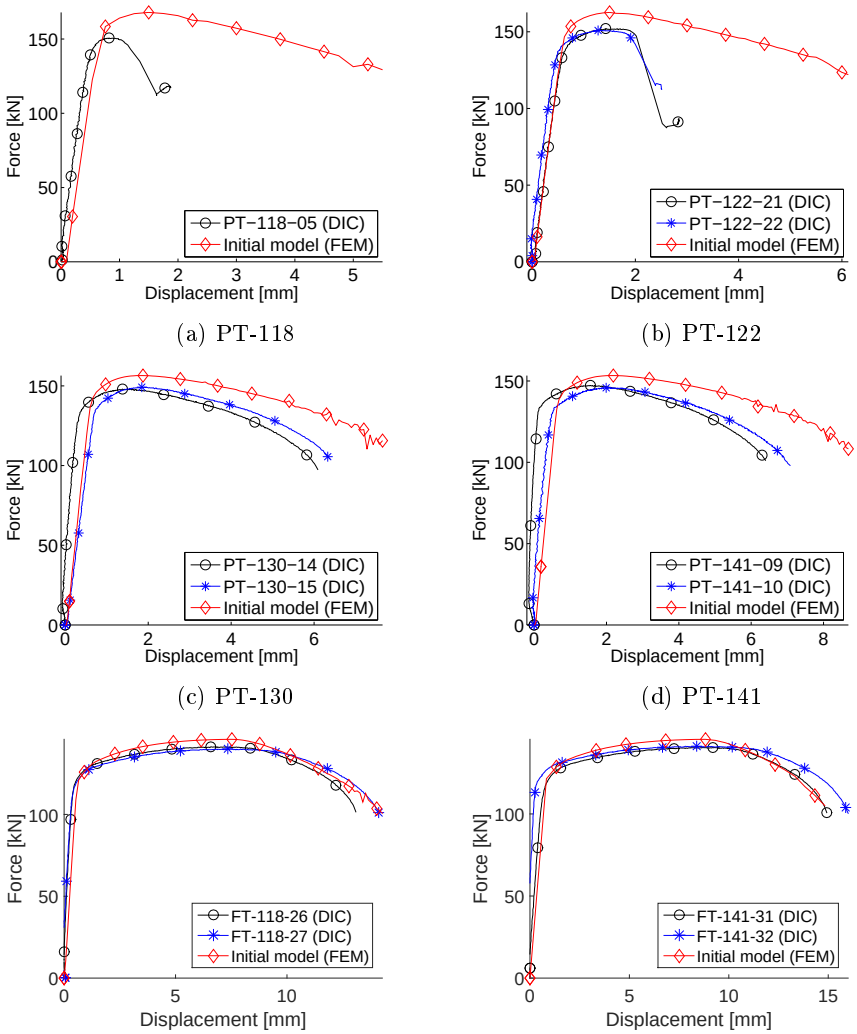

(a) PT-118 (b) PT-122

(c) PT-130 (d) PT-141

(e) FT-118 (f) FT-141

Figure 6.6: Force-displacement curves for the initial FE models

- A higher load level is present in the FE models. From Table 6.2 it is observed less deviation as the number of threads in the grip length increases. The maximum deviation is registered for PT-118 with a deviation of 11.4%, whereas a deviation of 3.16% is observed for the FT-141.

- Noise is observed at the final stage in the numerical simulations. This is due to the small elements at the root of the threads, which will reach the prescribed fracture stress, before bolt failure occurs.
- The physical behaviour of the fully threaded bolts is well represented in the FE models. However, a stiffer behaviour is observed among the partially threaded bolt models, where fracture initiates at a later stage.
- Bolt failure occurred in all FE models. This differ from the experiental tests, where thread stripping occurred in the partially threaded bolt tests with grip lengths 118mm and 122mm.

6.2 Parametric study

Due to deviation between the experiments and the initial FE models, it is of interest to identify what parameters may influence the failure mode of the FE models. The failure mode, thread stripping, which occurred in the PT bolts with grip lengths 118mm and 122mm, has not been recreated in the initial models. This is of specific interest, and will provide guidelines for further work. Investigations concerning fully threaded FE models, will therefore not be prioritized, as the behaviour of the initial models is considered accurate enough. Closer investigations will be performed with regards to the variation of nut geometry and strength, as well as a sensitivity study due to the mesh refinement.

6.2.1 Validation of nut strength material

As described in Chapter 4, the hardness of the nut, tested by Vickers Hardness test, is approximately 76% compared to the fully and partially threaded bolts. Due to the limited number of tests performed, it is difficult to say if this reflects the true situation. However, it is of interest to study if a reduction in material strength may influence the behaviour of the bolts, since reduced nut material provokes thread stripping according to Alexander [18]. A study have been carried out, where the yield stress of the nut was reduced by 10%, 15%, 20% and 25% of the yield stress of the bolt.

Figure 6.7 displays the effect of reducing the nut strength by force-displacement curves from the analyses. The study involves partially threaded bolt models with grip lengths 118mm, 122mm, 130mm and 141mm. Nut strength reduction is denoted NSR, where the two digit number describes the reduction of the yield stress. Tables 6.3 - Table 6.6 presents the observed forces and calculated external

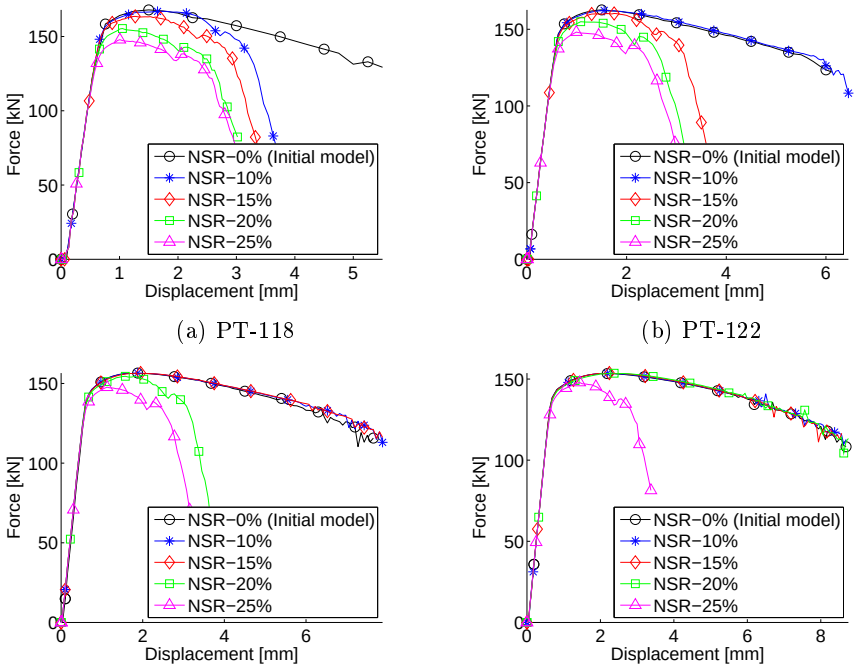

(a) PT-118

(b) PT-122

(c) PT-130

(d) PT-141

Figure 6.7: Force-displacement curves for the partially threaded FE models with reduced nut strength

Table 6.3: Results for test PT-118 with reduced nut strength

Model	$F_{t,Ed}$ [kN]	Deviation DIC average [kN]	Deviation DIC average [%]	External work [Nm]	Deviation DIC average [Nm]	Deviation DIC average [%]
Initial-0%	167.97	17.17	11.39	181.29	80.41	79.70
NSR-10%	166.94	16.14	10.70	206.12	105.2	104.3
NSR-15%	163.57	12.77	8.468	141.49	40.60	40.25
NSR-20%	155.37	4.570	3.031	102.98	2.092	2.073
NSR-25%	147.91	-2.890	1.916	93.392	-7.495	7.429

Table 6.4: Results for test PT-122 with reduced nut strength

Model	$F_{t,Ed}$ [kN]	Deviation DIC average [kN]	Deviation DIC average [%]	External work [Nm]	Deviation DIC average [Nm]	Deviation DIC average [%]
Initial-0%	162.67	17.18	7.38	183.90	24.54	15.40
NSR-10%	162.31	10.82	7.142	191.58	32.32	20.23
NSR-15%	160.30	18.81	5.816	221.91	62.56	39.26
NSR-20%	154.93	3.440	2.271	113.24	-46.10	28.93
NSR-25%	148.17	-23.32	12.19	96.950	-62.40	39.16

work for each grip length.

As predicted, the reduction in nut strength has a large impact on the failure mode. The models with small grip lengths appear to be more sensitive to nut strength reduction compared to models with larger grip lengths. Thread stripping occurred for all tested PT-118 in comparison to PT-141, where only a reduction of 25% ended with thread stripping. The changed failure mode affects the load capacity. With a nut reduction of 15%, thread stripping initiated in PT-118 and PT-122, in comparison to PT-130 and PT-141 where bolt failure occurred. This is in accordance to the failure modes observed in the laboratory tests.

From the laboratory work, internal and external thread stripping are considered as one failure mode. In this parametric study, the internal threads failed first. This is observed in Figure 6.8 which displays the course of events for FE simulation PT-118-NSR-15%.

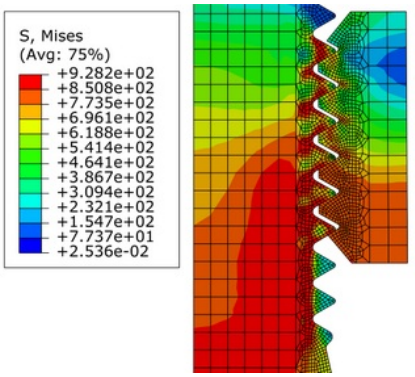

(a) At displacement 0.656mm

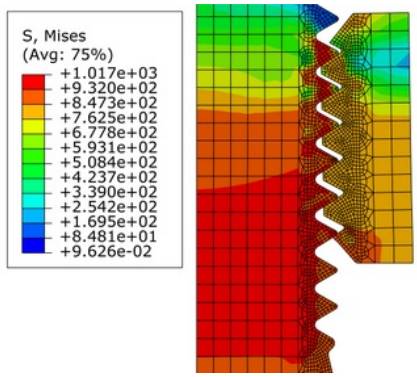

(b) At displacement 1.094mm

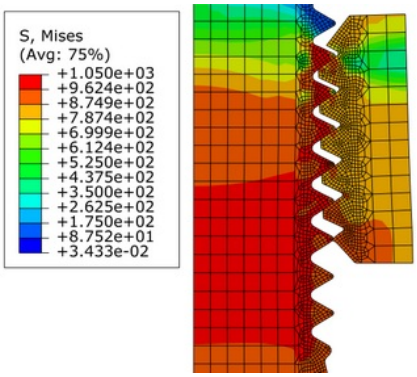

(c) At displacement 1.531mm

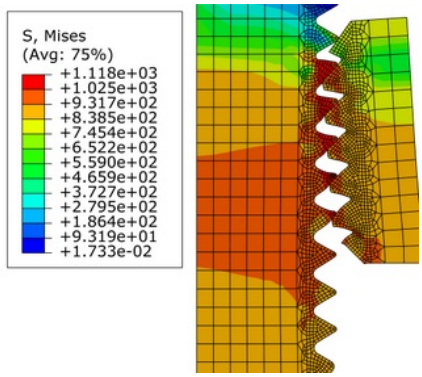

(d) At displacement 2.406mm

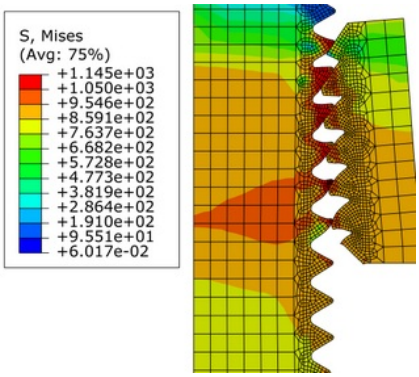

(e) At displacement 2.844mm

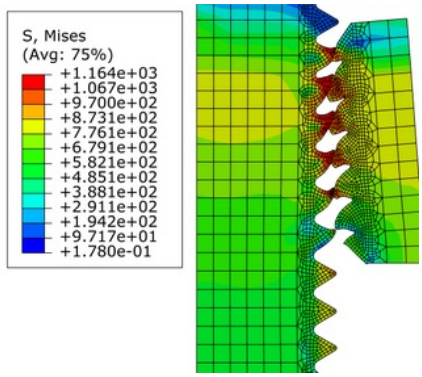

(f) At displacement 3.281mm

Figure 6.8: Deformation propagation through the PT-118-NSR-15% analysis

Table 6.5: Results for test PT-130 with reduced nut strength

Model	$F_{t,Ed}$ [kN]	Deviation DIC average [kN]	Deviation DIC average [%]	External work [Nm]	Deviation DIC average [Nm]	Deviation DIC average [%]
Initial-0%	156.49	7.88	5.30	233.59	29.64	14.53
NSR-10%	156.54	7.92	5.33	236.20	32.25	20.53
NSR-15%	156.53	7.91	5.33	247.71	43.75	11.10
NSR-20%	154.46	5.85	3.93	187.41	-16.54	8.83
NSR-25%	147.64	-0.98	0.66	116.50	-87.45	75.07

Table 6.6: Results for test PT-141 with reduced nut strength

Model	$F_{t,Ed}$ [kN]	Deviation DIC average [kN]	Deviation DIC average [%]	External work [Nm]	Deviation DIC average [Nm]	Deviation DIC average [%]
Initial-0%	153.34	6.79	4.63	272.68	31.62	13.12
NSR-10%	153.46	6.91	4.72	272.38	31.32	12.99
NSR-15%	153.69	7.14	4.87	280.98	39.92	16.56
NSR-20%	153.54	6.99	4.77	299.80	58.74	24.37
NSR-25%	147.85	1.3	0.89	155.25	-85.81	35.60

6.2.2 Validation of the threaded geometry

To improve the threaded geometry, one partially threaded and one fully threaded bolt, and one nut have been cut in two for further examination. Figure 6.9b displays the inspected components, where the investigated bolts were in good accordance with the predicted geometry calculated from ISO 68-1 [28]. However, it was observed that the nut geometry differ from the assumed geometry presented in the initial model, since the four outer threads are shorter compared with the inner threads. The detailed measurements found from the inspections are presented in Appendix C. Based on these measurements, the average height of the second outer threads, T2 and T6, in Figure 6.10, were measured to be 78.0% of the full height, while the lowest height was measured to be only 71.7% of the full height.

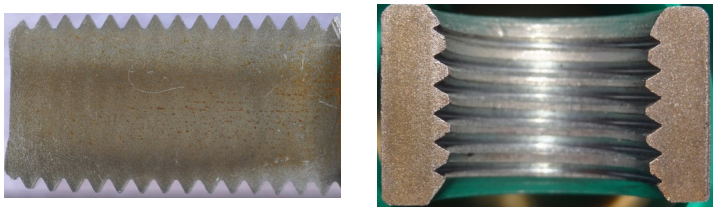

(a) Bolt cut in half (b) Nut cut in half

Figure 6.9: Investigated thread geometry

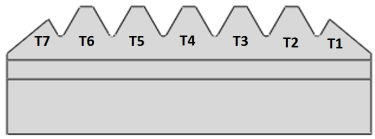

Figure 6.10: Internal threads

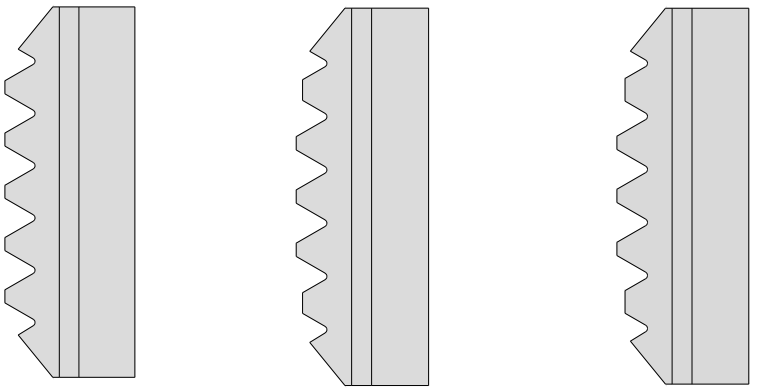

(a) Nut 0 (b) Nut 1 (c) Nut 2

Figure 6.11: Tested nut geometries

With reduced height of the initial threads, the shear area decreases, which may trigger thread stripping. Different nut geometries, regarding thread height of second outer threads, have been studied. Figure 6.11 illustrates the geometry of the tested nuts, where *Nut 0* refers to the initial model with full height of

second outer threads, in contrast to *Nut 1* and *Nut 2*, with corresponding thread heights of 78% and 71.7% of the initial height.

Figure 6.12 shows force-displacement curves of the tested geometries in both partially and fully threaded bolt FE models.

Despite test PT-118, the change in nut geometry does not appear to have any influence on the physical behaviour and failure mode in the FE models. Necking initiates in all the FE models, although thread stripping was the decisive failure mode in PT-118. From Figure 6.13, which shows the deformation propagation for FE simulation PT-118-Nut 1, necking initiates in the threaded part. This leads to slippage in two of the bearing threads, which results in thread stripping. As the grip length increased, the neck developed farther away from the threaded connection, and no slip between the threads were registered.

6.2.3 Mesh sensitivity

The initial FE models for the partially threaded bolts were modelled with coarser mesh due to required computational time. This resulted in a stiffer behaviour and a higher load level, compared to the experiments. A study has been carried out to clarify the sensitivity due to mesh refinement. As defined in the initial model, the local mesh refers to the threaded part, while the global mesh refers to the shank and the outer part of the nut. Table 6.7 describes the preselected element sizes of the models, where the size is approximately the same in both directions.

Table 6.7: Element sizes

Part	Coarse [mm] (initial)	Medium [mm]	Fine [mm]
Local mesh	0.2	0.1	0.1
Global mesh	1.0	0.5	0.3

Figure 6.14 displays the force-displacement curve for the mesh sensitivity study of the partially threaded bolt models. The mesh refinement has a significant impact of the hardening in the FE models. The hardening is considerable reduced beyond necking when a finer mesh is applied. Although mesh refinement requires more computational time, the improvement of the response is prioritized over computational efficiency. A slight reduction of 1-2% of the maximum load

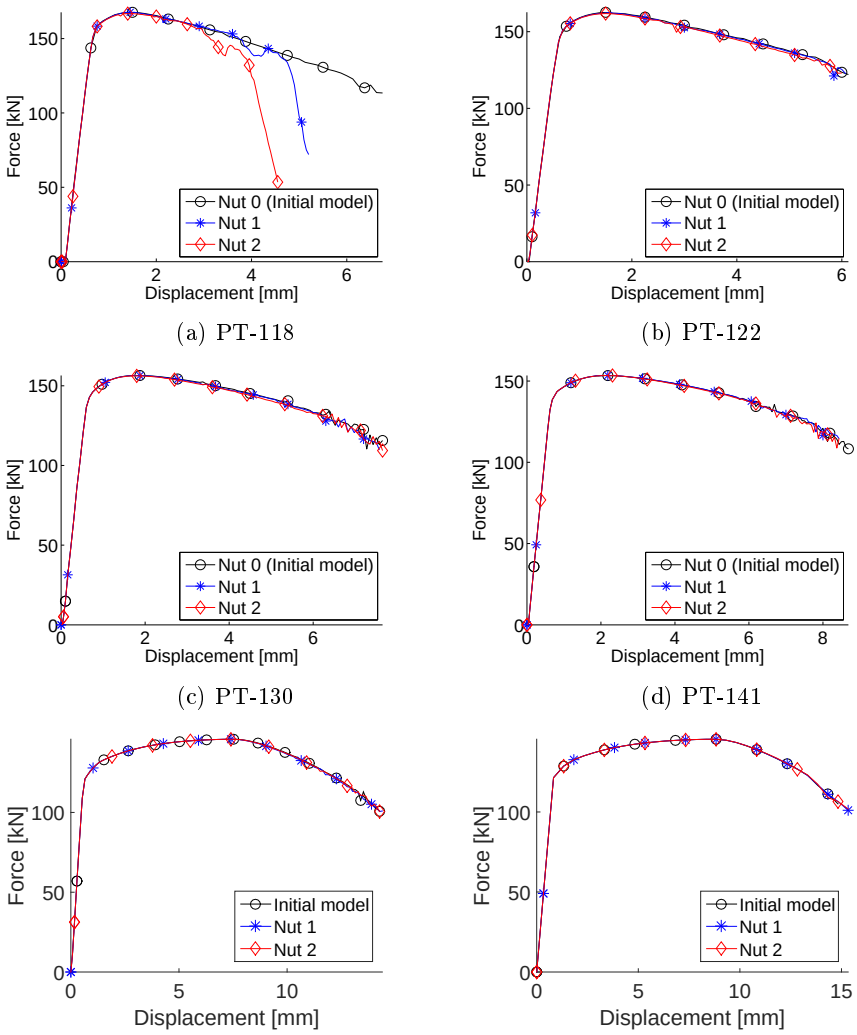

(a) PT-118 (b) PT-122

(c) PT-130 (d) PT-141

(e) FT-118 (f) FT-141

Figure 6.12: Force-displacement curves for the FE models with reduced thread height in the nut

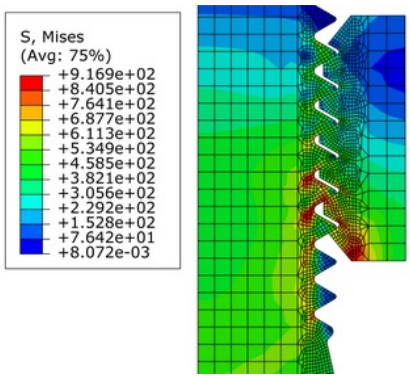

(a) At displacement 0.415mm

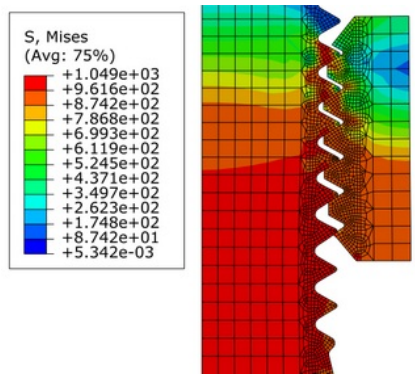

(b) Maximum force at displacement 1.450mm

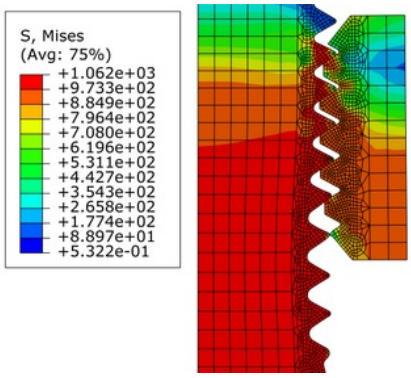

(c) Slip in first thread, $u = 2.15mm$

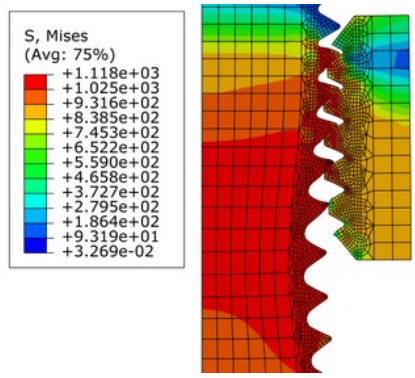

(d) Slip in second thread at displacement 3.80mm

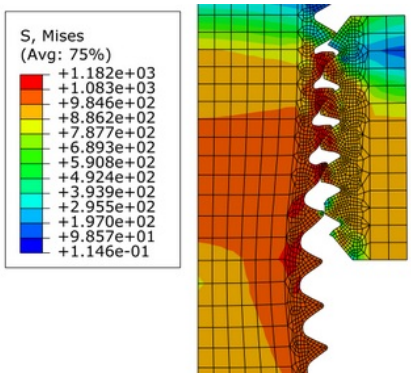

(e) Nut connect with new thread at displacement 4.3mm

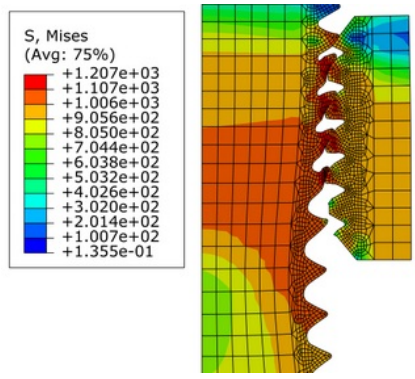

(f) Drop in load at displacement 4.8mm

Figure 6.13: Deformation propagation through the PT-118-Nut1 analysis

is registered with refined mesh.

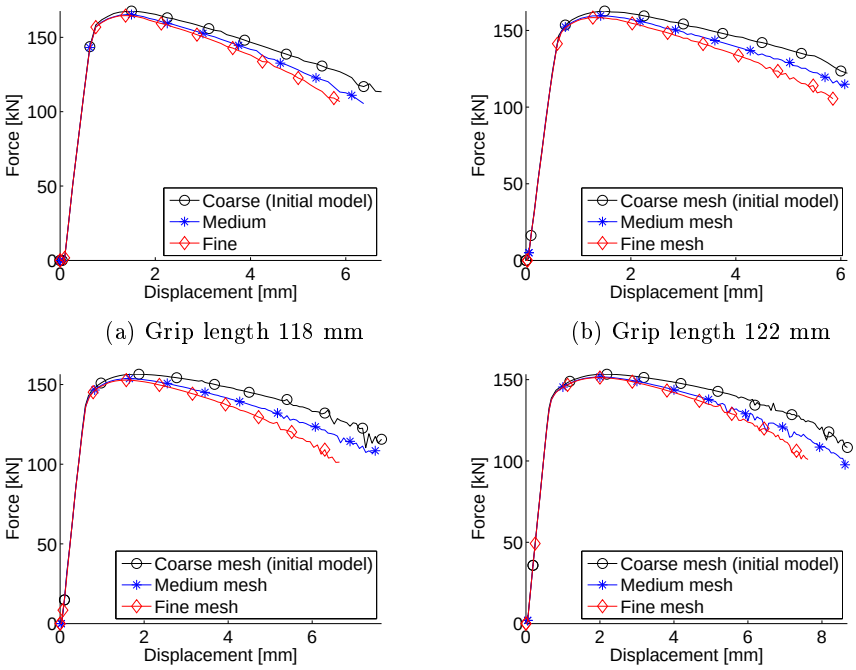

(a) Grip length 118 mm

(b) Grip length 122 mm

(c) Grip length 130 mm

(d) Grip length 141 mm

Figure 6.14: Force-displacement curves for mesh study

6.2.4 Final model

Some of the sensitive parameters of the initial finite element model have been identified in the parametric study. Based on these results, the final models have been created. Table 6.8 specifies the chosen parameters implemented in the final models. As the studied parameter for fully threaded bolt models show insignificant effect, the results retrieved from the initial models persist. As for the partially threaded bolt models, the average nut geometry, Nut 1, have been utilized with nut strength reduction of 15%. Nut 1 reflects the measured geometry more adequately, which affected the failure mode for PT-118. Nut strength reduction of 15% yielded the same failure mode in all the partially threaded bolt models

Table 6.8: Final parameters for FE models

FE model	Nut strength reduction	Thread geometry	Mesh refinement
PT-118	NSR-15%	Nut 1	Fine
PT-122	NSR-15%	Nut 1	Fine
PT-130	NSR-15%	Nut 1	Fine
PT-141	NSR-15%	Nut 1	Fine
FT-118	Initial model-0%	Nut 0	Initial
FT-141	Initial model-0%	Nut 0	Initial

as observed in the laboratory work. Although finer mesh gave a increase in CPU time, the behaviour was considerable improved when it was applied.

The final results are presented in Figure 6.15, where the force-displacement curves for the final models are compared with the laboratory results retrieved from DIC. Table 6.9 presents the tensile forces $F_{\mathrm{t,Ed}}$ and the external work calculated, and presents deviations from the average values from the DIC analyses.

Table 6.9: Final FE models

Model	$F_{\mathrm{t,Ed}}$ [kN]	Deviation DIC average [kN]	Deviation DIC average [%]	External work [Nm]	Deviation DIC average [Nm]	Deviation DIC average [%]
PT-118	158.78	7.98	5.29	116.11	15.23	15.09
PT-122	156.37	4.88	3.22	157.31	-2.04	1.28
PT-130	152.61	3.10	2.69	190.38	-13.57	6.65
PT-141	151.08	4.53	3.09	250.15	9.09	3.77
FT-118	145.88	4.88	3.35	1007.9	80.21	7.96
FT-141	145.45	4.59	3.16	1171.22	2.13	0.182

A generally good accordance is observed between the numerical and the experimental results, where the correct failure mode occurs in the numerical models, viz. thread stripping in the partially threaded models PT-118 and PT-122, and bolt failure the partially threaded models PT-130 and PT-141 and fully threaded models FT-118 and FT-141.

Despite an increase in maximum load, which was observed in all the finite models, the material seems to capture the behaviour registered in the laboratory

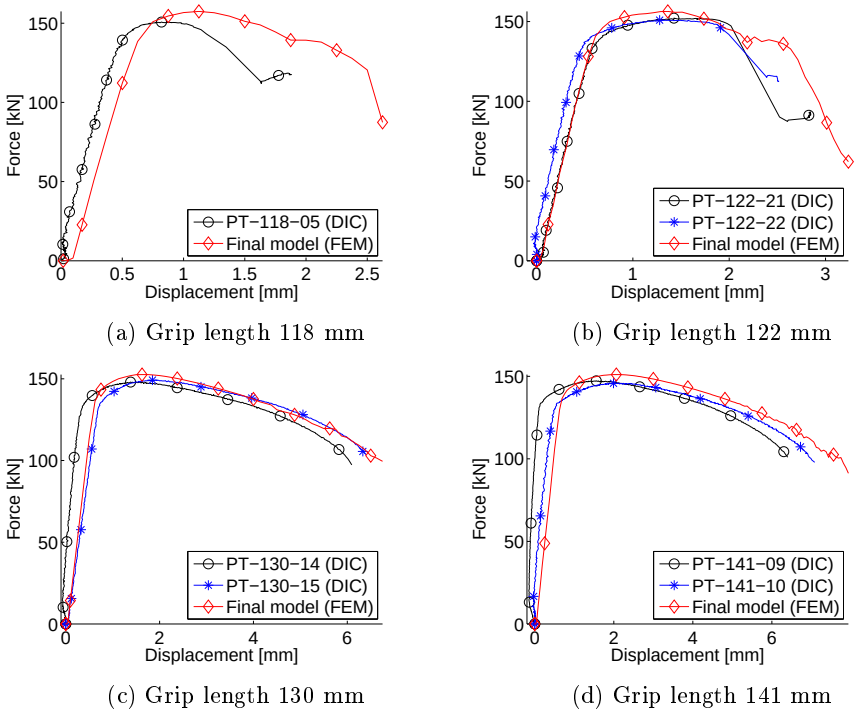

(a) Grip length 118 mm

(b) Grip length 122 mm

(c) Grip length 130 mm

(d) Grip length 141 mm

Figure 6.15: Force-displacement curves for final models of partially threaded bolts

tests. This mainly applies to the fully threaded models, where larger deviation is registered for the partially threaded bolts. Especially PT-118 model, where largest deviation in maximum force is found to be 5.29% and 15.23% for external work. This is due to a stiffer behaviour, where maximum force occurs at a larger displacement. The external work is in good accordance to the external work calculated for the laboratory tests, presented in Section 4.4.

7 Discussions

This chapter includes evaluation of the experimental and numerical results, which will further be compared with analytical results based on calculations retrieved from NS-EN 1993-1-8 [17]. The main features of this part of the project will be presented, where possible errors will be highlighted.

7.1 Load capacity

The numerical simulations presented in Section 6.2.4 show that the overall physical behaviour is captured with a reasonable accuracy, where the desired failure modes were successfully recreated. The maximum load deviation is less than 5.29% for the simulations which generate thread stripping, i.e. PT-118 and PT-122, and less than 3.09% for simulations which ended in bolt failure.

A higher maximum load is registered in all the numerical simulations compared to the load level observed in the laboratory work. From Chen et al. [2] and Fransplass et al. [4] a similar tendency is observed by the use of axisymmetric elements. As distinct from a three dimensional model, the axisymmetric model will not be able to recreate the helical threads. This simplified geometry may cause a stiffer behaviour.

The dimensions may also affect the load capacity. The measurements carried out from the laboratory tests, show a small variance due to bolt and nut diameter, while the numerical simulations were carried out using the average dimensions measured. According to Equation 4.1, the load capacity will decrease if the bolt diameter is reduced.

7.2 Sensitive parameters

As the initial models for PT-118 and PT-122 failed to recreate the desired failure mode, some of the sensitive parameters related to thread stripping were investigated. As predicted, distinctions in nut geometry and material affect the failure mode. It was further observed that the simulations with a low number of threads in the grip length were particularly sensitive. This is in accordance with the theory derived by Alexander [18] and the observations in the laboratory work.

A nut geometry study was carried out, where the thread height of the second outer threads were significantly reduced, in accordance to measurements of the cut nut. These results show that only the PT-118 analyses were affected, where the remaining simulations showed insignificant variance compared to results carried out for the initial models. With few threads in the grip length, the neck initiates close to the nut, which results in a reduction of the shear surface. This leads to a higher load concentration on the threaded assembly, where thread stripping is provoked.

Based on the results from Vickers Hardness test, a considerable deviation in hardness of the tested nut and bolts was registered. The nut hardness was measured to be 76.7% of the partially threaded bolt and 78.9% of the fully threaded bolt. Several factors may influence the differences registered between the bolts and the nut, where chemical composition, fabrication of the threaded part and temperature during processing have an impact. The simulations were implemented with a reduced yield stress in the nut material, to account for the reduced hardness that was observed. This mainly resulted in plastic deformations in the nut, in form of bending, which reduced the shear area. The finite element analyses were greatly affected by the nut strength reduction, where all the partially threaded configuration resulted in internal thread stripping, with the corresponding nut strength reduction measured from Vickers hardness test. A reduction of 15% however, was found suitable to recreate the failure modes observed in the experimental results. With only one examined nut by Vickers hardness test, it is difficult to conclude what nut strength is reasonable.

The use of an axisymmetric model may also affect the failure mode, as a centric position of the bolt in the nut is predetermined. This will give a uneven load distribution on the threads, which may lead to thread stripping, especially if the gap between the threads is of significance.

7.3 Thread stripping comparisons

As the threaded connection was wedged together in the experiments, it was hard to identify the initiate failure in thread stripping, whether it was in the internal or external threads. The nut was pulled off in an attempt to identify the thread failure. Figure 7.1 shows the initial and final observation of a PT-118 test. From closer examination of the bolt, bolt thread failure seem to be the decisive failure mode. However, uncertainties are related to this method, as the initial thread failure is not determined, and the required force to pull off the nut may influence the observed thread failure.

Figure 7.1: Observed thread stripping for test PT-118-01

The deformation propagation of the final model PT-118 is displayed in Figure 7.2. Similar to PT-122, external thread stripping was decisive. As predicted, the initial contribution of stress concentrates on the threads closest to the bearing surface, before spreading out. At displacement $1.125mm$ maximum load is reached, and the stress distribution congregates at the threads, which eventually fails in external thread stripping. This was also the determining failure mode in the numerical analyses carried out in Kolberg and Willand's master thesis [34], where they studied bolted connectors in road safety barriers. Similar failure

modes was also observed in the work presented by of Fransplass et al. [35], where different thread run-out combinations were studied due to thread stripping sensitivity. Although a reduction in nut strength provokes internal thread stripping, which is registered in the parametric study, the combination with finer mesh and changed nut geometry is decisive. With slimmer threads in the bolt, external thread stripping is assumed to be the appropriate failure mode.

From Figure 7.2, it is observed that the nut is moving outwards as the threads are connected. It is reasonable to assume that a small movement in radial direction may appear, however in what extent is uncertain. The simplified load constraint may also affect the radial movement, as the bearing surface of the bolt remains horizontal throughout the analysis. A more accurate recreation of the loading would be obtained by modelling the washers used in the laboratory work, as seen in Figure 4.3a.

Due to limited knowledge of the bending capacity of the threads, it is hard to determine at what deformation the threads actually will fail. From Figure 7.2 the failure criteria $W = W_{\mathrm{cr}}$ is reached, and the first element is deleted at the displacement 2.125mm. However, a considerable load reduction is first observed at the displacement 2.500mm.

7.4 Comparison with analytical results

Table 7.1 shows the comparison of the analytical load capacity compared with the numerical and experimental results. As described in Section 4.6, the tension resistance provided by NS-EN 1993-1-8 [17] is highly conservative compared to both the experimental and numerical results. As the design code is general for all bolts and include safety factors due to geometrical and material imperfections, a higher load capacity is predicted by the NS-EN 1993-1-8 [17]. For bolts with property class 8.8, the nominal ultimate tensile stress, f_{ub}, is 800 MPa. It was of interest to study if the ultimate tensile stress retrieved from the material tests, gave a better prediction of the load capacity. From the material tests, presented in Chapter 5, the ultimate tensile stress was measured as 1036 MPa for partially threaded bolts and 984 MPa for fully threaded bolts. The safety factors are neglected. *EC3 nominal* is the load capacity defined in Equation 4.2, where *EC3 adapted* is modified with ultimate tensile stress according to the material tests and with no material corrections applied. The design code defined by Alexander [18] is also taken into consideration, where the calculations, carried out in Appendix D, is based on the same measurements utilized in the FE models.

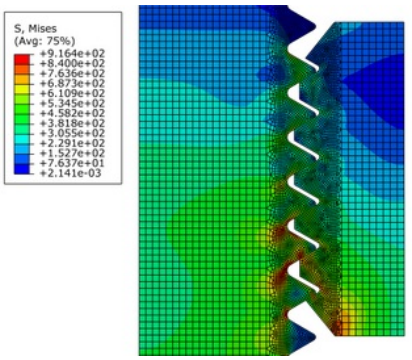

(a) At displacement 0.379mm

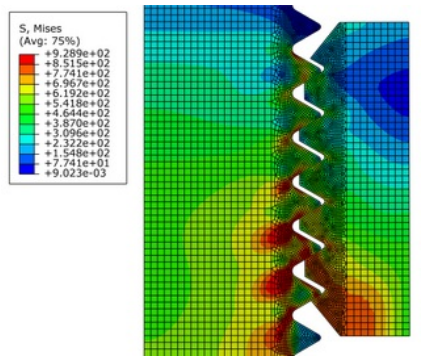

(b) At displacement 0.500mm

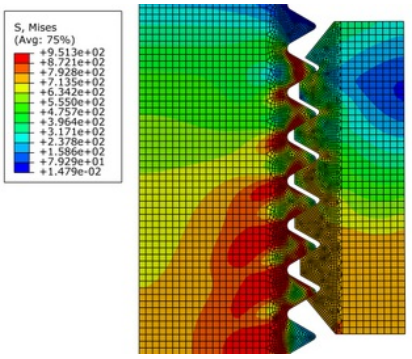

(c) At displacement 0.625mm

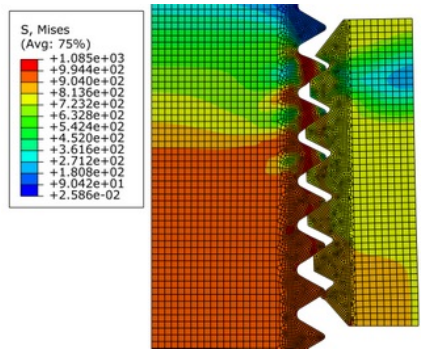

(d) Maximum force at displacement 1.125mm

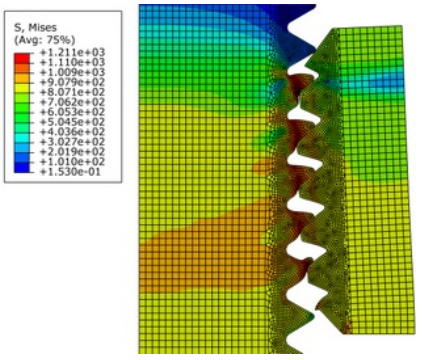

(e) W_{cr} reached at displacement 2.125mm

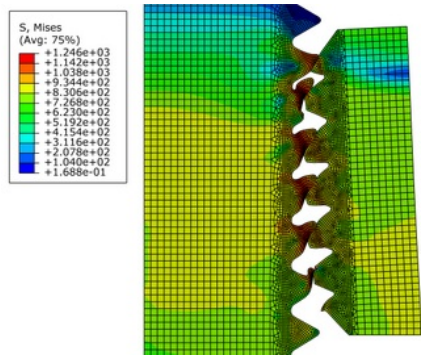

(f) Severe reduction in load at displacement 2.500mm

Figure 7.2: Deformation propagation through the final PT-118 analysis

Table 7.1: Comparison of load capacity

	Partially threaded [KN]	Fully threaded [KN]
Experiments	145.26	139.95
Simulations	151.08	145.67
EC3 nominal	90.43	90.43
EC3 adapted	146.4	139.15
Alexander	140.63	123.44

From Table 7.1 it is registered that the *EC 3 adapted* is in accordance with the capacity observed in the experiments. The design load calculated by Alexander is conservative, but gives a better prediction of the capacity compared to NS-EN 1993-1-8, where nominal values are utilized. This is as predicted, since the design calculations always should remain conservative, due to safety.

The load capacities presented in Table 7.1 refers to the bolt failure capacity. Although a nut strength reduction of 15% was used in the calculations by Alexander, bolt failure remained decisive. The number of threads in the grip length was emphasized as a factor provoking thread stripping by Alexander, however, this is not taken into account in the calculations.

8 Conclusions

As predicted, the design resistance according to NS-EN 1993-1-8 [17] gives a conservative estimate compared with the load capacities observed in the laboratory work. The method developed by Alexander showed to be suitable as the prediction gave more reliable load capacity, although it remained conservative.

The numerical simulations succeeded in recreating the physical behaviour within reasonable accuracy. However, a higher load level, up to 5.3%, were registered in all the numerical analyses. With similar observations in previous work, it is assumed to be caused by the simplified axisymmetric model, where the helical shape is ignored.

The number of threads in the grip length is found to be decisive for the failure mode of the bolt and nut assembly. With three full threads in the grip length, the partially threaded bolts tested failed due to thread stripping, i.e internal or external thread failure. This is of specific interest as the required number of full threads in the grip length is determined as one to avoid thread stripping, according to NS-EN 1090-2 [1]. With an increased number of threads in the grip length, the capacity of absorbing energy is significantly improved. Fully threaded bolts are therefore preferable when subjected to tension.

From the Vickers Hardness test, a large deviation of hardness between the nut and the bolt has been noticed. This was further studied in numerical analyses, and showed to provoke thread stripping, similar to finite observations made by Alexander [18].

The experimental results are successfully recreated in the finite element analyses with sufficient accuracy. With limited number of threads in the grip length, the models are more sensitive due to material and geometrical imperfections.

8.1 Suggestions for further work

The following list presents suggestions for further work for bolt and nut assemblies subjected to tension.

- To decrease the deviation of maximum load, a three-dimensional model with representative geometry including the washers should be examined.
- The failure mode thread stripping is defined for both internal and external thread failure, as no reliable observation of the failure could be determined from the experiments. Further investigation of tests failed in thread stripping should be carried out, where the nut is cut off instead on pulled off.
- The friction coefficient should be carefully examined, as the threaded assembly consist of a large contact surface. Even though the friction coefficient only show small impact on the threaded assembly carried out by Chen [2], a low friction may provoke thread stripping, and should therefore be further investigated.
- Quasi-static tests are carried out in this thesis. However, under extreme conditions, where extreme loads are applied, it is more adequate to believe that the prescribed situation occurs under dynamic conditions. Higher strain rates should therefore be tested by both experimental work and numerical analyses.
- Additional bolt and nut tests should be conducted by Vickers hardness test to identify the strength ratio.

Part II

T-stub connections

9 Literature review

A lot of research has been done on T-stub connections over the years, and the equivalent T-stub is widely accepted as a simplified model used to characterize the behaviour of the tension zone of a bolted joint. Some of the previous work performed on T-stub connections will be presented in this chapter. The articles and thesis presented focus on the overall behaviour of the T-stub rather than the behaviour of the tension bolts.

9.1 Girão Coelho et al.: "Finite-Element Modeling of the Nonlinear Behaviour of Bolted T-stub Connections" [5]

Girão Coelho et al. have created finite element models that provide accurate predictions of the deformations of a T-stub up to failure. Both T-stubs made out of rolled profiles, HR-T-stubs, and two plates welded together, called WP-T-stubs, are considered. The bolt is modelled as an equivalent bolt presented in Bursi et al. [36]. The threads are neglected and the deformation of the head and nut are assumed to be symmetric. The finite element models are calibrated from existing experimental work. A parametric study considers the influence of geometry and material properties. It was found that the physical response of the system is highly dependent on the positioning of the bolts. The article emphasises the failure modes of a T-stub and corresponding ductility levels. The failure mode of the T-stub depends on the relation between the flexural resistance of the flanges and the axial resistance of the bolts. Eurocode 3 does not account for material strain hardening effects, which implies that the resistance of the flanges and bolt is based on plastic conditions. Neither are any limits imposed to the ductility of connections that mainly depend on material ductility (bolt and flange) and structural discontinuities (welds and bolt holes). Concerning these conditions,

Girão Coelho et al. propose four possible failure mode topologies that all represent different ductility properties.

9.2 Swanson: "Characterization of the Strength, Stiffness and Ductility Behaviour of T-Stub Connections" [6]

Swanson has done thorough investigations of the behaviour of T-stub connections with both tension and shear bolts. The experimental work consists of 48 component T-stub tests and 10 component clip angle tests which are all evaluated based on their strength, stiffness and ductility. According to Swanson, high-strength fasteners are designed so that tension failure of the bolt will occur before thread stripping. From experimental observations and results from finite element analyses, a monotonic stiffness model is developed. Based on observations from the experimental program, a cyclic model is also developed. T-stubs that were proportioned such that a flange mechanism and stem yielding developed simultaneously gave the most desirable behaviour.

9.3 Swanson et al.: "Advanced finite element modeling of bolted T-stub connection components" [7]

Swanson et al. have implemented both two and three dimensional finite element models to investigate the behaviour of T-stub flanges. The results are compared to experimental data. The T-stubs considered consist of tension bolts and shear bolts. The tension bolts are pretensioned. The shanks of the tension bolts are modelled as prismatic shafts, neglecting the reduced area of the threaded part of the bolt. This yields a larger force in the FE model than in the experimental results. It is also pointed out that nominal values are used for the material properties, and this also influences the results. Discrepancies are observed in flange deformation and slip response in the tree dimensional model, but due to the computational costs of the model no further investigations are performed. Instead, two dimensional models are considered to examine the characteristics of flange deformation, stress distributions, bolt bearing stiffness, and the stiffness of the stem. It was observed that bending effects in tension bolts reduced their axial

strength. Multi-directional plate bending is observed in the flanges of the four-bolt T-stubs tested. The flange capacity and post-yield stiffness appear to be independent of the pretension, but the flange deformations are affected. Flange thickness and tension bolt location influence the pressure distributions between the T-stub flange and column flange. The force distribution from stem into the flange appears to be approximately uniform across the width of the T-stub.

10 Laboratory work

This chapter describes the experimental work conducted on bolted T-stub connections. 18 quasi-static tests have been performed on a variation of T-stub connections to investigate the failure modes of the bolts when the connection is subjected to pure tension. The yielding of the flanges will impose bending stresses on the bolts. According to Swanson [7], this effect may reduce the tension resistance of the bolts. It is of interest whether thread failure may be a concern in this situation as well as in pure tension, as investigated in Part I. All T-stubs are made out of S355 steel and all bolts used are M16x70 bolts with property class 8.8. Both partially and fully threaded bolts have been considered.

10.1 Geometry

Each connection consist of two T-stubs, two bolts and nuts, where the nuts are finger tightened. Five configurations of the connection have been tested where a combination of the following parameters is changed for each configuration:

- The bolt type used in the connection. The failure mode of both partially and threaded bolts are of interest. From the pure tension tests in Part I thread stripping was only observed for partially threaded bolts, but this might change when the stresses enforced on the bolt come from a combination of tension and bending.
- The center distance, w, between bolt holes in T-stub, presented in Figure 10.1. Variation of bolt placement will change the bending stresses applied. By increasing the center distance of the bolts the bending stresses will also increase.
- The number of nuts used on each bolt in the connection. By adding more nuts on the bolt it can be determined if it is possible to achieve a differ-

ent failure mode if the number of threads subjected to the combination of bending and tension effects increases.

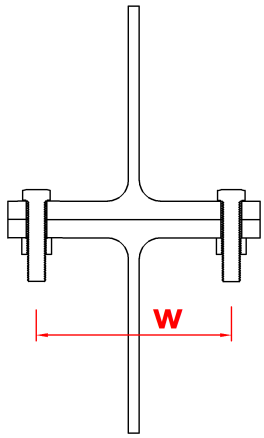

Figure 10.1: Center distance between bolt holes in a T-stub connection

Specifications of the different configurations and number of tests performed for the given configuration are presented in Table 10.1. Each test is given a name that will be used throughout this thesis. The first part of the name indicates the center distance between the bolts in the connection. The bolt type is denoted PT for partially threaded bolts and FT for fully threaded bolts. The very last two digits denote the unique test number.

The geometries of the five different configurations are given in Appendix F. The T-stubs are based on the geometry of a HEB220 profile where one of the flanges is removed. The center distance, w, between the bolts is determined from required values for bolt access [37]. The center distance of 120 mm is also given in [38]. The center distance of 170 mm is checked according to minimum distance from edge provided by NS-EN 1993-1-8 [17].

The T-stubs are designed according to the theory of the equivalent T-stub presented in Section 2.2. The effective lengths of the two T-stubs are determined such that failure Mode 2 gives the lowest resistance. Recall that Mode 2 involves tensile bolt fracture in combination with flange yield mechanisms. The calculations of l_{eff} are presented in Appendix E.

Table 10.1: T-stub configurations tested

Test	Center distance [mm]	Bolt type	Number of nuts
T120-FT-01	120	FT	1
T120-FT-02	120	FT	1
T120-FT-03	120	FT	1
T120-FT-04	120	FT	1
T120-FT-05	120	FT	1
T120-FT-06	120	FT	1
T120-PT-01	120	PT	1
T120-PT-02	120	PT	1
T120-PT-03	120	PT	1
T120-PT-04	120	PT	1
T120-PT-05	120	PT	2
T120-PT-06	120	PT	2
T170-FT-01	170	FT	1
T170-FT-02	170	FT	1
T170-FT-03	170	FT	1
T170-PT-01	170	PT	1
T170-PT-02	170	PT	1
T170-PT-03	170	PT	1

10.2 Test setup

All tests are performed in a servo hydraulic test machine. The test specimen is fastened by clamping of the webs as indicated in Figure 10.2a. The load is applied as a constant velocity acting on the lower web. For the tests with fully threaded bolts the velocity applied was in general 0.05mm/s, while it was 0.03mm/s for all tests with partially threaded bolts to ensure quasi-static conditions. The upper web is withheld from translation in all directions.

Figure 10.2b shows the full test setup including the equipment used for the DIC analyses. The force was logged using the machine at a frequency of 1 Hz, and DIC registered the deformation of the connection at the same frequency.

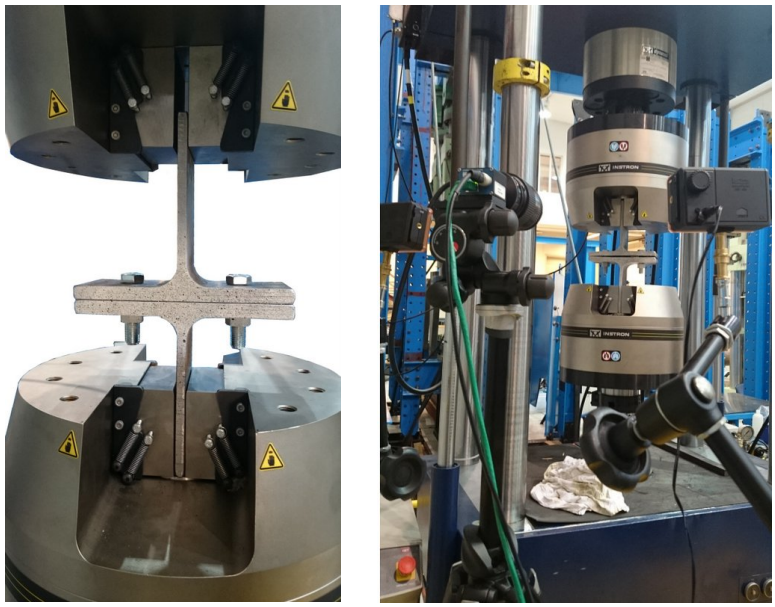

(a) Detailed view (b) Overview

Figure 10.2: Test setup

10.3 DIC

Two-dimensional DIC analysis is utilized to retrieve elongation of the T-stub connections. The process is displayed in Figure 10.3 and 10.4, where a vector measures the distance between two nodes placed approximately in the middle of each flange and at the position of the bolts. Due to disturbance in the mesh applied along the edges of the flanges, a smaller element mesh is employed. Due to insignificant deviation of the flange thickness measured during the tests, no corrections are taken into account when withdrawing the displacements of the T-stub.

Disturbance of the light sources in the laboratory during tests T120-PT-04 and T170-PT-01 made it impossible to perform DIC analysis for these tests.

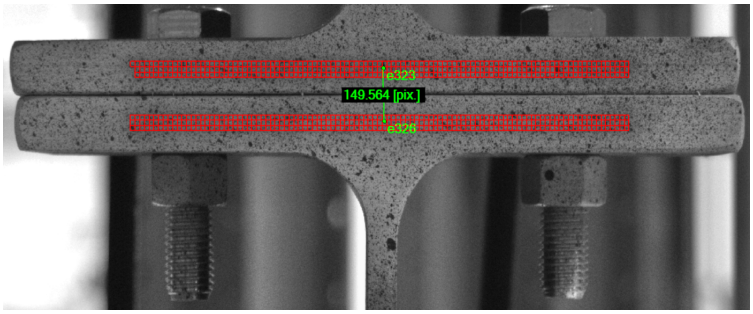

(a) Initial vector length

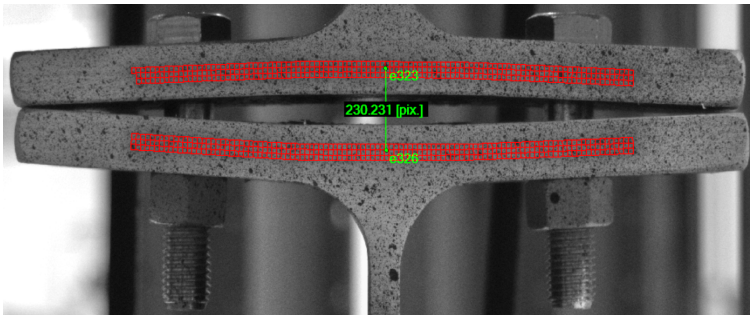

(b) Final vector length

Figure 10.3: DIC analysis of the bolted T-stub connection

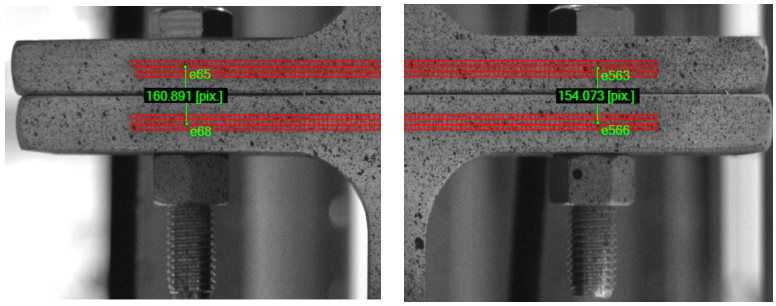

(a) Left side (b) Right side

Figure 10.4: DIC analysis of the flanges at the position of bolts in the T-stub connection

10.4 Results

The force-displacement curves for all tests where displacement has been retrieved from DIC are presented in Figure 10.5. The failure mode of the bolts and maximum force, $F_{t,Ed}$, observed in each test is presented in Table 10.2. In addition the external work in each test is presented. This is calculated as described in Section 4.4. All tests exhibited the desired failure mode as described in Section 10.1. Both thread stripping and bolt failure occurred in the tests.

From Table 10.2 and Figure 10.5 the following is observed:

- The average maximum force of the connections with bolt center distance 120mm is 228kN for both partially and fully threaded bolts. This is also the case for the configurations with center distance 170mm where the average maximum force is 153kN.
- The T120-FT configuration is able to absorb more than double the amount of energy than the T120-PT configurations. This ratio decreases when the bending stresses on the bolts increases. The T170-FT configurations are able to absorb 73% more energy compared to the T170-PT configurations.
- All tests with partially threaded bolts and only one nut experienced thread stripping at failure. When adding an extra nut and doubling the number of threads holding the bolt in place, bolt failure occurred. This led to an increase of 71.27% in energy absorbed by the system. The average maximum force only increased by 6.20%.

Table 10.2: Results from laboratory tests of T-stub connections

Test	Failure mode	$F_{t,Ed}$ [kN]	External work [Nm]
T120-PT-01	TS	232.06	555.06
T120-PT-02	TS	225.40	515.46
T120-PT-03	TS	228.59	503.15
T120-PT-04	TS	226.35	-
T120-PT-05	B	240.91	888.03
T120-PT-06	B	243.57	908.82
T120-FT-01	TS	229.59	987.10
T120-FT-02	TS	229.91	1231.2
T120-FT-03	B	228.88	1227.0
T120-FT-04	B	229.60	1218.4
T120-FT-05	B	227.98	1202.6
T120-FT-06	TS	225.10	1110.5
T170-PT-01	TS	152.28	-
T170-PT-02	TS	148.17	852.21
T170-PT-03	TS	157.47	1212.2
T170-FT-01	B	154.17	1924.4
T170-FT-02	TS	154.48	1980.7
T170-FT-03	TS	151.95	1555.8

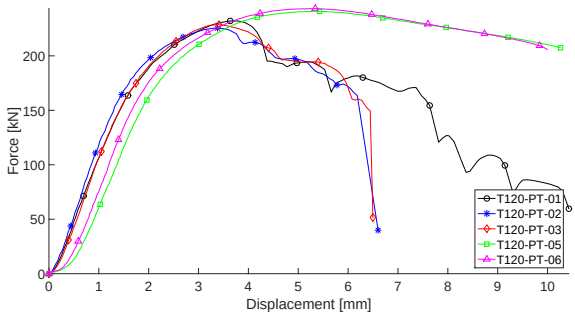

(a) Partially threaded bolts with center distance 120 mm

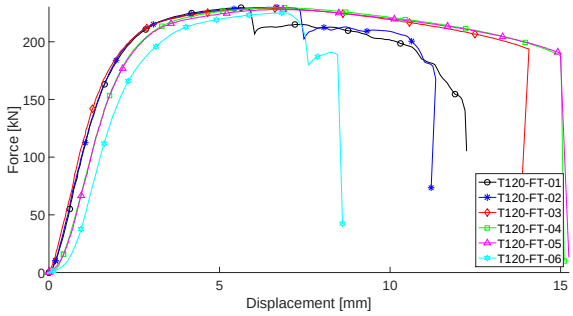

(b) Fully threaded bolts with center distance 120 mm

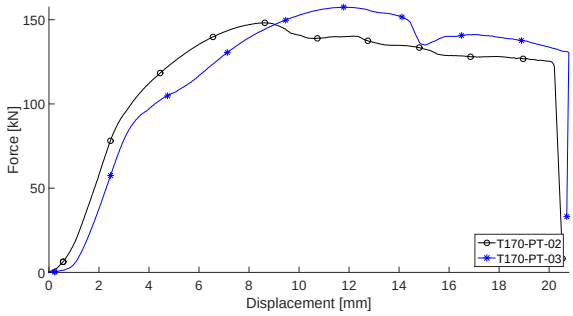

(c) Partially threaded bolts with center distance 170 mm

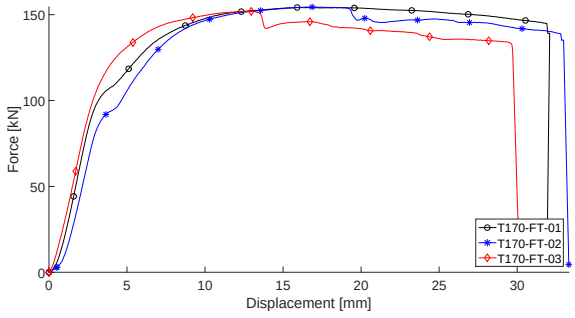

(d) Fully threaded bolts with center distance 170 mm

Figure 10.5: Force-displacement curves for laboratory tests

- Several of the tests with center distance of 170mm display sudden changes in force level when the connection has reached the plastic domain. This will be further examined in Section 10.5.

10.5 Deformation patterns and failure modes

Figure 10.7 displays the deformation of the test T170-PT-03 at certain points in time. As seen in Figure 10.5c, the force drops when the deformation between the webs is approximately $14.4 - 14.9$mm. By comparing Figures 10.7d and 10.7e a change in the deformation of the flange by the left bolt can be seen.

To verify if this is actually the case the vertical displacements along different points of the flanges are compared. Figure 10.6 shows how the gap between the flanges develops at the position of each bolt in addition to the deformation under the web. At the time $t = 486$ s the flanges suddenly deform at a higher rate under the left bolt.

When the deformation of the bolts at these time steps are considered further, it is observed that the right bolt and nut move as a rigid body but the left bolt and nut move relative to each other. The number of threads on the bolt below the left nut is reduced in Figure 10.7e compared to Figure 10.7d. This slip is considered an initial thread stripping which leads to a reduction in force until the nut threads reach the next thread on the bolt and again establishes contact.

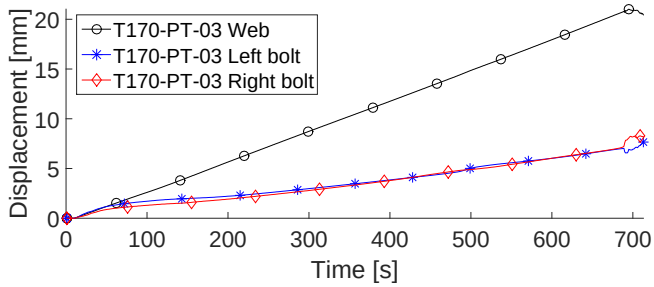

Figure 10.6: Displacements of flange measured at web and bolt positions for T170-PT-03

This behaviour is also observed for tests T170-FT-02 and T170-FT-03. It is however not observed in any of the configurations with bolt center distance

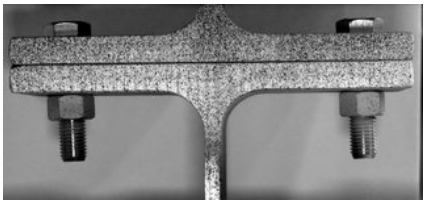

(a) Start, $t = 0$ s

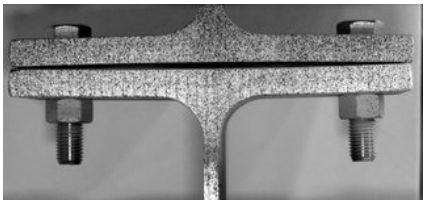

(b) Yielding, $t = 121$ s

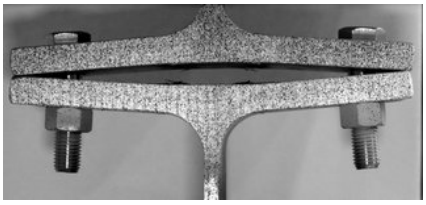

(c) Maximum force, $t = 404$ s

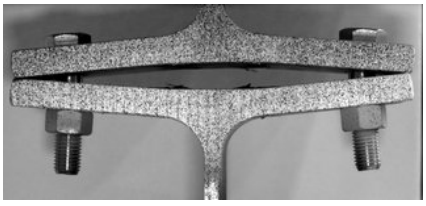

(d) Before drop in force, $t = 486$ s

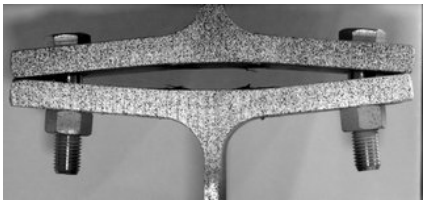

(e) Drop in force, $t = 499$ s

(f) Before fracture, $t = 689$ s

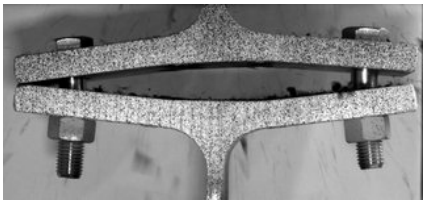

(g) Fracture, $t = 690$ s

Figure 10.7: The course of events for test T170-PT-03

120mm. Therefore, it is reason to believe that this initial thread stripping happens due to the bending of the bolt, which is significantly higher for the T170-configurations as seen in Figure 10.9. After the initial thread stripping both bolt failure and thread stripping is observed as the final failure mode.

10.6 Discussions

From the calculations given in Appendix E the design load of the connections with bolt center distance 120mm is $F_{t,Rd,T120} = 171.90$kN. For the connections with center distance 170mm it is $F_{t,Rd,T170} = 122.80$kN. As expected, all registered maximum forces are higher than the corresponding design loads. The method described in Section 2.2 is sufficient for the determination of the capacity of a T-stub connection subjected to tension. All tests exhibit the desired failure mode, which implies that the design code correctly predicts the failure mode of the T-stub.

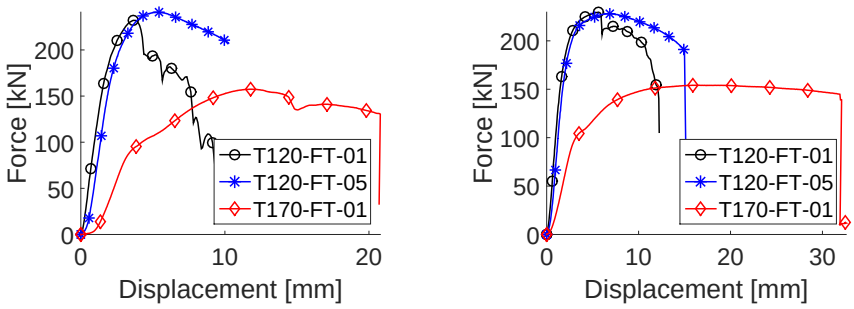

(a) T-stubs with partially threaded bolts (b) T-stubs with fully threaded bolts

Figure 10.8: Force-displacement curves for T-stubs with different center distances between bolt holes

In Figure 10.8, representative force-displacement curves for different center distances are plotted together. The average maximum force for the T120 configurations with only one nut is 49.0% larger than for the average maximum force of the T170 configurations for both bolt types. Due to the increased bending stresses, the bolts in the T170 configurations are subjected to larger bending deformations, see Figure 10.9. As expected, this reduces the tension resistance of the bolts.

(a) Bolt center distance 120 mm

(b) Bolt center distance 170 mm

Figure 10.9: Deformations of M16x70 bolts

A graphical presentation of the external work calculated for each test is given in Figure 10.11. As mentioned in Section 10.4, the T120 configurations with fully threaded bolts are able to absorb more than double the amount of energy compared to those with partially threaded bolts although the average maximum tension load, $F_{t,Ed}$, is the same. This is due to the fact that all joints with partially threaded bolts and only one nut experience thread stripping at failure. When the nut height is increased, the number of threads subjected to stresses caused by the loading increase, reducing the stress distribution on each individual thread. This leads to bolt failure and an increase in the average ductility of the system by 71.27%. In general, the joints with fully threaded bolts are more ductile than the configurations with partially threaded bolts. This is caused by the variation in grip length as discussed in Section 4.6.

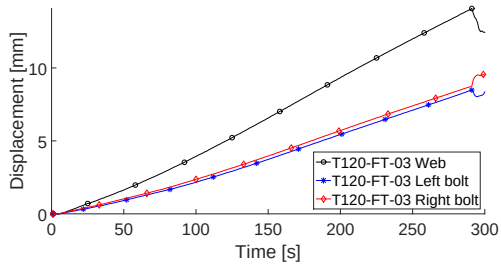

Figure 10.10: Deformation of flange at specified points

DIC analyses of the deformation of the flanges measured at the position of the bolts reveal that the deformations are asymmetrical. Figure 10.10 displays this trend for the test T120-FT-03. Similar behaviour is observed for all configurations presented in Table 10.1. When the nuts are tightened, the geometrical imperfections of the flanges and the bolts may affect the position of the nut relative to the bolt, which may cause this asymmetry. Small deviations in bolt hole positions, and the positions of the bolts relative to the hole, may also cause uneven loading conditions. These possible inaccuracies are difficult to measure, but the experimental work conducted always results in fracture of only one of the two bolts, indicating that some form of inaccuracy appears in every test. This asymmetry may trigger failure of the bolt at an earlier stage than for a perfectly symmetric test.

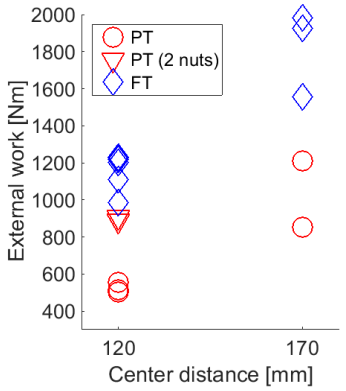

Figure 10.11: Graphical presentation of external work for all test configurations of T-stub connections

The initial thread stripping observed in the configurations with bolt center distance 170 mm is assumed to be a result of the increased bending effects compared to the T120 configuration. Even though the bolts are able to sustain a considerable amount of deformation before the next thread is stripped or the bolt fails in the cross-section, this is a undesirable behaviour because of the uncertainties associated with thread stripping.

It is not possible to establish a deformation pattern for the T120-FT configurations based on this experimental work since both thread stripping and bolt failure is observed. The failure mode appears to be random based on these results, and more thorough investigations are advised.

11 Identification of material parameters

Three material tests have been carried out for the all the components in the T-stub connection, which consist of partially and fully threaded M16x70 bolts and HEB220-flange (S355). Due to similar behaviour observed among the material test series, one test of each component was set as the basic test and acts as the foundation for the material model. The same approach is utilized for these tests, as for the material tests carried out in Chapter 5. Only a brief description is therefore given in the following chapter.

11.1 DIC

DIC is utilized to retrieve the deformation of the specimen. The bolts were carried out the same way presented in Section 5.1, while the HEB220-flange tests required an additional camera. With two cameras, the elongation in both the width and thickness were identified, and a sufficient measurement of the true cross-section area was obtained.

11.2 Calibration of the material parameters

As described in Section 2.5 and Section 5.2, hardening parameters need to be implemented to describe the material behaviour after yielding. With the same procedure as for the M16x160 bolts, Voce Rule with Bridgman's correction method were employed in the models. These parameters were further implemented and calibrated in finite element analyses to achieve a representative behaviour of the material tests.

11.2.1 Material test simulations

Three dimensional FE models have been implemented for the material tests using Abaqus/Explicit. Due to negligible differences in the geometry of fully threaded and partially threaded material tests, the same finite element model is utilized for both the bolt models. To reduce the required computational time, one quarter of the material tests have been modelled, where symmetry constrains are applied along the symmetry axes to establish a full recreation of the tests. The material models contain the same element type, C3D8R, utilized in the initial model of the T-stub connections. For further details of the element type, see Section 12.1.2. The material models are calibrated using fine mesh to diminish errors which coarse mesh might induce. An element size of 0.5mm is assumed to give a proper description of the material behaviour. Due to mesh-sensitivity, the fracture criterion is determined for different element sizes, ranging 0.5 mm-1 mm. Figure 11.1 shows the finite element models employed in Abaqus.

(a) M16x70 (b) S355

Figure 11.1: Material tests

11.2.2 Final material test simulation

Figure 11.2 shows the relation between engineering stress and area reduction of the material tests compared with the resulting finite element models. With the final material parameters implemented in the numerical models, a good accordance is observed. The corresponding material parameters are listed in Table 11.1. These parameters will further be implemented in the finite element analyses of the T-stub connections.

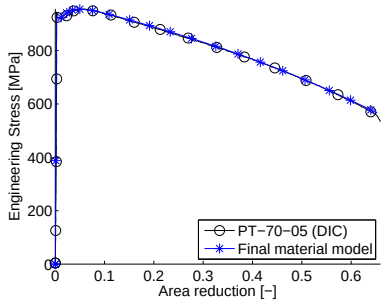

(a) Partially threaded M16x70

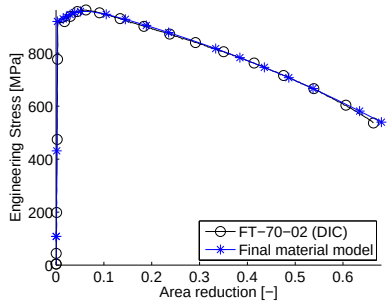

(b) Fully threaded M16x70

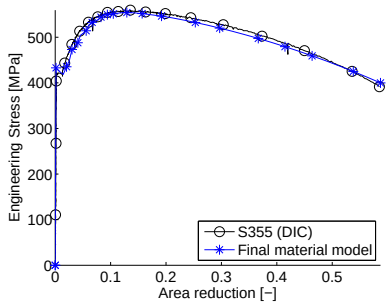

(c) HEB220-flange (S355)

Figure 11.2: Engineering stress-area reduction for the material tests of M16x70 and HEB220

Table 11.1: Hardening and fracture parameters

	PT-70	FT-70	HEB220-flange (S355)
σ_0 [MPa]	932.2	930.1	424.0
θ_1 [MPa]	7874	7634	7662
Q_1 [MPa]	155.1	195.0	252.1
θ_2 [MPa]	$-1.000 \cdot 10^4$	-7700	$-1.232 \cdot 10^4$
Q_2 [MPa]	-77.09	-97.45	-83.91
θ_3 [MPa]	220.0	219.7	404.9
Q_3 [MPa]	-2000	805.8	105.0
W_{cr} [MPa]	1575	1656	654.2

12 Finite element models

Finite element models of the four different T-stub connections have been created using the finite element program Abaqus/Explicit. Abaqus/Explicit is capable of handling nonlinear behaviour in a way that is desirable for the conduction of quasi-static simulations with contact. The finite element analysis in Abaqus/Explicit is performed using an explicit integration scheme as described in Section 2.8.

The geometry of the T-stub is based on the geometry described in Appendix F. The flange thickness was measured from the parts used in the laboratory work. To represent the geometry of the threads a fine mesh must be applied, and this implies that the system will become computationally ineffective. To reduce the computational time required by the full system the threads on the bolt and nut assemblies have been ignored in the first part of this work. A study of the effective tension area of a simplified bolt has been performed to establish which diameter this simple bolt model should have to properly recreate the load level.

SimLAB Metal Model is used to implement the material in all FE models. The material properties for the T-stub and bolt materials are defined in Chapter 11.

Since thread stripping was observed in the laboratory work, an attempt has been made to investigate two models of the connection with threaded bolts. This is further described in Section 12.3.

Four initial models of the connections were created to act as a basis for further models that can represent the behaviour of the system as accurate as possible. The models are based on default settings and basic elements. The purpose of these models is to act as robust basis models for further investigations of different parameters that may impact the physical response of the connection.

In order to increase the computational efficiency, the deformation of the con-

nection is assumed symmetric about two planes. In the laboratory work the deformation observed was not symmetric, but this assumption reduces the finite element model to a quarter of the connection studied in the laboratory work, hence the computational cost is also reduced.

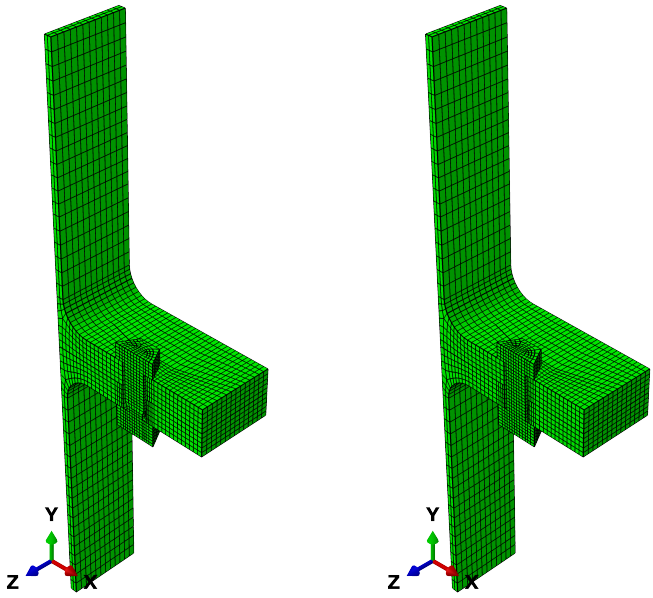

(a) Partially threaded (b) Fully threaded

Figure 12.1: Finite element model of T-stub connection with center distance 120 mm between the bolt holes

12.1 Initial model

Initial models have been made for four of the configurations tested in the laboratory. Both bolt types and both bolt positions have been considered, but only the general height of one nut. Each model is made to recreate the laboratory work as accurately as possible. All models have the same boundary conditions, loading,

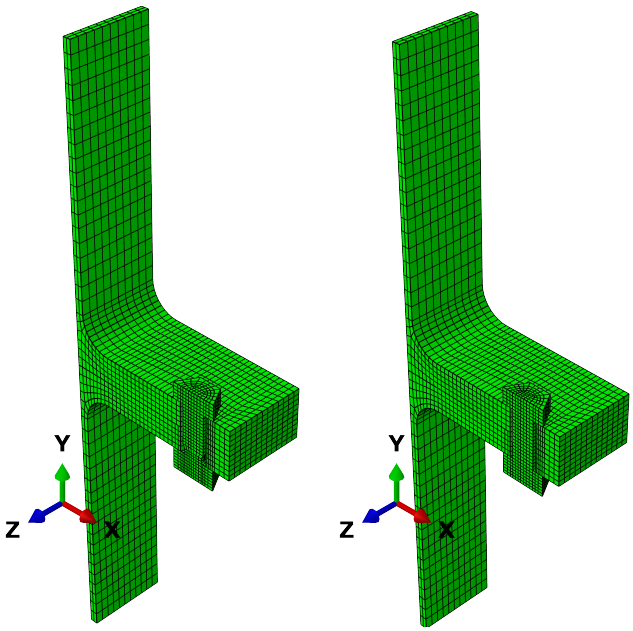

(a) Partially threaded (b) Fully threaded

Figure 12.2: Finite element model of T-stub connection with center distance 120 mm between the bolt holes

interactions and mesh presented in this section.

Figures 12.1 and 12.2 show the initial models for all test configurations. Initially two half T-stubs are placed with an initial gap of 0.15mm between the flanges and the bolt is placed in the center of the bolt hole.

12.1.1 Simplified bolt

A simplified finite element model of the bolt without threads is used. Because the bolt has no threads, the bolt and nut is modelled as one part. The models will therefore not be able to fail due to thread stripping, but they should be able to recreate the physical response up to failure for the tests where this is the case.

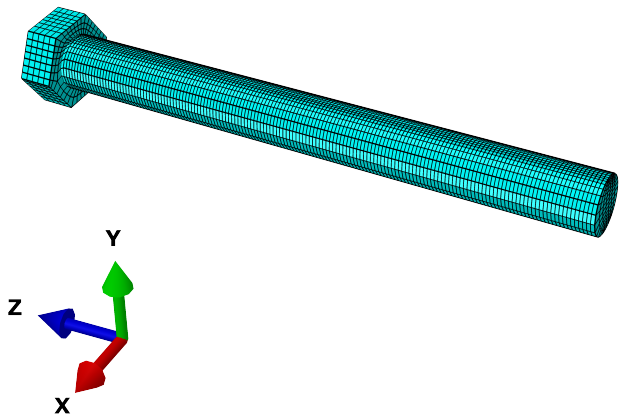

Figure 12.3: Simple model of M16x160 bolt

Ignoring the threads implies that the diameter of the bolt may be altered to properly represent the tensile stress area of the bolt. To find the ideal diameter

of the simplified bolt a study is performed on a M16x160 bolt without threads. By recreating the grip length of 118 mm, applying a velocity at the bolt head and using the material properties in Table 5.1, the model in Figure 12.3 should be able to recreate the physical response of the fully threaded bolt presented in Figure 4.19a.

Three diameters of the simple bolt have been considered:

- The nominal outer diameter of the bolts, 16.00mm.
- The basic pitch diameter of external thread [28], 15.35mm.
- The diameter of the tensile stress area defined in NS-EN ISO 898-1 [39], 14.14mm.

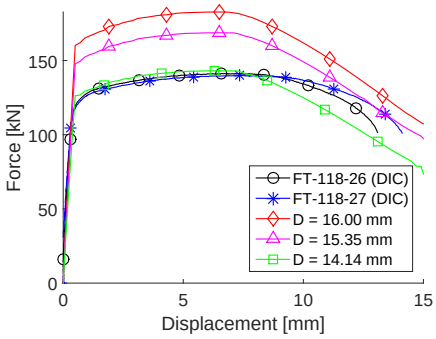

Figure 12.4: Force-displacement curve for simple M16x160 bolt

The force-displacement curves from the three diameters are compared with the results from the laboratory work in Figure 12.4. It is clear that the tensile stress area defined by NS-EN ISO 898-1 is best suited to recreate the load level of the threaded M16 bolt.

Disregarding the threads in the bolt and nut assembly implies that the connection between these must be reconsidered. Thus it is chosen to model the bolt and nut as one part. The models are presented in Figure 12.5.

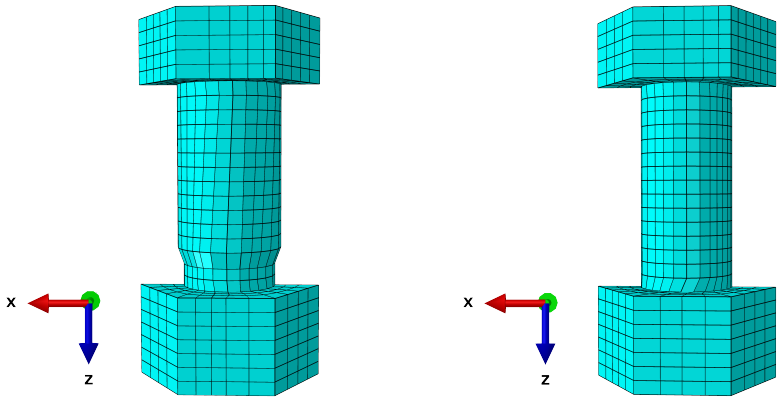

(a) Partially threaded (b) Fully threaded

Figure 12.5: Simple bolt models

12.1.2 Mesh and element characteristics

The initial model is meshed using C3D8R elements. This is a 8-node linear brick element with reduced integration and hourglass control. This element is preferred to the 8-node linear brick element C3D8 because it is more computational effective and it does not exhibit shear locking behaviour. Elements with reduced integration may exhibit hourglassing. This is prevented by applying hourglass control in Abaqus/Explicit.

The meshed parts are displayed in Figures 12.5 and 12.6. An overview of the different element sizes applied in the initial model is given in Table 12.1. A fairly coarse mesh is applied to the initial model in order to save computational time. The plastic deformation of the flange observed in the laboratory tests implies that the mesh has to be fine in this part of the initial model. The applied mesh in the web is coarse to reduce the number of degrees of freedom in the system.

12.1.3 Boundary conditions

To reduce computational time only a quarter of the connection is modelled. This is done by utilizing the symmetry about the XY-plane and YZ-plane in point S as displayed in Figure 12.7. In Abaqus/Explicit the XY symmetry is enforced

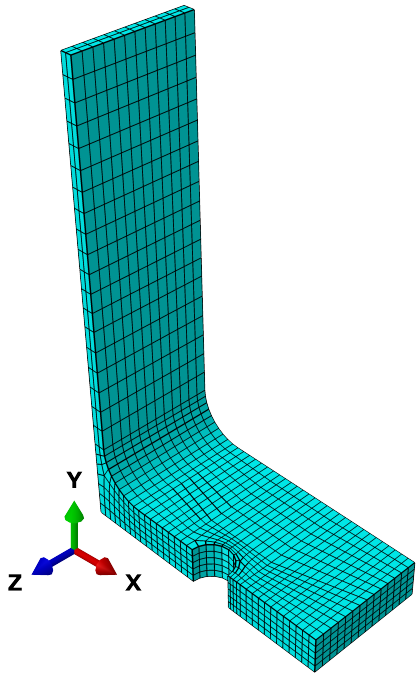

Figure 12.6: Mesh of T-stub

Table 12.1: Element sizes applied in initial models

Part	Element size [mm]
Web of T-stub	8
Flange of T-stub	3
Bolt	2

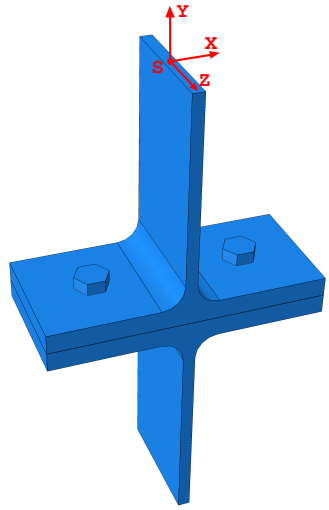

Figure 12.7: Full model of T-stub

by fixing the translation in the z-direction and the rotational degrees of freedom in the x- and y-direction as shown in Figure 12.8a. Figure 12.8b displays how the YZ symmetry is enforced by fixing the translation in the x-direction and the rotational degrees of freedom in the y- and z-direction.

To represent the boundary conditions used in the laboratory work all translational degrees of freedom in the upper half of the upper web in the initial model are fixed.

The load is applied as a velocity acting on the lower web to recreate the quasi-static conditions from the laboratory work. To limit the amount of kinetic energy created by this velocity a smooth step is applied. This will gradually increase the

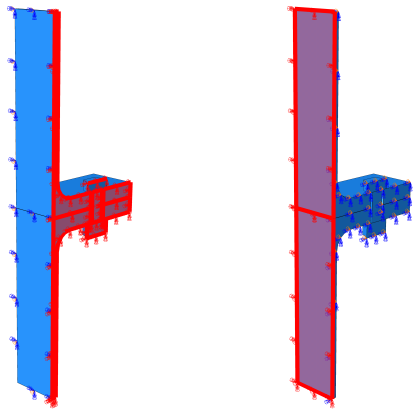

(a) XY-plane (b) YZ-plane

Figure 12.8: Symmetry boundary conditions

velocity up to full amplitude at time t as discussed in Section 6.1.5.

12.1.4 Interactions

The interactions in the initial model are controlled by the general contact algorithm in Abaqus/Explicit. This contact formulation is chosen because it allows simple definitions of contact and it is not necessary to specify the surfaces that may be in contact.

The general contact algorithm in Abaqus/Explicit enforces contact constraints using a penalty method that searches for penetrations in the current configuration. The penalty stiffness relates the contact force to the penetration distance. To avoid influencing the time increment but still make the penetration non-significant the penalty stiffness is chosen automatically by Abaqus/Explicit [40].

The general contact requires at least one friction coefficient. In the initial models the friction coefficient, μ is assumed to be 0.4 based on the value given for surfaces blasted with shot or grit in NS-EN 1090-2 [1]. Note that it is possible to have different friction coefficients between different surfaces in the model when using a general contact formulation. This is not utilized in this case, even though the friction coefficient for the bolt against the T-stub might be lower than the friction coefficient between the T-stubs. A study of the friction coefficients

impact on the model will be conducted.

12.1.5 Computational efficiency

According to Section 2.8, time scaling is applied to reduce the computational cost. By testing different velocities it is found that it is possible to use a velocity of 1000 mm/s on the T-stubs without the appearance of inertia forces.

12.1.6 Results of initial models

The initial configurations described in Section 12.1 are all implemented for four different configurations of the T-stub. Figure 12.9 shows where the displacements of the models are retracted.

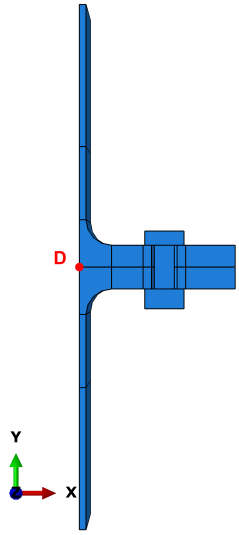

Figure 12.9: Displacements retracted from point D

The force-displacement curves for the initial models are given in Figure 12.10 and 12.11. As a basis of comparison the curves from the corresponding configuration from the laboratory work are included in the plots. To eliminate the discrepancy of the displacement the curves are moved to coinside at a given point

for each configuration. A displacement of 0.2 mm and force 15 kN are used for the T120-PT configuration, 0.3 mm and 20 kN for the T120-FT configuration, and 0.16 mm and 15 kN for the T170 configurations.

From Figures 12.10 and 12.11, and Table 12.2 the following observations are made:

- The response in the elastic domain is too stiff in the finite element models.
- The maximum force of the initial models are greater than the maximum forces observed in the laboratory work.
- The deformation of the connections, and especially the bolts, are much larger than observed in the corresponding laboratory tests.

Table 12.2: Results of initial FE models

Model	$F_{t,Ed}$ [kN]	Deviation DIC average [kN]	Deviation DIC average [%]	External work [Nm]	Deviation DIC average [Nm]	Deviation DIC average [%]
T120-PT	249.33	21.23	9.307	3996.8	3472.2	661.9
T120-FT	253.78	25.27	11.06	5234.9	4072.1	350.2
T170-PT	223.10	75.48	49.36	11320	10281	989.3
T170-FT	235.30	81.64	53.13	12061	10241	562.6

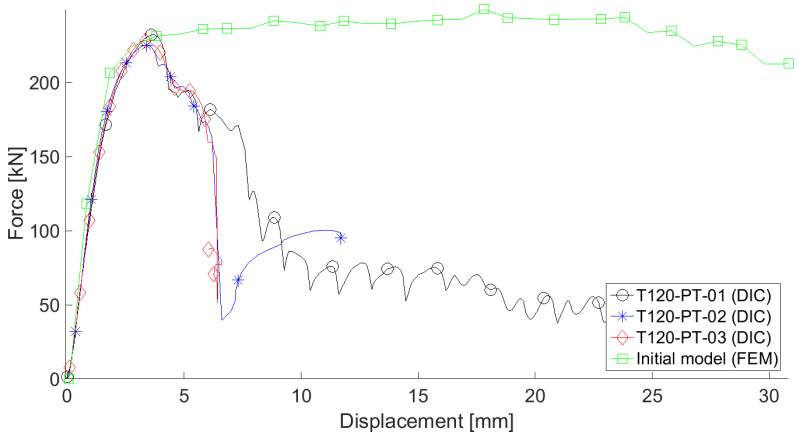

(a) Partially threaded bolts, center distance 120 mm

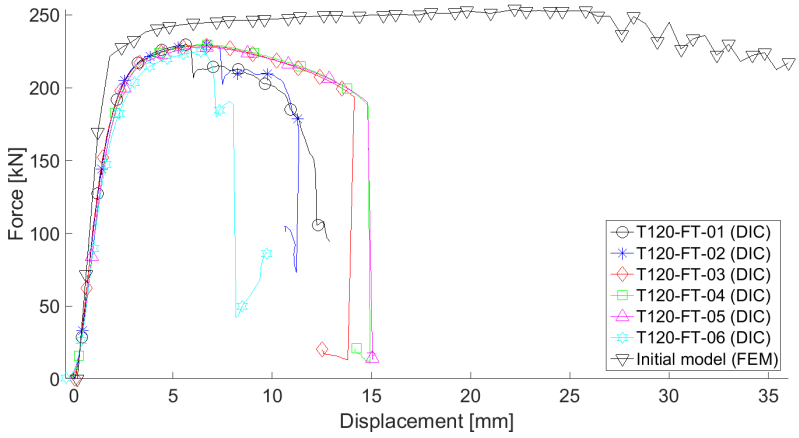

(b) Fully threaded bolts, center distance 120 mm

Figure 12.10: Force-displacement curves for initial FE models

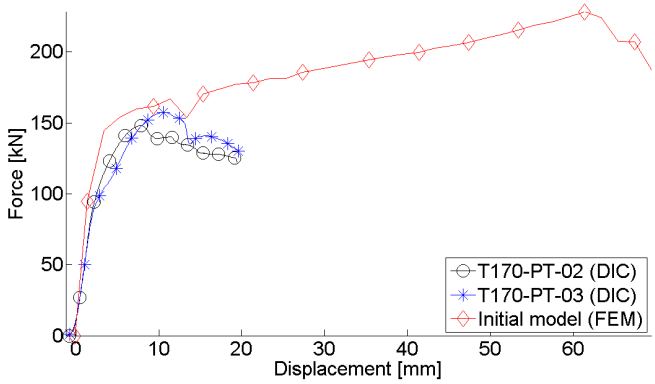

(a) Partially threaded bolts, center distance 170 mm

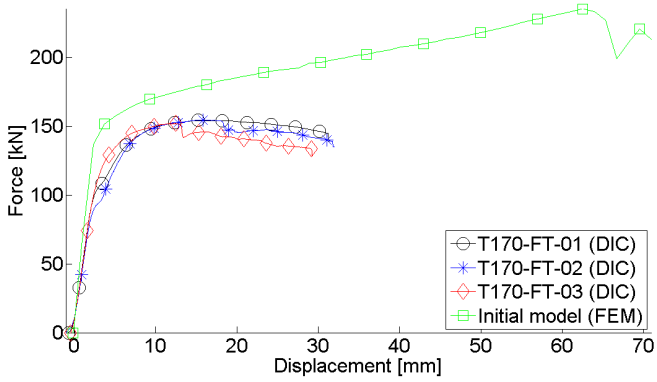

(b) Fully threaded bolts, center distance 170 mm

Figure 12.11: Force-displacement curves for initial FE models

12.2 Parametric study

A parametric study will be conducted to explore the significance of element size, friction coefficients and placing of bolts in the FE models. In addition the simplified model of the partially threaded bolt is investigated.

Due to small variations between the different configurations and uniform trends for all the initial models the parametric studies will only be conducted for the T120-FT model. When the results from each study are combined, the final models for each configuration are presented in Section 12.2.5.

Note that output data was retrieved more frequently for the analyses in the parametric study than for the initial models, and this revealed disturbances in the deformation of the flanges that was not observed for the initial models.

12.2.1 Mesh sensitivity

Due to the large differences between the initial finite element models and the laboratory work in maximum force, a study of the mesh sensitivity is conducted.

It is important that the element sizes in the parts of the model where plastic deformation takes place are small enough to correctly represent the deformation. Linear interpolation between nodes also indicate that the element size must be small to properly represent the curved deformation. Both the flange and bolt are subjected to plastic deformations which indicates that a mesh refinement may affect the physical response of the model.

Three different mesh configurations have been tested; fine, medium and coarse. The approximate element sizes used in each configuration are presented in Table 12.3. The elements have the same magnitude in all three directions.

Figure 12.12 display the force-displacement curves for the different meshes. As predicted, the chosen element sizes influence the response of the FE model. However, the difference in force level and displacements are larger than expected. The disturbance observed is also a reason to investigate further.

Large reduced integration elements are prone to exhibit hourglassing as described in Section 6.1.2. The artificial strain energy used to prevent hourglassing modes are plotted with the internal energy for each mesh configuration for the

Table 12.3: Element sizes used in study of mesh sensitivity

	Coarse [mm]	Medium (Initial model) [mm]	Fine [mm]
Web	8	8	8
Flange	6	3	2
Bolt	2	2	1

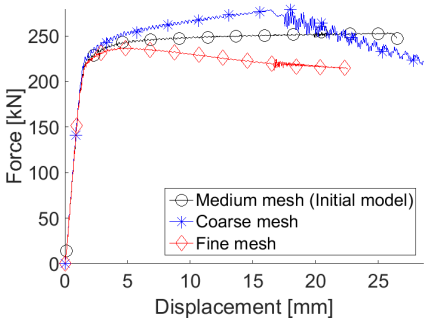

Figure 12.12: Force-displacement curves for different mesh configurations of the T120-FT FE model

T120-FT model in Figure 12.13. For the coarse and medium mesh the ratio $\frac{\text{Art. strain energy}}{\text{Internal energy}}$ is 15.4% and 13.7%, respectively. However, this ratio is only 7.33% for the fine mesh, which is acceptable when enhanced hourglass control is applied.

The maximum force observed in the fine mesh is $F_{\text{t,Ed,fine}} = 236.90\text{kN}$. This is 3.67% higher than the average force of the T120-FT laboratory tests. The lower level of artificial strain energy in the fine mesh model also leads to less disturbance in the physical response. The fine mesh is applied in the studies conducted on bolt placement and friction coefficients.

12.2.2 Friction coefficient

Due to the uncertainty concerning the friction coefficient, a study is conducted. With many surfaces in contact this may affect the physical response of the system.

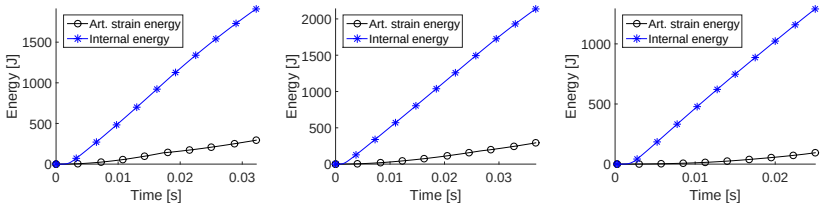

(a) Coarse mesh (b) Medium mesh (c) Fine mesh

Figure 12.13: Artificial strain energy in T120-FT model for different mesh configurations

The main focus of this parametric study is to check if a change in friction coefficient is enough to influence the physical response of the FE model. In addition to the friction coefficient, $\mu = 0.4$, used in the initial models, a frictionless model has been tested. Also a higher friction coefficient, $\mu = 0.8$, has been checked for comparison. The same coefficient is applied to the whole model through the general contact property.

The nature of the problem indicates that the sliding in the system is insignificant. The movement of the bolt inside the bolt hole is assumed to be most affected. A change in the coefficient should not affect the response of system considerably.

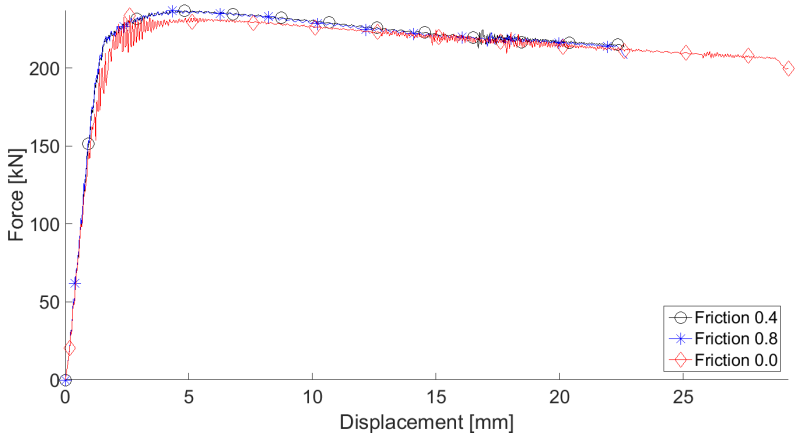

Figure 12.14: Different friction coefficients in T120-FT

The force-displacement curves for T120-FT with different friction coefficients are presented in Figure 12.14. There is little difference between $\mu = 0.4$ and $\mu = 0.8$. As expected $\mu = 0.0$ has a lower force level and a response with more disturbance.

12.2.3 Placement of bolt

According to NS-EN 1090-2 [1] the difference between the nominal diameter of the bolt hole and the nominal diameter of the bolt, referred to as the nominal clearance, should be 2mm for M16 bolts. In the initial model the bolt is placed in the middle of the bolt hole, but the nominal clearance indicates that this is not the only possible positioning of the bolt. Moving the bolt inside the hole may lead to additional bending effects and furthermore influence the tension resistance of the bolt. Figure 12.15 displays the different bolt placements considered. It is chosen to only move the bolt along the x-axis, positioning the shank in such a way that it is in contact with the flanges.

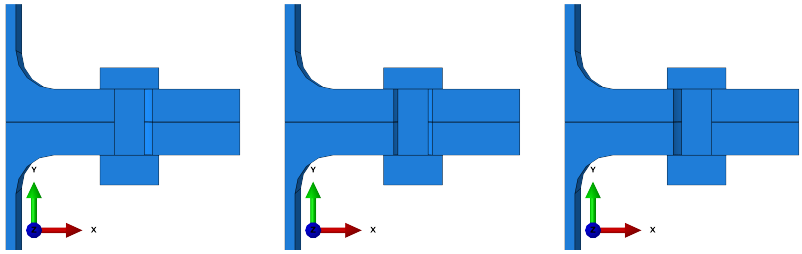

(a) Moved left (b) Not moved (initial) (c) Moved right

Figure 12.15: Bolt placements relative to bolt hole

The resulting force-displacement curves are presented in Figure 12.16. Small variations in maximum force, $F_{\mathrm{t,Ed}}$, are observed and presented in Table 12.4. The left position increases the load capacity by 3%, while the right position reduces the capacity by approximately 2%. The right position has a load capacity 1.91% higher than the average maximum load in the laboratory work.

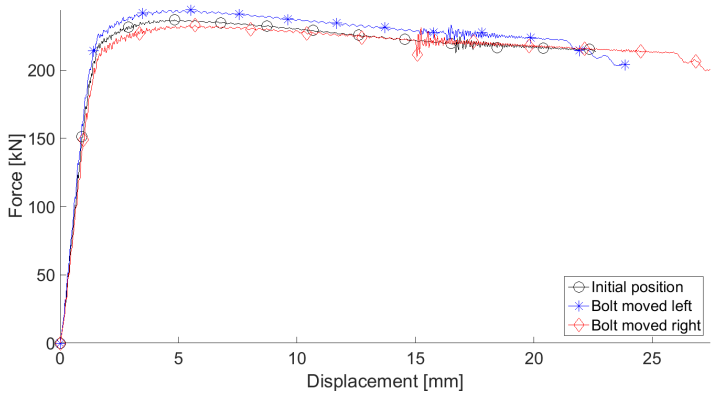

Figure 12.16: Force-displacement curves for different bolt placings

Table 12.4: Maximum forces observed for different bolt placings

	Initial position	Bolt moved left	Bolt moved right
$F_{t,Ed}$ [kN]	236.90	244.03	232.88

12.2.4 The partially threaded bolt

During the parametric study, an error made in the geometry for the initial model of the partially threaded bolt was discovered. The diameter of the effective tension area of the threaded bolt was applied to the non-threaded part of the shank, causing the diameter of the threaded part to become 11.64mm rather than 14.14mm. To correct this error an analysis with the correct dimensions was performed. For comparison an analysis using the bolt model in Figure 12.5b with the material properties of the partially threaded bolt was also performed.

Figure 12.17 displays the behaviour of the T120-PT with different bolt models and dimensions. The initial model corresponds to the initial model in Figure 12.1a, which gave an acceptable agreement with the DIC data for the corresponding configuration. The geometry used for the fully threaded bolts, denoted "FT bolt", only differs 2.95% from the maximum force observed in the initial model. The updated geometry of the partially threaded bolt yields a maximum force of 294kN, which is 17.95% higher than the initial model. Based on these observations, the geometry of the partially threaded bolts in the T120-PT and T170-PT models are changed to the same geometry used in the fully threaded models T120-FT and T170-FT when implementing the results from this para-

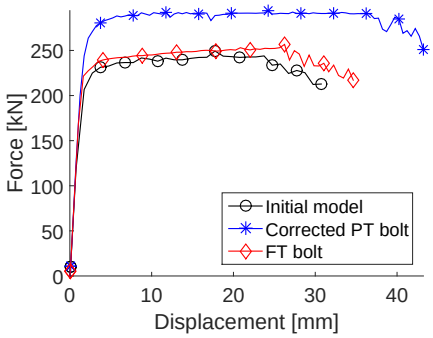

Figure 12.17: Force-displacement curves for different geometries of partially threaded bolt for the T120 joint

metric study into the final FE models in Section 12.2.5.

12.2.5 Results of final models

Based on the results from the parametric study performed, the final models may be assembled. The same changes are applied to each of the initial models. It is chosen to use the mesh refinement described in section 12.2.1 and to change the positioning of the bolt as shown in Figure 12.15c. The friction coefficient remains similar to the one used in the initial model, $\mu = 0.4$. Since the geometry of the partially threaded bolt model is similar to the geometry of the fully threaded bolt, the only difference between the models is the material properties of the bolts.

The behaviour of the final models are presented in terms of force-displacement curves in Figures 12.18 and 12.19, and maximum force level and external work in Table 12.5. The force-displacement curves from DIC analyses presented in Section 10.4 are included for comparison.

12.3 Model with threads

An attempt to include the threads in the models has been made. This threaded bolt model is based on a similar model used by Kolberg and Willand [34]. The bolts have been modelled as shown in Figure 12.20, where the geometric properties of the threads described in Appendix B are interpreted. The helical shape

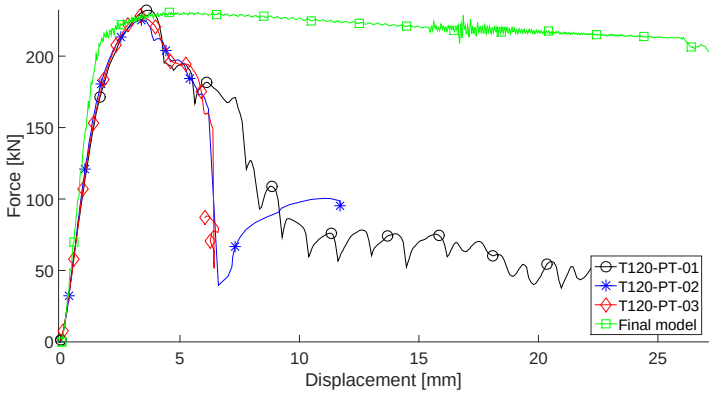

(a) Fully threaded bolt, center distance 120 mm

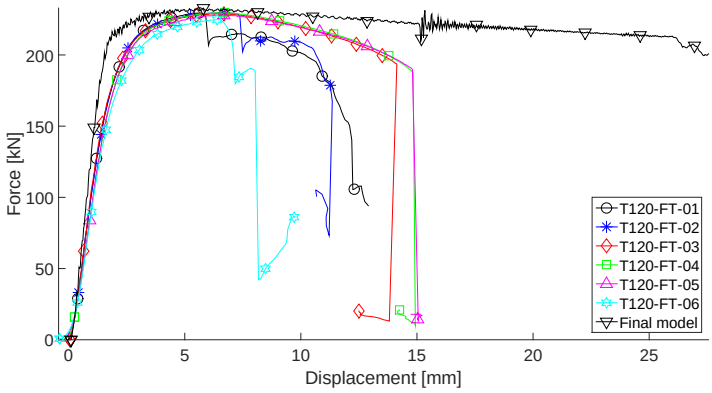

(b) Fully threaded bolt, center distance 120 mm

Figure 12.18: Force-displacement curves for final FE models

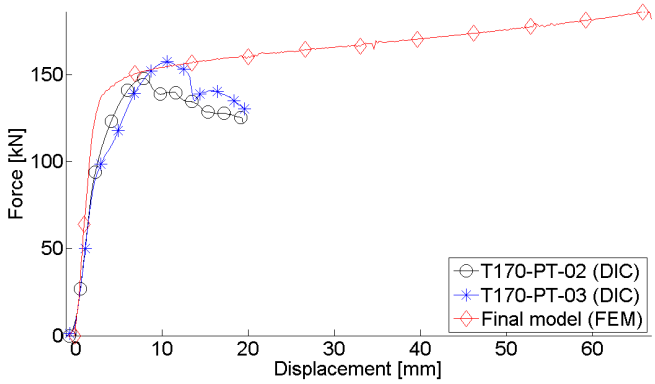

(a) Fully threaded bolt, center distance 170 mm

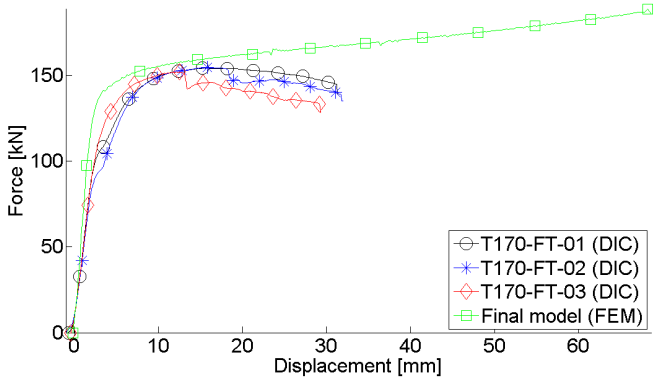

(b) Fully threaded bolt, center distance 170 mm

Figure 12.19: Force-displacement curves for final FE models

Table 12.5: Results of final FE models

Final model	$F_{t,Ed}$ [kN]	Deviation DIC average [kN]	Deviation DIC average [%]	External work [Nm]	Deviation DIC average [Nm]	Deviation DIC average [%]
T120-PT	230.07	1.97	0.864	829.74	305	58.2
T120-FT	232.88	4.37	1.91	1108.6	54.2	4.66
T170-PT	186.40	33.5	21.9	10949	9910	954
T170-FT	187.13	33.5	21.8	11311	9490	521

is neglected due to difficulties when attempting to mesh the complex geometry. Instead, circular threads are used. The bolt and nut are made out of individual parts that will be held together by use of tie constraints. This allows for different mesh sizes in different regions of the bolt and nut. All mesh sizes applied are based on the sizes used by Kolberg and Willand [34]. All other parameters remain similar to the ones in the initial models described in section 12.1. The yield stress of the nut is reduced by 15% of the yield stress of the bolt according to the results found in Part I.

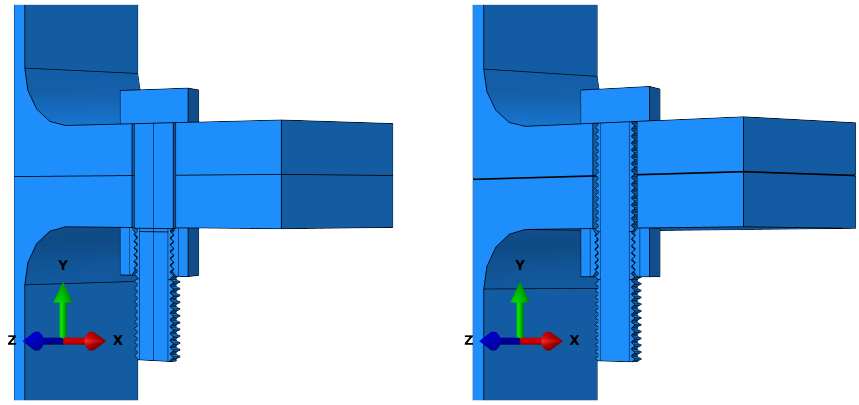

(a) Partially threaded bolt (b) Fully threaded bolt

Figure 12.20: FE models including threads for the T-stub connection with bolt hole center distance 120 mm

The full model of the T-stub connection where threads are included is very computational demanding and must be conducted on a supercomputer. Due to

the limited time span of the project there was not enough time to calibrate the mass scaling necessary to get a proper result. The analysis performed by use of the supercomputer resulted in fracture of the web subjected to loading. These results are not considered relevant and will not be discussed further.

12.4 Stiffness of the T-stub connections

Large deviation of stiffness between the laboratory tests and the numerical simulations in Section 12.1.6 calls for a closer investigation. The average stiffness, k_{av}, for each bolt hole center distance is calculated and presented in Table 12.6. The deviation between DIC and the initial FE models is 13.87% for the T120 configurations and 57.50% for the T170 configurations.

Table 12.6: Calculations of stiffness k_{av} for T-stub connections

T-stub connection	$k_{\text{av,DIC}}$ [kN/mm]	k_{av} [kN/mm]	Deviation [%]
T-120	129.6	147.5	13.87
T-170	41.57	65.52	57.50

To identify possible errors related to the FE model, the stiffness was calculated in according to NS-EN 1993-1-8 [17]. The calculations are carried out in Appendix G. As the stiffness calculations are based on the relation $n = 1.25m$, which is clearly not the case in the T170 configuration, a simplified method was also taken into consideration. The flange was then assumed to behave like a cantilever, where the prying forces were ignored. Figure 12.21 displays the deviation between the average stiffness retrieved from the numerical and experimental results compared with the calculated stiffness.

Observed in Figure 12.21 the stiffness based on calculations from NS-EN 1993-1-8 is significantly stiffer compared to the average stiffness from the numerical and experimental results for T120 and T170. The main reason for the large deviation is assumed to be the contribution from the prying forces. From the laboratory tests, a small contact surface between the flanges throughout the test was observed. This results in a reduction of the prying forces, which again results in a lower stiffness of the system. Similar behaviour was observed in the numerical simulations. The initial gap length of 0.15mm implemented between the flanges may be an important factor causing the low contact surface. Figure 12.22 displays the observed deformation at force 145kN for FE model T170 and

corresponding laboratory test. A small contact surface between the flanges appears to be in both the numerical and experimental test.

The stiffness retrieved from the simplified model, show to be too soft compared with the laboratory tests for T120. In contrast to T120, similar stiffness was observed for T170. Although a softer behaviour is predicted for the T170, the assumption of absent prying forces will be invalid, although the contribution to the stiffness is small.

Factors involving the setup of the T-stub and geometrical imperfections may also have an impact of the stiffness deviation observed in Figure 12.21. Pretension of the bolts were not applied in the tested T-stub connections . From previous work carried out by Swanson in Chapter 9, pre-tensioning of the bolts will affect the deformation of the flange. This may affect the low stiffness registered in the laboratory tests.

The tested components were carefully examined and measured before testing. In total 18 measurements of the thickness were carried out for each T-stub. Deviations of the thickness within the same T-stub flange was discovered. In T120, the thickness varied between 0.75 mm, where a deviation of 0.78 mm was registered for T170. Variations in the effective length and the bolt diameter will also affect the stiffness, as seen in the formulas for stiffness coefficients presented in Section 12.4.

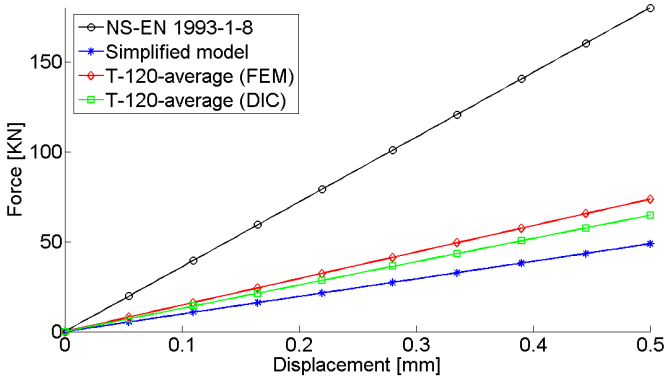

(a) T120

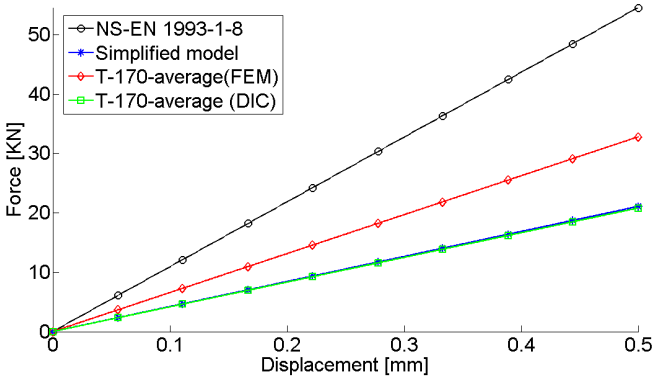

(b) T170

Figure 12.21: Stiffness comparison

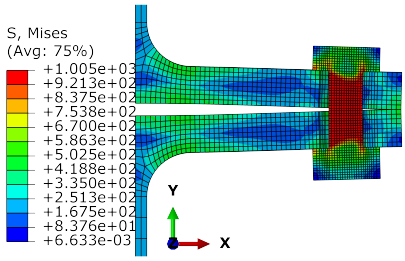

(a) FE model T170-FT

(b) DIC T170-FT

Figure 12.22: Comparison of contact surface between the flanges

13 Discussions

In Table 13.1, the design resistance, $F_{\mathrm{t,Rd}}$, calculated according to NS-EN 1993-1-8 [17], is compared to the average maximum loading observed in the laboratory, $F_{\mathrm{t,Ed}}$, and the adapted design resistance ,$F_{\mathrm{t,Rd,adapted}}$, with material properties defined in Chapter 11 and neglection of the the empirical and general partial factors. There is no difference between partially and fully threaded bolts for the two configurations. The adapted design resistance $F_{\mathrm{t,Rd,adapted}}$ provides good accuracy when predicting the maximum force in the laboratory work, only differing by $3.0 - 8.5\%$.

Table 13.1: Design loads for the T120 and T170 configurations

	$F_{\mathrm{t,Ed,DIC}}$ [kN]	$F_{\mathrm{t,Rd}}$ [kN]	$F_{\mathrm{t,Rd,adapted}}$ [kN]
T120	228	156	221
T170	153	107	140

None of the initial models of the T-stub configurations are able to represent the behaviour observed in the laboratory. Deviations are in the range $9.3 - 53.1\%$ for the maximum forces presented in Table 12.2. For the final models of the T120 configuration the deviation in maximum force is less than 2%, and for the T170 configurations it is reduced to approximately 22%, see Table 12.5. These reductions are mainly due to the mesh refinement applied in the parametric study. Also, Section 12.2.3 describes how the position of the bolt relative to the bolt hole affects the force level to some extent.

The main issue is the element sizes in the mesh. If the elements are too large they become overly stiff, hence the stress distributions will not be represented correctly. The refinement of the mesh presented in Section 12.2.1 improves the response of the FE models, especially for the T120 configurations up to maximum force.

Table 13.2: Forces in final models measured at the point of maximum forces $F_{t,Ed,DIC}$ in DIC

	F_t [kN]	Deviation DIC average [kN]	Deviation DIC average [%]	External work [Nm]	Deviation DIC average [Nm]	Deviation DIC average [%]
T170-PT	155.48	2.56	1.68	1556.0	516.83	49.73
T170-FT	160.06	6.41	4.17	2257.3	436.96	24.01

The overall behaviour of the final models for the T170 configurations does not correspond well with the behaviour observed in the laboratory work. However, up to the point of maximum force observed in the laboratory work, $F_{t,Ed,DIC}$, the deviation in force, F_t, from DIC is only 1.68% for the partially threaded and 4.17% for the fully threaded model, see Table 13.2. The complexity of the stress distribution from both tension and bending in the T170 configurations is hard to represent correctly without very small elements in the flange and bolt. When using an explicit solver this mesh refinement leads to a very small critical time step, Δt_{cr}, causing the solution to become very computational demanding.

The differences in external work presented in Table 13.2 are caused by the deviation in force and the deviation in stiffness. Recall from Section 12.4 that the stiffness in the FE model is found to be 57.5% higher than the stiffness calculated from the experimental results.

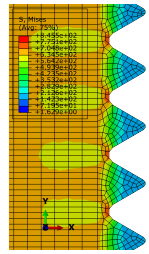

Figure 13.1: Stress concentrations in the roots of the threads

The simplified bolt geometry does also influence the behaviour of the FE models. Neglecting the threads implies that thread stripping is not possible, but it also affects the deformation pattern of the bolt. The geometry of the threaded

bolt causes stress concentrations to form in the roots of the threads, see Figure 13.1. These stress concentrations may initiate fracture of the bolt. A smooth shank will not exhibit this effect, causing the simple bolt to withstand larger deformations than the bolts in the laboratory work.

Figure 13.2 displays the deformations of the flanges for the T120-FT configuration at given points in time. The deformation of the flanges measured at the bolts are compared with measures retrieved from DIC at the time of maximum force and the time of fracture. The results are presented in Table 13.3. Similar figures and measures are presented for the T170-FT in Figure 13.3 and Table 13.4.

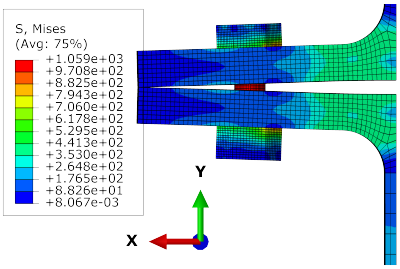

(a) Final FE model, $t = 151$ s

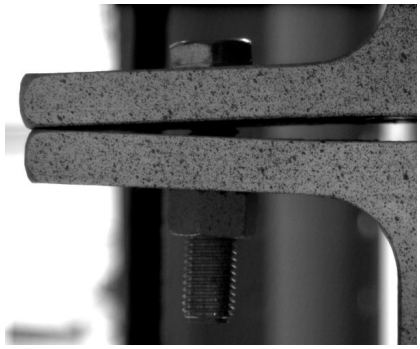

(b) T120-FT-03 (DIC), $t = 151$ s

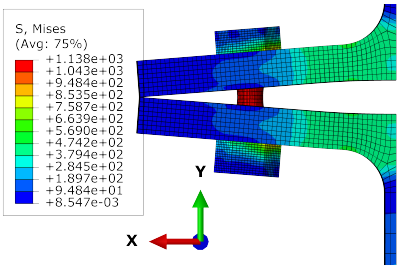

(c) Final FE model, $t = 291$ s

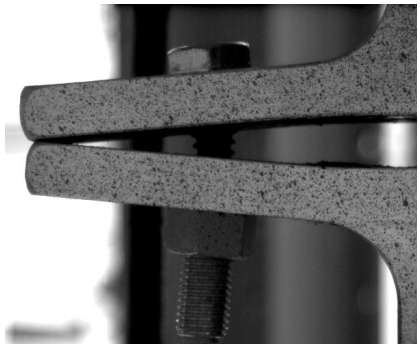

(d) T120-FT-03 (DIC), $t = 291$ s

Figure 13.2: Deformation of flanges for final FE model T120-FT and T120-FT-03

The deformations of the flanges at the position of the bolts are smaller in

Table 13.3: Vertical distance between flanges measured at the position of the left bolt for the T120-FT configuration

Given point	Model	Measured distance [mm]	Deviation DIC [mm]	Deviation DIC [%]
Maximum force $t = 151$ s	T120-FT-03 (DIC)	3.998	-	-
	Final FE model	3.070	0.928	23.21
Fracture $t = 291$ s	T120-FT-03 (DIC)	8.752	-	-
	Final FE model	7.550	1.02	13.72

Table 13.4: Vertical distance between flanges measured at the position of the left bolt for the T170-FT configuration

Given point		Measured distance [mm]	Deviation from DIC [mm]	Deviation from DIC [%]
t = 139 s	T170-FT-01 (DIC)	1.494	-	-
	Final model	1.237	0.2568	17.2
t = 383 s	T170-FT-01 (DIC)	4.827	-	-
	Final model	4.204	0.6232	12.9
t = 625 s	T170-FT-01 (DIC)	8.161	-	-
	Final model	7.130	1.031	12.6

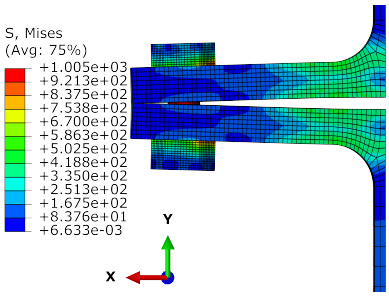

(a) Final FE model, $t = 139$ s

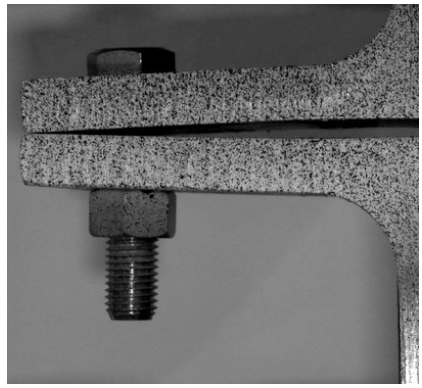

(b) T170-FT-01 (DIC), $t = 139$ s

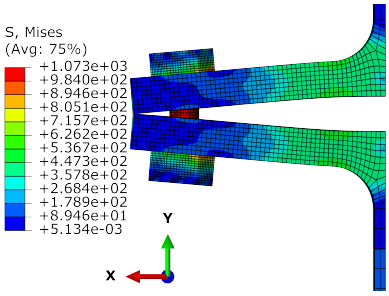

(c) Final FE model, $t = 383$ s

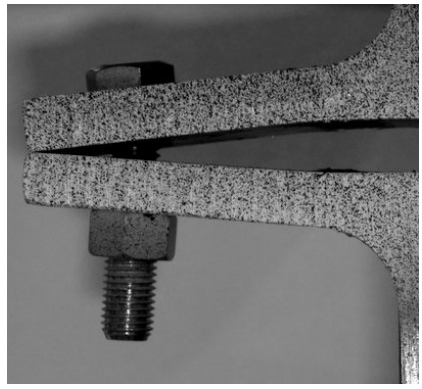

(d) T170-FT-01 (DIC), $t = 383$ s

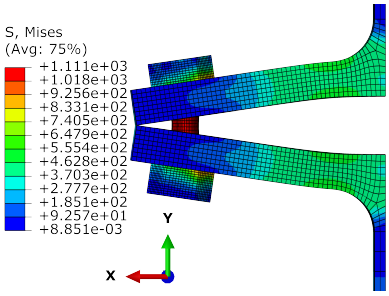

(e) Final FE model, $t = 625$ s

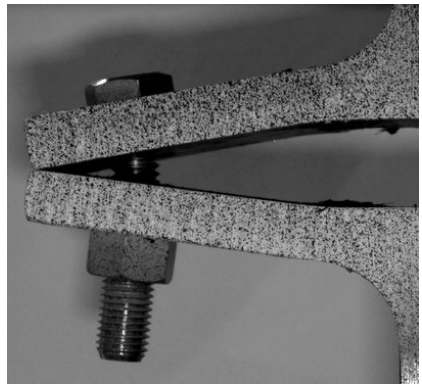

(f) T170-FT-01 (DIC), $t = 625$ s

Figure 13.3: Deformation of flanges for final FE model T170-FT and T170-FT-01

the FE models. This implies that the elements in the flanges are too large to properly represent the deformations. Elements employing linear interpolation can only represent a linear deformation between the nodes of the element. To represent a non-linear deformation between the flanges such as the one observed in the flanges in Figure 13.2d, the mesh must be very fine. Not even the finest mesh configuration tested in Section 12.2.1 is able to represent the deformations of the system correctly. An additional mesh refinement has not been considered in this thesis due to the computational requirements and the limited time span of the project.

The observation of smaller deformations of the flanges implies that the deformation of the bolts are also smaller than what is observed in the laboratory work. As discussed, the simplified bolt will withstand larger deformations than the threaded bolts before fracture. When the simplified bolt is less deformed in the FE model, even though the deformations of the flanges under the webs are similar, fracture will be initiated after much larger deformations in the finite element model.

The symmetric boundary conditions applied also indicate that the bolts are uniformly loaded. This behaviour is however not observed in the laboratory work. Furthermore, it is assumed that the disturbance in the force-displacement curves are caused by these symmetry conditions.

14 Conclusions

In the laboratory work conducted on simple T-stub connections the load capacity is similar for joints with partially and fully threaded bolts. Thread stripping is observed in all joints where partially threaded bolts have been utilized. Stripping of the threads is a brittle failure mode and leads to a less ductile behaviour of the T-stub connection. It is possible to avoid thread stripping of the partially threaded bolt by increasing the number of threads on the nut. Fully threaded bolts have exhibited both thread stripping and bolt failure, hence it is not possible to establish a certain pattern of failure modes based on the experimental work in this thesis.

The bolt center distance affects both the loading capacity and the ductility of the connection. As observed in previous studies conducted by Girão Coelho et al. [5] and Swanson et al. [7], an increase in bending effects on the bolt will reduce the load capacity of the system. Additionally, this increased bolt center distance increases the ductility. The increase in bolt center distance also leads to such large bending deformations of the bolt that an initial thread stripping is observed for both the partially and fully threaded bolts.

The finite element models are able to predict the behaviour of the joints up to maximum force for the T120 configurations. When the center distance is increased to 170 mm, the stress distribution in the bolt becomes so complex that it is difficult to represent it due to the demanding computational requirements.

14.1 Suggestions for further work

Based on the results and discussions regarding the simple T-stub connections considered in this thesis some further work is suggested.

- Based on the observations of failure mode for fully threaded bolts in the laboratory work it is not possible to verify what causes thread stripping. The experimental work in this thesis is limited in terms of configurations and number of tests. More experimental work is advised in order to gather information regarding failure modes of T-stub connections with fully threaded bolts.

- It is of great interest to find out why the force level of the T170 configurations is not reduced when the simple bolt starts to neck. Previous studies show that it is possible to get satisfactory results from the finite element model when utilizing more symmetry planes. This would reduce the size of the system, making it easier to employ additional mesh refinement without increasing the computational cost tremendously.

- The friction coefficient is assumed similar between all surfaces in the connection, but as previously mentioned, it might vary between the bolt and nut, the bolt and flange, and flange-to-flange. It is possible to check the influence of different friction coefficients between different surfaces by defining them specifically in Abaqus/Explicit. This might influence the disturbance in the responses of the finite element models.

- Further investigations of the effects of asymmetry in a simple model will help understand the asymmetry observed in the laboratory work of this thesis.

- The fully threaded finite element models presented in Section 12.3, employing the determining properties of thread stripping in Part I would give valuable insight to the behaviour of the threaded parts of the connections when subjected to both tension and bending. The case of pure tension in steel joints is rare, and a combination of loads on a threaded bolt and nut assembly causing thread stripping, and especially the initial thread stripping, is of interest. These analyses require a combination of time scaling and mass scaling, and must be conducted on a supercomputer due to the computational costs.

Bibliography

[1] NS-EN 1090-2:2008+A1:2011, Execution of steel structures and aluminium structures - Part 2: Technical requirements for steel structures, 2012.

[2] Jien-Jong Chen and Yan-Shin Shih. A study of the helical effect on the thread connection by three dimensional finite element analysis. *Nuclear Engineering and Design*, 191(2):109 – 116, 1999.

[3] JW Hobbs, RL Burguete, and EA Patterson. Investigation into the Effect of the Nut Thread Run-Out on the Stress Distribution in a Bolt Using the Finite Element Method. *ASME. J. Mech*, 125(3):527–532, 2003.

[4] H. Fransplass, M. Langseth, and O.S. Hopperstad. Numerical study of the tensile behaviour of threaded steel fasteners at elevated rates of strain. *International Journal of Impact Engineering*, 54(0):19 – 30, 2013.

[5] Ana M Girão Coelho, Luís Simões da Silva, and Frans SK Bijlaard. Finite-element modeling of the nonlinear behavior of bolted t-stub connections. *Journal of structural engineering*, 132(6):918–928, 2006.

[6] James A Swanson. *Characterization of the strength, stiffness, and ductility behavior of T-stub connections*. PhD thesis, Georgia Institute of Technology, 1999.

[7] James A Swanson, Daniel S Kokan, and Roberto T Leon. Advanced finite element modeling of bolted t-stub connection components. *Journal of Constructional Steel Research*, 58(5):1015–1031, 2002.

[8] Per Kr. Larsen. *Dimensjonering av stålkonstruksjoner*. Tapir Akademisk Forlag, 2nd edition, 2010.

[9] Reidar Bjorhovde, André Colson, and Riccardo Zandonini. In *Connections in Steel Structures*, pages xii – xiii. Pergamon, Oxford, 1996.

[10] Hilde Ersland. Endeplateskjøt for hulprofiler. Master's thesis, Norwegian University of Science and Technology, 2011.

[11] Egil Fagerholt. Field Measurements in Mechanical Testing Using Close-Range Photogrammetry and Digital Image Analysis. 2011.

[12] O.S. Hopperstad and T. Børvik. Materials mechanics part1. University Lecture, 2013.

[13] Aase G. Roberg Reyes. Uniaxial behaviour. University Lecture, 2006.

[14] Aase G. Roberg Reyes. General stress-strain relations. University Lecture, 2006.

[15] Y. Bai, X. Teng, and T. Wierzbicki. Application of Stress Triaxiality Formula for Plane Strain Fracture Testing. *ASME. J. Eng. Mater. Technol.*, (021002-021002-10), 2009.

[16] Mohammad Mashayekhi. Element selection criteria. University Lecture.

[17] NS-EN 1993-1-8:2005+NA:2009 Eurocode 3: Design of steel structures - Part 1-8: Design of joints, 2009.

[18] E. Alexander. Analysis and design of threaded assemblies. *SAE Technical Paper*, (770420), 1977.

[19] Svein I. Sørensen and Jan Arve Øverli. *TKT4222 Concrete Structures 3, Compendium.* Department of Structural Engineering, NTNU.

[20] Bing Pan, Kemao Qian, Huimin Xie, and Anand Asundi. Two-dimensional digital image correlation for in-plane displacement and strain measurement: a review. *Measurement Science and Technology*, 20(6):062001, 2009.

[21] NS-EN 1993-1-1:2005+na:2008 Eurocode 3: Design of steel structures - part 1-1: General rules and rules for, 2008.

[22] Yun Ling. Uniaxial true stress-strain after necking. *AMP Journal of Technology*, 5, 1996.

[23] George E. Jr. Dieter. *Mechanical Metallurgy.* Mc Grow-Hill Book Company, 1961.

[24] G. Le Roy, G.E. Embury, and M.F. Ashby. A model of ductile fracture based on the nucleation and growth of voids. *Acta Metallurgica*, 29(8):1509–1522, 1981.

[25] Robert D. Cook, David S. Malkus, Michael E. Plesha, and Robert J. Witt. *Concepts and applications of finite element analysis.* John Wiley & Sons, INC, 4th edition, 2002.

[26] J. P. Den Hartod. The mechanics of plate rotors for turbo-generators. *Trans ASME*, (APM S1-1):1–10, 1929.

[27] D. G. Sopwith. The distribution of load in screw threads. *Proceedings of the Institution of Mechanical Engineers*, 159(1):373–383, 1948.

[28] ISO 68-1:1998, ISO general purpose screw threads – Basic profile – Part 1: Metric screw threads, 1998.

[29] ISO 965-1:2013, ISO general purpose metric screw threads – Tolerances – Part 1: Principles and basic data , 2013.

[30] NS-EN ISO 4014:2011, Hexagon head bolts - Product grades A and B, 2011.

[31] Kjell Magne Mathisen. Solution of the nonlinear dynamic equilibrium equations. University Lecture.

[32] Kjell Magne Mathisen. Solution methods for contact problems. University Lecture.

[33] Quasi-static Analysis abaqus inc. `http://imechanica.org/files/l5-quasi-static.pdf`. Accessed: 2015-02-15.

[34] Bendik M Kolberg and Eirik T Willand. Behaviour and Modelling of Bolted Connectors in Road Safety Barriers. Master's thesis, Norwegian University of Science and Technology, 2014.

[35] H. Fransplass, M. Langseth, and O.S. Hopperstad. Tensile behaviour of threaded steel fasteners at elevated rates of strain. *International Journal of Mechanical Sciences*, 53(11):946 – 957, 2011.

[36] OS Bursi and Jean-Pierre Jaspart. Benchmarks for finite element modelling of bolted steel connections. *Journal of Constructional Steel Research*, 43(1):17–42, 1997.

[37] Stahlbauzeichnungen. SZS Pub. B2, Zürich 1980.

[38] Per Kr. Larsen, Arild H. Clausen, and Arne Aalberg. Stålkonstruksjoner: profiler og formler, 2003.

[39] NS-EN ISO 898-1:2013, Mechanical properties of fasteners made of carbon steel and alloy steel - Part 1: Bolts, screws and studs with specified property classes - Coarse thread and fine pitch thread, 2013.

[40] Dassult Systemes. Abaqus Analysis User's Guide, 2015.

Appendices

Appendix A: Corretions of elongation retrived from DIC

This appendix presents the corrections assosiated with the retrived elongation from DIC. As the elongation vector was applied on the middle of the nut and the bolt head, and not at the grip length, the retrieved elongation had to be corrected. The contribution from the bolt and the nut were therefore measured at the initial and final image, and then subtracted from the final displacement. Figure 1 illustrate the measured lengths, C1 and C2, which are listed in Table 1.

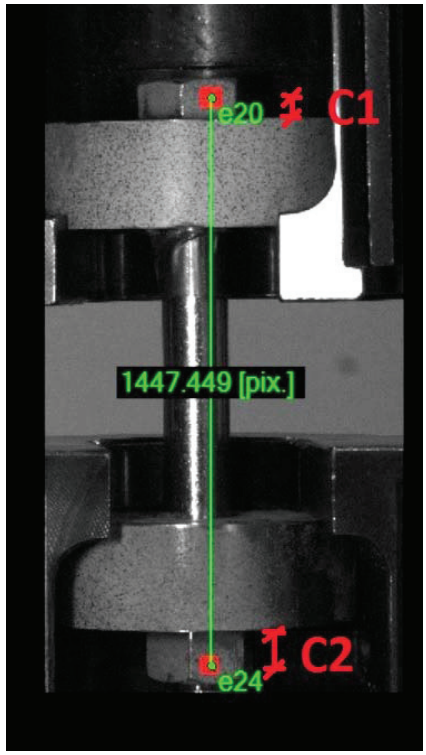

Figure 1: Measured elongation

Test	C1 start	C1 end	C2 start	C2 end
	[pix]	[pix]	[pix]	[pix]
DG-118-04	54.718	53.223	67.721	64.395
DG-118-05	55.871	56.704	72.377	71.861
DG-122-21	50.605	50.605	67.442	65.698
DG-122-22	62.58	61.209	68.282	68.283
DG-130-14	46.993	47.767	65.907	65.304
DG-130-15	48.967	48.047	67.202	64.311
DG-141-09	50.831	51.803	76.546	78.459
DG-141-10	52.48	51.907	68.352	68.985
FG-118-26	51.72	50.128	49.193	49.927
FG-118-27	52.824	50.007	64.631	62.813
FG-141-31	41.462	38.481	72.688	72.888
FG-141-32	48.007	46.256	72.329	73.422

Table 1: Measured distance C1 and C2 from DIC.

With kown diameter of the bolt tests, the contribution from the nut and the bolt head was converted from pixel to mm, as calculated in Table 2. Table 3 shows the final contribution from the nut and bolt head.

Test	Diameter [pix]	Diameter [mm]	Ratio [mm/pix]
DG-118-04	172.032	15.88	0.092308408
DG-118-05	171.825	15.82	0.09207042
DG-122-21	172.885	15.87	0.091795124
DG-122-22	172.207	15.87	0.092156533
DG-130-14	173.13	15.85	0.091549703
DG-130-15	172.488	15.85	0.09189045
DG-141-09	172.745	15.84	0.091695852
DG-141-10	173.603	15.86	0.091357868
FG-118-26	172.664	15.84	0.091738869
FG-118-27	171.098	15.85	0.092636968
FG-141-31	171.745	15.84	0.092229759
FG-141-32	170.399	15.82	0.09284092

Table 2: Convertion ratio

Test	C1 [pix]	C2 [pix]	Total displacement [pix]	Total displacement [mm]
DG-118-04	-1.495	-3.326	-4.821	-0.4450
DG-118-05	0.833	-0.516	0.317	0.0292
DG-122-21	0	-1.744	-1.744	-0.1601
DG-122-22	-1.371	0.001	-1.37	-0.1263
DG-130-14	0.774	-0.603	0.171	0.0157
DG-130-15	-0.92	-2.891	-3.811	-0.3502
DG-141-09	0.972	1.913	2.885	0.2645
DG-141-10	-0.573	0.633	0.06	0.0055
FG-118-26	-1.592	0.734	-0.858	-0.0787
FG-118-27	-2.817	-1.818	-4.635	-0.4294
FG-141-31	-2.981	0.2	-2.781	-0.2565
FG-141-32	-1.751	1.093	-0.658	-0.0611

Table 3: Final contribution from the nut and the bolt head.

Appendix B: Geometry of the bolts

This appendix present the geometry of the bolts, M16x160. The geometry is based on measurements of the bolts carried out in the laboratory using a micrometer, in addition to specifications described in ISO 68-1. The average measurements were utilized in the numerical simulations, and will be presented in this appendix.

Global geometry, carried out from the laboratory tests:

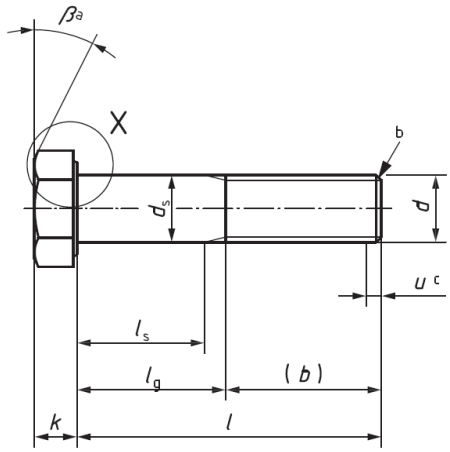

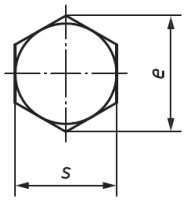

General geometry:

Wrench size: $s := 24\text{mm}$

Bolt diameter: $d_b := 15.85\text{mm}$

Bolt head height: $h_b := 14.20\text{mm}$

Nut height: $k := 10\text{mm}$

Nut minor diameter: $D_1 := 14.06\text{mm}$

Number of threads in the nut: $n_t := 7$

Specific geometry:

	M16x160 PT bolt:	M16x160 FT bolt:
Length of threaded part:	$b_{PT160} := 44mm$	$b_{FT160} := 160mm$
Length of unthreaded part:	$l_{g.PT160} := 116mm$	$l_{g.FT160} := 0mm$
Number of threads:	$n_{t.PT160} := 22$	$n_{t.FT160} := 80$

	M16x70 PT bolt:	M16x70 FT bolt:
Length of threaded part:	$b_{PT70} := 32mm$	$b_{FT70} := 70mm$
Length of unthreaded part:	$l_{g.PT70} := 38mm$	$l_{g.FT70} := 0mm$
Number of threads:	$n_{t.PT70} := 16$	$n_{t.FT70} := 35$

Local geometry, carried out from ISO 68-1:

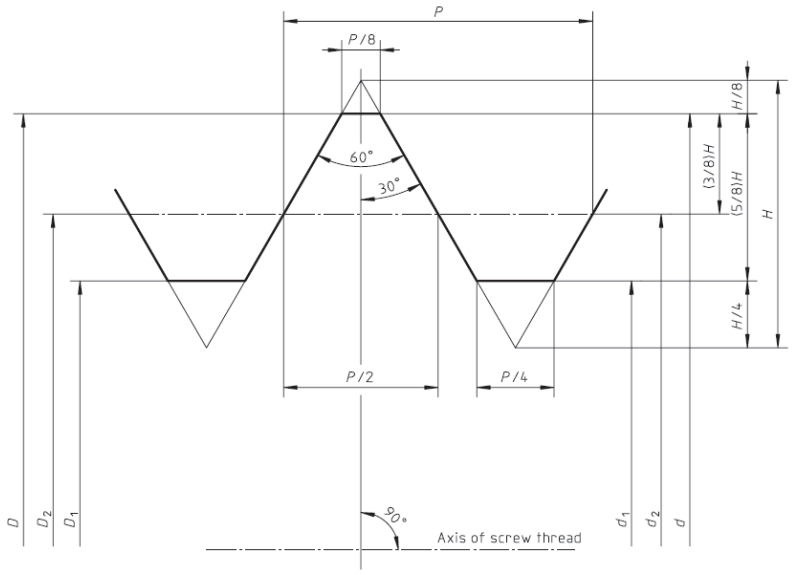

where

D	is the basic major diameter of internal thread (nominal diameter)
d	is the basic major diameter of external thread (nominal diameter)
D_2	is the basic pitch diameter of internal thread
d_2	is the basic pitch diameter of external thread
D_1	is the basic minor diameter of internal thread
d_1	is the basic minor diameter of external thread
H	is the height of fundamental triangle
P	is the pitch

Figure 3: Description of geometry of the threads

ISO 68-1 gives the relation between the pitch, P, and the height, H, of the thread;

$$P := 2mm$$

$$H := \frac{\sqrt{3}}{2} \cdot P$$

The threads are not as lined as shown in Figure 3. The rounded edges are taken into account in ISO 965-1, where a minimum root radius is presented. From table 14 in ISO 965-1, the minimum root radius is 250µm. The ideal radius can often be set to H/6, and is used in our calculation. Figure 4 illustrate the final geometry of the threaded assembly.

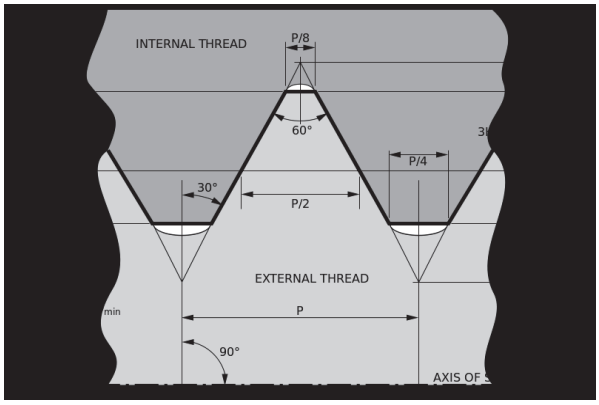

Figure 4: final geometry of the internal and external threads

Appendix C: Nut geometry

This appendix presents the nut geometry of a nut cut in half. This investigation was carried out as there was no sufficient measuring instrument for finding the physical geometry of the threads. Photo editing software was utilized to retrieve the measured heights. These measurements provide the basis for further studies carried out for single bolts.

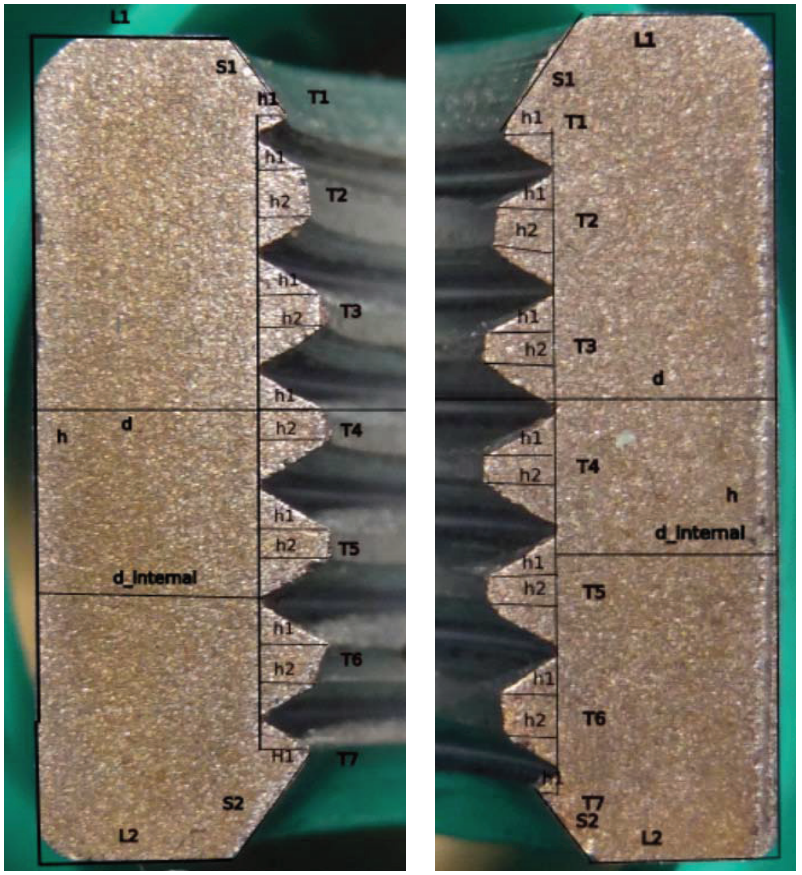

a) Left side of measured nut (LS) b) Right side of measured nut (RS)

Figure 1: Nut measurements

Thread	T1	T2	T3	T4	T5	T6	T7
h1 [mm]	0.48535823	0.77450934	0.97609101	1.03442286	1.12550367	1.05842921	0.74863981
h2 [mm]	-	0.78905647	1.12722352	1.15201814	1.12557533	0.84015058	0.75035966
Pitch [mm]	-	2.00349112	2.029074	2.02384277	2.02312616	2.09622012	-

Table 1: Measurements of each thread at left side of nut

Thread	T1	T2	T3	T4	T5	T6	T7
h1 [mm]	0.77393605	1.06602525	1.10250057	1.02216887	0.86157714	0.2847798	0.2847798
h2 [mm]	-	1.10916502	1.12442876	1.06595359	0.83241122	0.65182614	-
Pitch [mm]	-	2.00857903	2.02914566	2.00843571	2.03939315	2.0186832	-

Table 2: Measurements of each thread at right side of nut

Measurements in unit mm	LS	RS	Average
L1	3.344	2.921	3.132
L2	3.315	2.980	3.147
L average	3.329	2.950	3.140
h	14.427	14.079	14.253
S1	0.871	1.934	1.403
S2	2.360	1.478	1.919
d	-	-	23.715
d_internal	3.885	3.565	3.725

Table 3: comparison of the measurements on right and left side of nut

	LS	RS	Average
Average height of T3-T5 [mm]	1.090	1.082	1.086
Average height of T2,T6 [mm]	0.866	0.822	0.844
Average height of T2,T6 [%]	79	76	78
Average height of T1, T9 [mm]	0.617	0.529	0.573
Average heigh of T1,T7 [%]	57	49	53

Table 4: Comparison of thread heights

Appendix D: Load capacity calculations

This appendix present the calculations of load capacity developed by Alexander. The calculations are based on the same assumptions used in the numerical analyses regarding geometry and nut strength, where a nut strength reduction of 15% is used.

Geometry

Pitch size: $P := 2mm$

Height of thread triangle: $H := \sqrt{3} \cdot \frac{P}{2} = 1.732 \cdot mm$

Root radius: $R := \frac{H}{6} = 0.289 \cdot mm$

Nut height: $m := 14.196mm$

Length of bell mounted section: $LB := \frac{m - 5 \cdot P}{2} = 2.098 \cdot mm$

Minor nut diameter: $D_1 := 14.06mm$

Major nut diameter: $D := D_1 + \frac{2 \cdot 5 \cdot H}{8} = 16.225 \cdot mm$

Basic pitch nut diameter: $D_2 := D - \frac{2 \cdot 3 \cdot H}{8} = 14.926 \cdot mm$

Design countersink diameter: $D_c := 1.08 \cdot D = 17.523 \cdot mm$

Mean diameter of Bell Mounted section: $D_m := \frac{D + D_1}{2} = 15.143 \cdot mm$

Basic major bolt diameter: $d := 15.85mm$

Basic minor bolt diameter: $d_1 := d - \frac{2 \cdot 5 \cdot H}{8} = 13.685 \cdot mm$

Basic pitch bolt diameter: $d_2 := d - \frac{2 \cdot 3 \cdot H}{8} = 14.551 \cdot mm$

Minor bolt diameter: $d_3 := d_1 - \frac{H}{6} = 13.396 \cdot mm$

Ultimate tensile strength for PT bolt: $\sigma_{sPT} := 917\text{MPa}$

Ultimate tensile strength for PT nut: $\sigma_{nPT} := 917\text{MPa}\cdot 0.85 = 779.45\cdot\text{MPa}$

Ultimate tensile strength for FT bolt: $\sigma_{sFT} := 804.9\text{MPa}$

Ultimate tensile strength for FT nut: $\sigma_{nFT} := 804.9\text{MPa}\cdot 0.85 = 684.165\cdot\text{MPa}$

Width across flats: $s := 24\text{mm}$

Tolerance for basic minor diameter,nut: $T_{D1} := 0.475\text{mm}$

Tensile stress area: $A_s := \frac{\pi}{4}\cdot\left(\frac{d_2 + d_3}{2}\right)^2 = 153.358\cdot\text{mm}^2$

$A_{si} := 0.78540\cdot\left(d_2 - 0.43301\cdot P + R\right)^2 = 153.359\cdot\text{mm}^2$

Length of threaded engagement: $LE := m - \left(D_c - D_1 - T_{D1}\right)\cdot 0.6 = 12.403\cdot\text{mm}$

Shear area for bolt threads: $AS_{s1} := \left(\frac{LE - LB}{P}\right)\cdot\pi\cdot D_1\cdot\left[\left(\frac{P}{2}\right) + \frac{\left(d_2 - D_1\right)}{\sqrt{3}}\right] = 292.106\cdot\text{mm}^2$

$AS_{s2} := \left(\frac{LB}{P}\right)\cdot\pi\cdot D_m\cdot\left[\left(\frac{P}{2}\right) + \left(\frac{d_2 - D_m}{\sqrt{3}}\right)\right] = 32.859\cdot\text{mm}^2$

$AS_s := AS_{s1} + AS_{s2} = 324.965\cdot\text{mm}^2$

Shear area for nut threads: $AS_n := \left(\frac{LE}{P}\right)\cdot\pi\cdot d\cdot\left[\left(\frac{P}{2}\right) + \frac{\left(d - D_2\right)}{\sqrt{3}}\right] = 473.536\cdot\text{mm}^2$

Strength ratio: $R_{s.PT} := \frac{\sigma_{nPT}\cdot AS_n}{\sigma_{sPT}\cdot AS_s} = 1.239$

$R_{s.FT} := \frac{\sigma_{nFT}\cdot AS_n}{\sigma_{sFT}\cdot AS_s} = 1.239$

Strength reduction factors:

$$\text{ratio} := \frac{s}{D} = 1.479$$

For $1.4 \le \frac{s}{D} < 1.9$ the reduction factor C1 is

$$C_1 := -\left(\frac{s}{D}\right)^2 + 3.8\cdot\left(\frac{s}{D}\right) - 2.61 = 0.823$$

For $1 < R_s \le 2.2$ the reduction factor C2 is

$$C_{2.PT} := 5.594 - 13.682\cdot R_{s.PT} + 14.107\cdot R_{s.PT}^{\ 2} - 6.057\cdot R_{s.PT}^{\ 3} + 0.9353\cdot R_{s.PT}^{\ 4} = 0.981$$

$$C_{2.FT} := 5.594 - 13.682\cdot R_{s.FT} + 14.107\cdot R_{s.FT}^{\ 2} - 6.057\cdot R_{s.FT}^{\ 3} + 0.9353\cdot R_{s.FT}^{\ 4} = 0.981$$

and for $R_s \ge 1$ gives the reduction factor

$$C_3 := 0.897$$

Load capacity for PT bolts:

Bolt breaking load: $F_{bb.PT} := \sigma_{sPT}\cdot A_{si} = 140.63\cdot kN$

Bolt stripping load: $F_{bs.PT} := \sigma_{sPT}\cdot AS_s\cdot C_1\cdot C_{2.PT}\cdot 0.6 = 144.396\cdot kN$

Nut stripping load: $F_{ns.PT} := \sigma_{nPT}\cdot AS_n\cdot C_1\cdot C_3\cdot 0.6 = 163.472\cdot kN$

Load capacity for FT bolts:

Bolt breaking load: $F_{bb.FT} := \sigma_{sFT}\cdot A_{si} = 123.438\cdot kN$

Bolt stripping load: $F_{bs.FT} := \sigma_{sFT}\cdot AS_s\cdot C_1\cdot C_{2.FT}\cdot 0.6 = 126.744\cdot kN$

Nut stripping load: $F_{ns.FT} := \sigma_{nFT}\cdot AS_n\cdot C_1\cdot C_3\cdot 0.6 = 143.488\cdot kN$

Appendix E: Calculation of effective length of the T-stub connections

This appendix presents the calculations of the effective length of a T-stub connection in accordance to Eurocode NS-EN 1993-1-8.

Geometry HEB 220

General for both T-stub connection series

Length of T-stub connection 1 and 2: $L := 100\text{mm}$

Width of T-stub connection: $b := 220\text{mm}$

Thickness of web $t_w := 9.6\text{mm}$

Thickness of flange $t_f := 16\text{mm}$

Radius of milled T-stub connection: $r := 18\text{mm}$

T-120

Distance between the bolts: $w_{120} := 120\text{mm}$ — Profiler og formler: Table 1.3

Distance between the bolt and the milled flange: $m_{120} := \left[\frac{\left(w_{120} - t_w\right)}{2}\right] - 0.8 \cdot r = 40.8 \cdot \text{mm}$ — EC3-1-8: Figure 6.8a

Distance between bolt and the horizontal edge: $e_{120} := \frac{\left(b - w_{120}\right)}{2} = 50 \cdot \text{mm}$

Distance between the bolt and the vertical edge: $e_{1\_120} := \frac{L}{2} = 50 \cdot \text{mm}$

Distance from bolt to edge: $n_{120} := \min\left(e_{120}, 1.25 \cdot m_{120}\right) = 50 \cdot \text{mm}$

T-170

Distance between the bolts in T-170: $w_{170} := 170\text{mm}$ — Profiler og formler: Table 1.3

Distance between the bolt and the milled flange: $m_{170} := \left[\frac{\left(w_{170} - t_w\right)}{2}\right] - 0.8 \cdot r = 65.8 \cdot \text{mm}$ — EC3-1-8: Figure 6.8a

Distance between bolt and the horizontal edge: $e_{170} := \frac{\left(b - w_{170}\right)}{2} = 25 \cdot \text{mm}$

Distance between the bolt and the vertical edge: $e_{1\_170} := \frac{L}{2} = 50 \cdot mm$

Distance from bolt to edge: $n_{170} := \min\left(e_{170}, 1.25 \cdot m_{170}\right) = 25 \cdot mm$

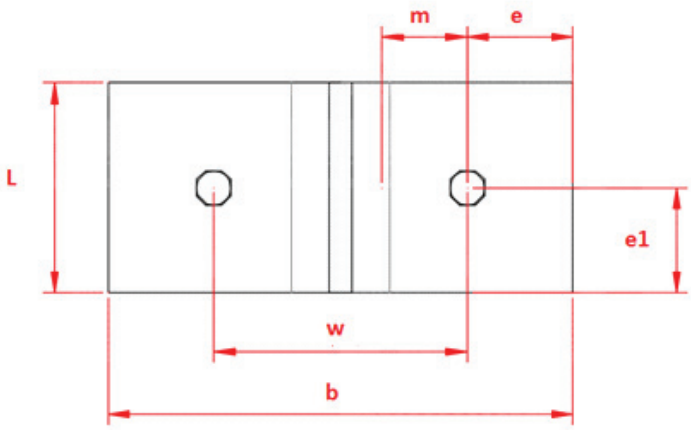

Figure 1: AutoCAD illustration of the top flange seen above

Material S355

The values for yield stress of the S355 material and the ultimate tensile stress of the bolts are based on pervious observations

Yield stress: $f_y := 400 \frac{N}{mm^2}$

Material factors: $\gamma_{M0} := 1.05 \quad \gamma_{M1} := 1.05 \quad \gamma_{M2} := 1.25$

Bolt M16 with property class 8.8

Cross section area: $A_{s.bolt} := 157 mm^2$

Profiler og formler: Table 6.1

Ultimate stress: $f_{ub} := 950 \frac{N}{mm^2}$

Bolt tension capacity

$k_2 := 0.9$

$F_{t.Rd} := \frac{\left(k_2 \cdot f_{ub} \cdot A_{s.bolt}\right)}{\gamma_{M2}} = 107.388 \cdot kN$ EC3-1-8: Table 3.4

Effective length of the T-stub

EC3-1-8: Table 6.4

Circular pattern:

$l_{eff.cp120} := \min\left(2 \cdot \pi \cdot m_{120}, \pi \cdot m_{120} + 2 \cdot e_{1\_120}\right) = 228.177 \cdot mm$

$l_{eff.cp170} := \min\left(2 \cdot \pi \cdot m_{170}, \pi \cdot m_{170} + 2 \cdot e_{1\_170}\right) = 306.717 \cdot mm$

Noncircular pattern:

$l_{eff.nc120} := \min\left(4 \cdot m_{120} + 1.25 \cdot e_{120}, 2 \cdot m_{120} + 0.625 \cdot e_{120} + e_{1\_120}\right)$

$l_{eff.nc120} = 162.85 \cdot mm$

$l_{eff.nc170} := \min\left(4 \cdot m_{170} + 1.25 \cdot e_{170}, 2 \cdot m_{170} + 0.625 \cdot e_{170} + e_{1\_170}\right)$

$l_{eff.nc170} = 197.225 \cdot mm$

$l_{eff.1\_120} := \min\left(l_{eff.nc120}, l_{eff.cp120}, L\right) = 100 \cdot mm$

$l_{eff.2\_120} := \min\left(l_{eff.nc120}, L\right) = 100 \cdot mm$

$l_{eff.1\_170} := \min\left(l_{eff.nc170}, l_{eff.cp170}, L\right) = 100 \cdot mm$

$l_{eff.2\_170} := \min\left(l_{eff.nc170}, L\right) = 100 \cdot mm$

Capacity of the T-stub connections

EC3-1-8: Table 6.2

As the effective length has been identified, the design loads can be calculated, and failure mode registered.

Failure Mode 1

T -120:

$$M_{pl.1.120.Rd} := 0.25 \cdot l_{eff.1\_120} \cdot t_f^2 \cdot \frac{f_y}{\gamma_{M0}} = 2.438 \cdot kN \cdot m$$

$$F_{T.1.120.Rd} := 4 \cdot \frac{M_{pl.1.120.Rd}}{m_{120}} = 239.029 \cdot kN$$

T - 170:

$$M_{pl.1.170.Rd} := 0.25 \cdot l_{eff.1\_170} \cdot t_f^2 \cdot \frac{f_y}{\gamma_{M0}} = 2.438 \cdot kN \cdot m$$

$$F_{T.1.170.Rd} := 4 \cdot \frac{M_{pl.1.170.Rd}}{m_{170}} = 148.212 \cdot kN$$

Failure Mode 2

T - 120:

$$M_{pl.2.120.Rd} := 0.25 \cdot l_{eff.2\_120} \cdot t_f^2 \cdot \frac{f_y}{\gamma_{M0}} = 2.438 \cdot kN \cdot m$$

$$F_{T.2.120.Rd} := \frac{\left(2 \cdot M_{pl.2.120.Rd} + n_{120} \cdot 2 \cdot F_{t.Rd}\right)}{m_{120} + n_{120}} = 171.971 \cdot kN$$

T - 170:

$$M_{pl.2.170.Rd} := 0.25 \cdot l_{eff.2\_170} \cdot t_f^2 \cdot \frac{f_y}{\gamma_{M0}} = 2.438 \cdot kN \cdot m$$

$$F_{T.2.170.Rd} := \frac{\left(2 \cdot M_{pl.2.170.Rd} + n_{170} \cdot 2 \cdot F_{t.Rd}\right)}{m_{170} + n_{170}} = 112.837 \cdot kN$$

Failure Mode3

T - 120 and T- 170:

$$F_{T.3.Rd} := 2 \cdot F_{t.Rd} = 214.776 \cdot kN$$

Conclusions

For both configurations of the T-stub connection, failure mode 2 will occur with a design load of 171.9 KN for T-120 and 122.8KN for T-170.

Sketches of the T-stub

Front view for both T -120 and T- 170

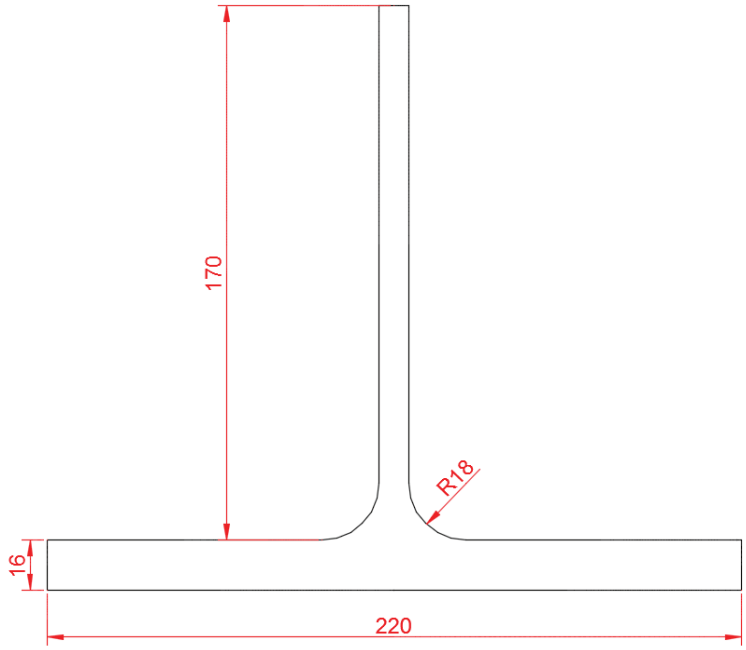

Top view for T-120

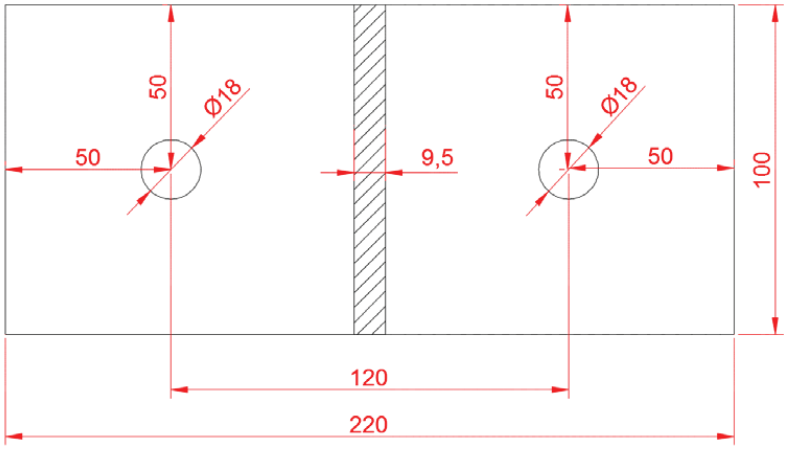

Top view for T-170

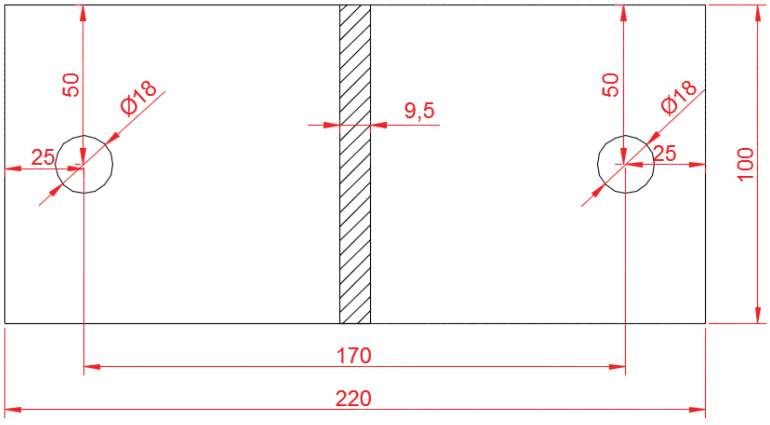

Appendix F: T-stub geometry

This appendix presents the geometry of the T-stub connections tested in the laboratory work. The sketches are also used as a basis for the geometry of the finite element models. All measures provided are in millimetre.

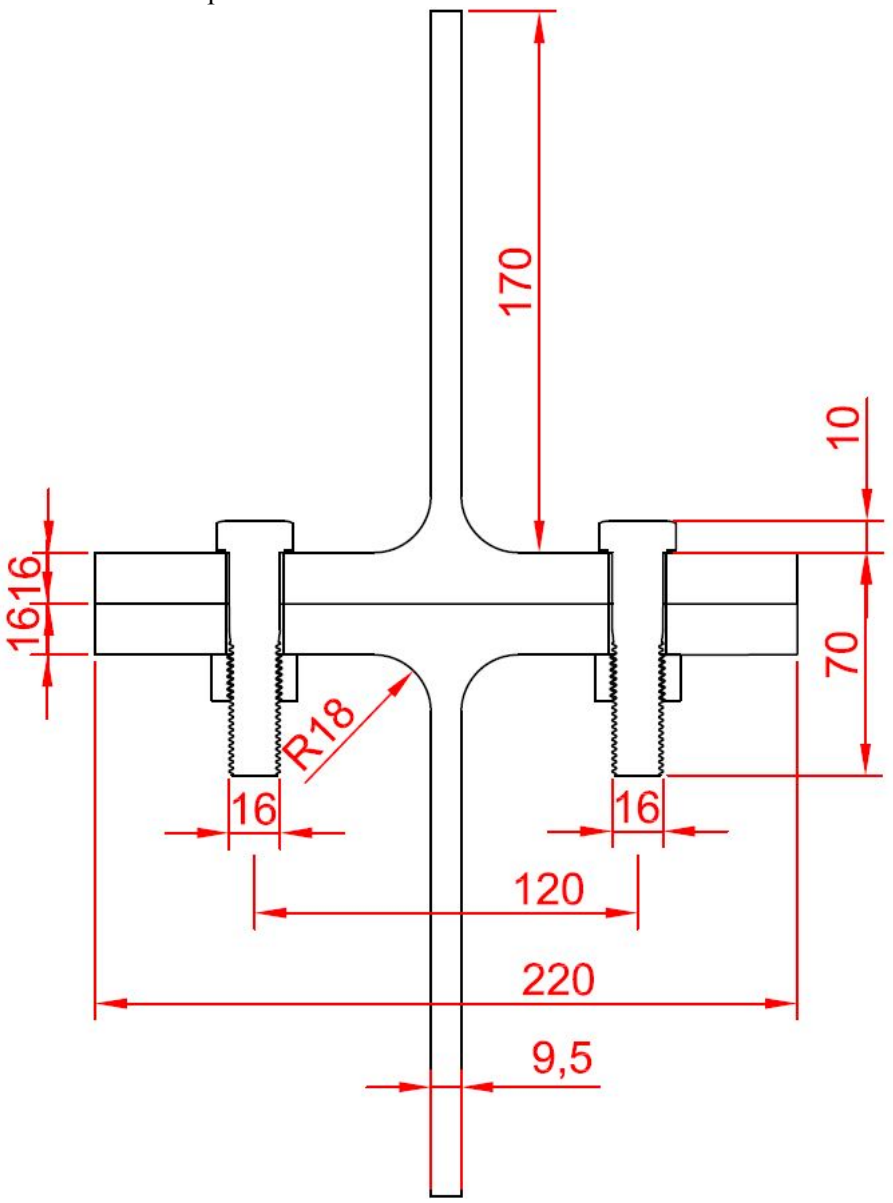

T120-PT: Center distance 120 mm, partially threaded bolts, one nut

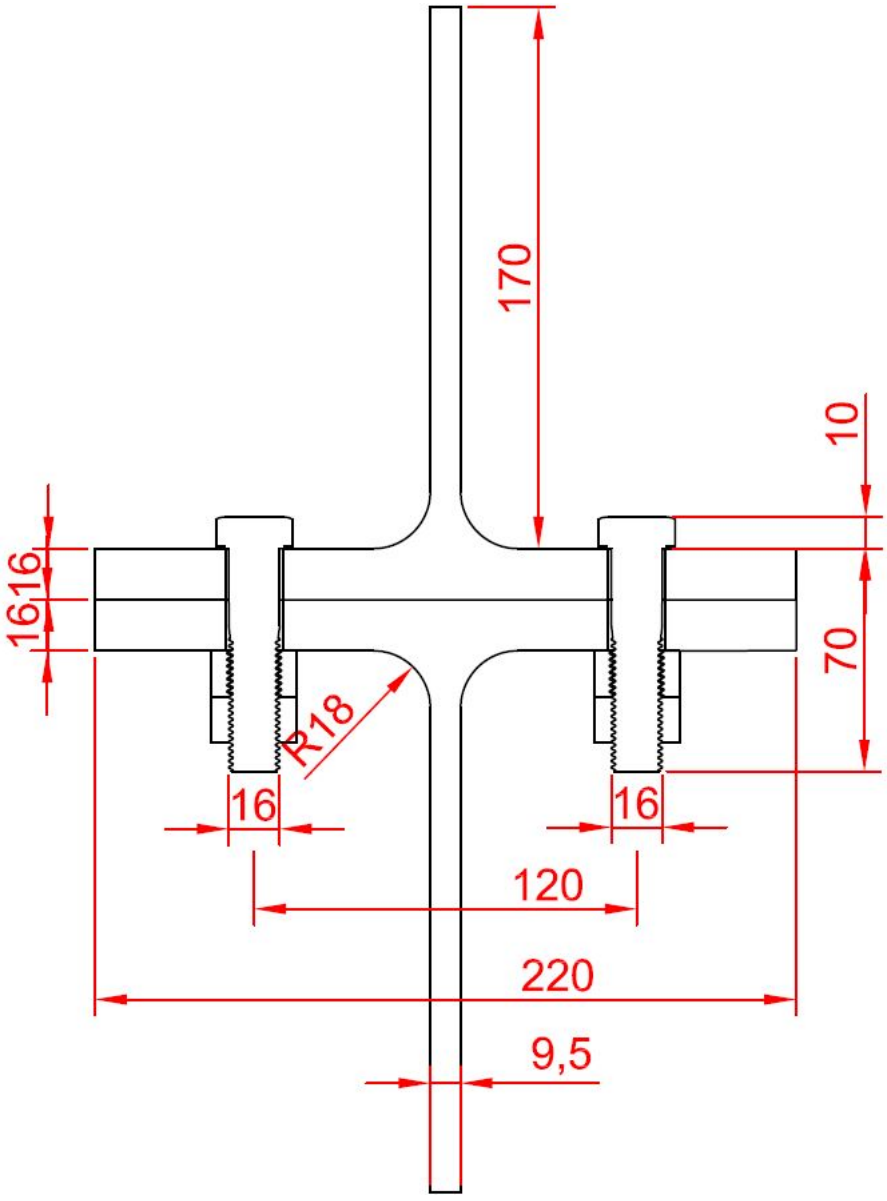

T120-PT: Center distance 120 mm, partially threaded bolts, two nuts

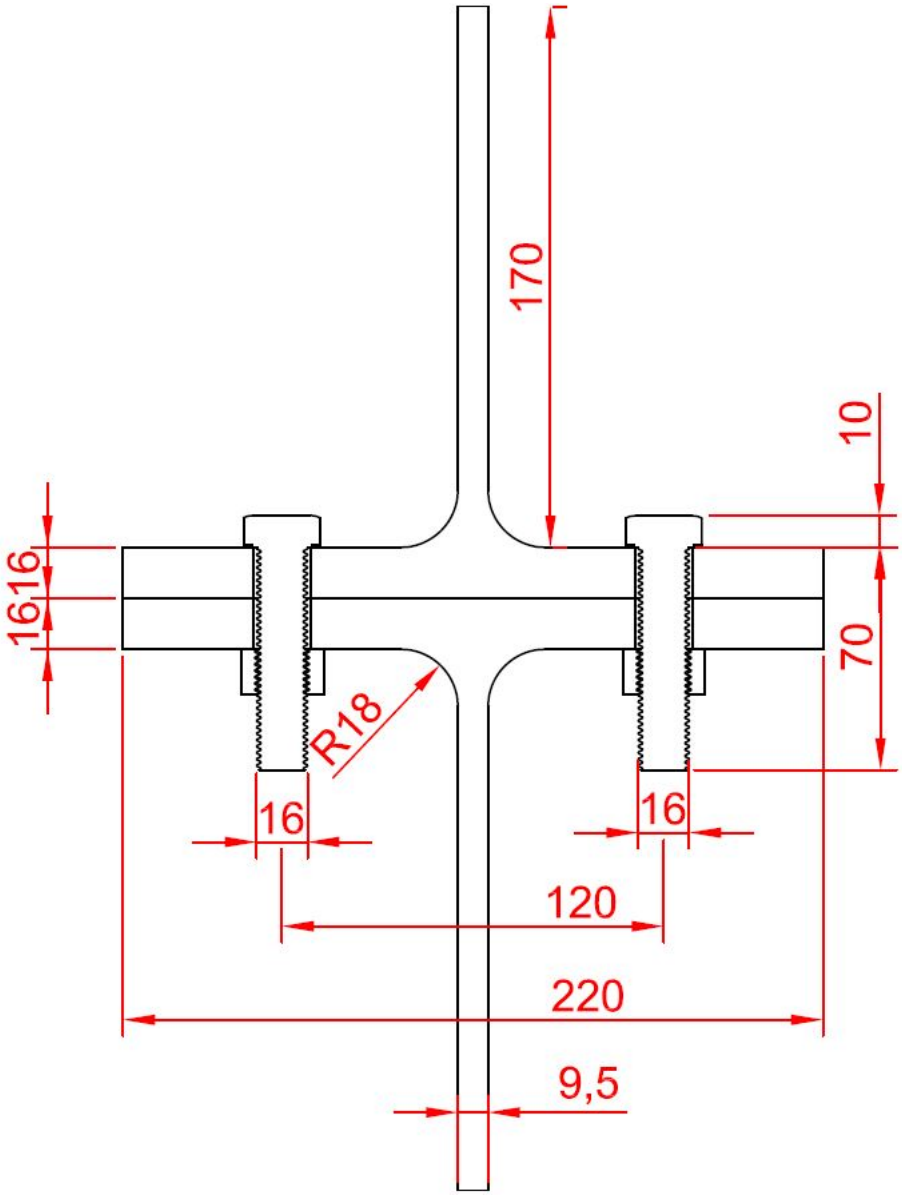

T120-FT: Center distance 120 mm, fully threaded bolts, one nut

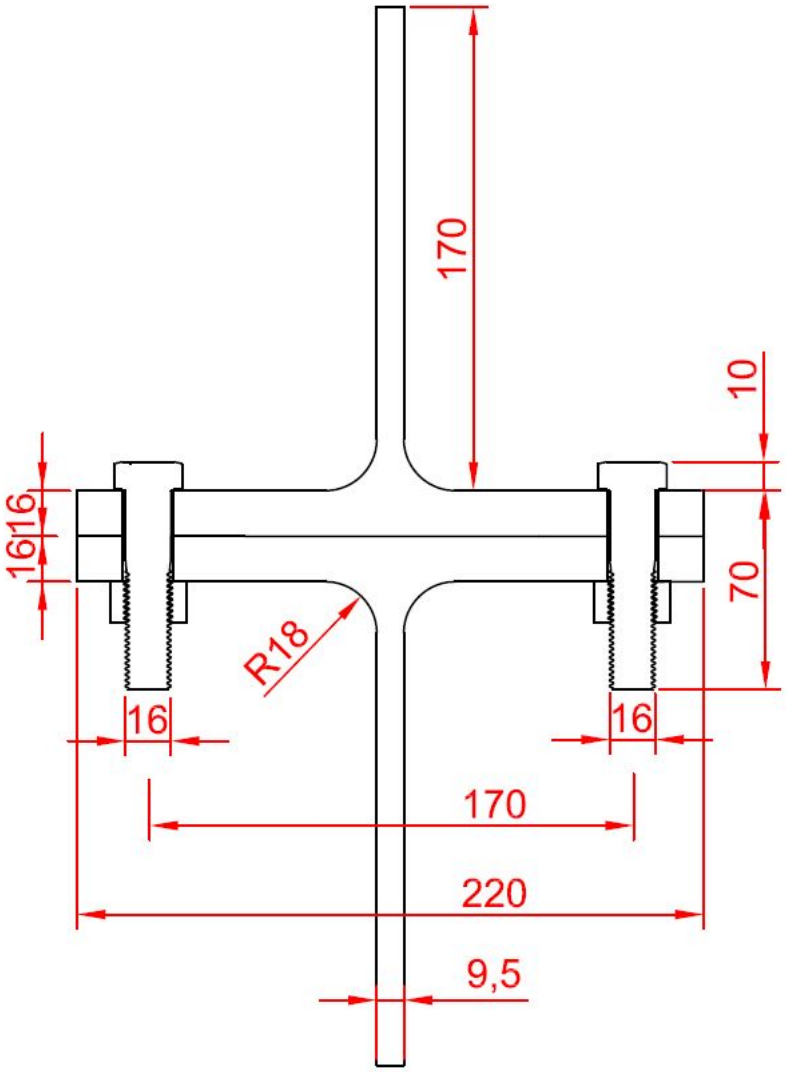

T170-PT: Center distance 170 mm, partially threaded bolts, one nut

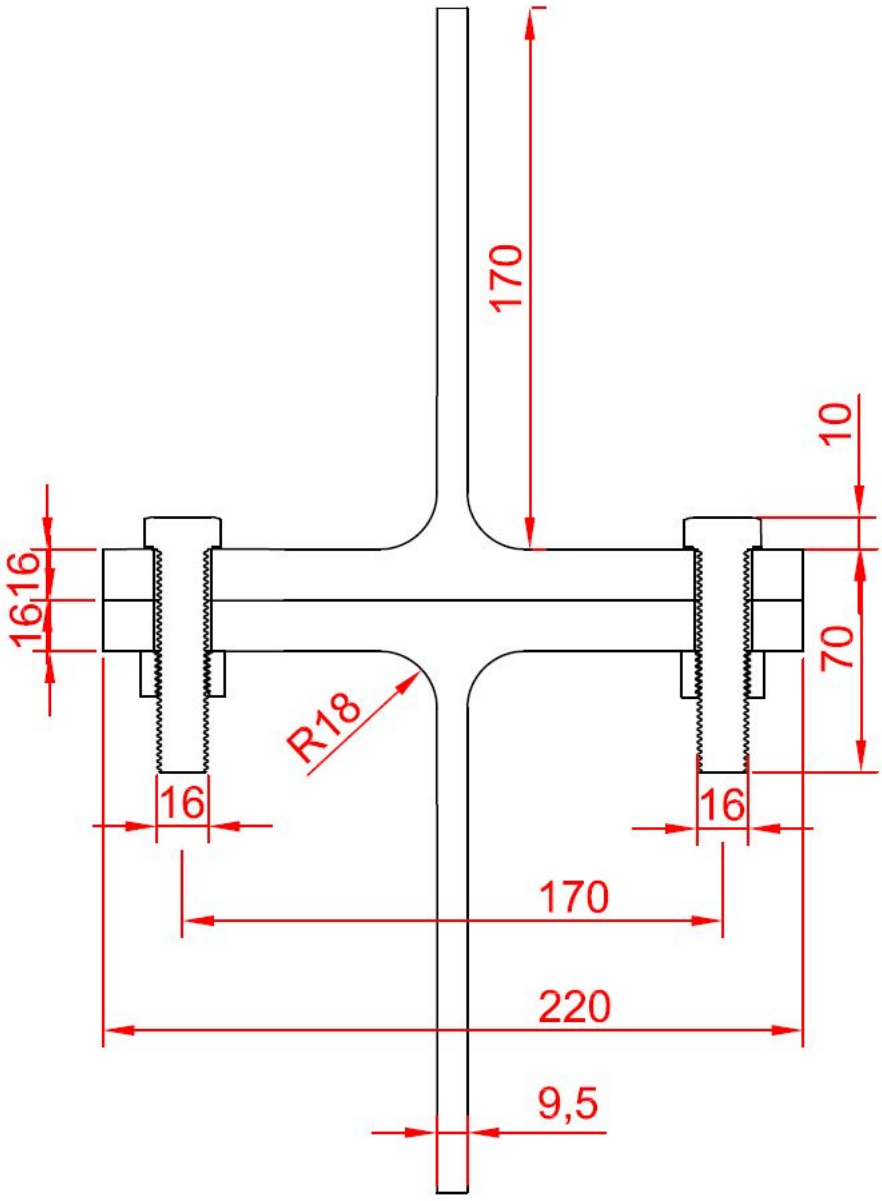

T170-FT: Center distance 170 mm, fully threaded bolts, one nut

Appendix G: Stiffness of the T-stub connection

This appendix contains the calculations regarding the stiffness of the T-stub connection. Two methods are utilized to define the stiffness, i.e. calculations retrieved from Eurocode NS-EN 1993-1-8 and a simplified method where the prying forces are ignored.

Geometry of the T-stub connection:

Average thickness of flange:	$t_f := 15.31\text{mm}$	
Length of flange:	$l_{eff} := 100\text{mm}$	
Average height of nut:	$h_n := 14.196\text{mm}$	
Height of bolt head:	$h_{bh} := 10\text{mm}$	
Clamp length of the upper T-stub:	$L_b := t_f + \frac{h_{bh}}{2} = 20.31\cdot\text{mm}$	
Optimal bolt diameter:	$d_b := 14.14\text{mm}$	
Cross section area of bolt:	$A_b := d_b^{2}\cdot\frac{\pi}{4} = 157.032\cdot\text{mm}^2$	
Young ' s Modulus	$E := 210000\frac{N}{\text{mm}^2}$	
Second moment of area:	$I := \frac{t_f^{3}\cdot l_{eff}}{12} = 2.991\times 10^{4}\cdot\text{mm}^4$	
Center distance between bolts, T-stub120:	$m_{120} := 40.8\text{mm}$	Appendix E
center distance between bolts, T-stub 170:	$m_{170} := 65.8\text{mm}$	Appendix E
Distance between the edge and bolt center, T-120:	$e_{120} := 50\text{mm}$	Appendix E
Distance between the edge and bolt center, T-170:	$e_{170} := 25\text{mm}$	Appendix E

Stiffness calculations from Eurocode NS-EN 1993-1-8

Stiffness coefficient for the bolt:

$$k_{c.FT} := \frac{1.6 \cdot A_b}{L_b} = 12.371 \cdot mm$$

EC 3-1-8: table 6.11

Stiffness coefficient for the flange:

$$k_{c.f.120} := \frac{0.9 \cdot l_{eff} \cdot t_f^{\,3}}{m_{120}^{\,3}} = 4.755 \cdot mm$$

EC 3-1-8: table 6.11

$$k_{c.f.170} := \frac{0.9 \cdot l_{eff} \cdot t_f^{\,3}}{m_{170}^{\,3}} = 1.134 \cdot mm$$

The total stiffness is divided by two to account for the total displacement of the T-stub connection.

$$k_{c.120.FT} := \frac{1}{\left(\frac{1}{k_{c.f.120}}\right) + \left(\frac{1}{k_{c.FT}}\right)} = 3.435 \cdot mm$$

Total stiffness for the T-120 with fully threaded bolts:

$$k_{120.FT} := E \cdot k_{c.120.FT}{}^{\cdot 0.5} = 360.673 \cdot \frac{kN}{mm}$$

$$k_{c.170.FT} := \frac{1}{\left(\frac{1}{k_{c.f.170}}\right) + \left(\frac{1}{k_{c.FT}}\right)} = 1.039 \cdot mm$$

Total stiffness for the T-170 with fully threaded bolts:

$$k_{170.FT} := E \cdot 0.5 k_{c.170.FT} = 109.043 \cdot \frac{kN}{mm}$$

Stiffness calculations from the simplified method

Simplified method is utilized, where the contribution from prying forces are ignored. An illustration is given in Figure 1.

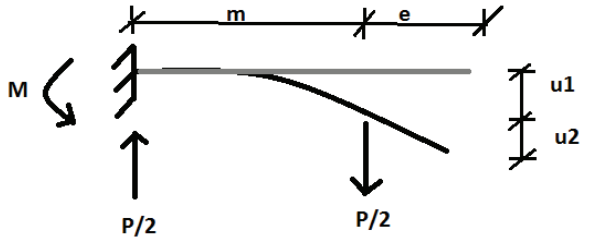

Figure 1: Simplified system of the T-stub connection

To identify the stiffness, a reference force of 50kN was employed. From the experimental results, this has shown to be within the elastic domain, and may therefore be utilized in the calculations to identify the elastic stiffness of the system.

$$P := 50kN$$

T -120:

$$u_{1.120} := \frac{P \cdot m_{120}^{3}}{2 \cdot 3 \cdot E \cdot I} = 0.09 \cdot mm$$

$$u_{2.120} := \tan\left(\frac{3 \cdot u_{1.120}}{2 \cdot m_{120}}\right) \cdot e_{120} = 0.166 \cdot mm$$

The total displacement for both flanges in T-120:

$$u_{tot.120} := 2 \cdot \left(u_{1.120} + u_{2.120}\right) = 0.512 \cdot mm$$

$$K_{simp.120} := \frac{P}{u_{tot.120}} = 97.736 \cdot \frac{kN}{mm}$$

T -170:

$$u_{1.170} := \frac{P \cdot m_{170}^{3}}{2 \cdot 3 \cdot E \cdot I} = 0.378 \cdot mm$$

$$u_{2.170} := \tan\left(\frac{3 \cdot u_{1.170}}{2 \cdot m_{170}}\right) \cdot e_{170} = 0.215 \cdot mm$$

The total displacement for both flanges in T-170:

$$u_{tot.170} := 2 \cdot \left(u_{1.170} + u_{2.170}\right) = 1.187 \cdot mm$$

$$K_{simp170} := \frac{P}{u_{tot.170}} = 42.124 \cdot \frac{kN}{mm}$$